CHAPTER–4

Ylide Decorated Monovalent Group 13 Carbenoids and Probing their potential towards Activation of Enthalpically Strong Bonds.
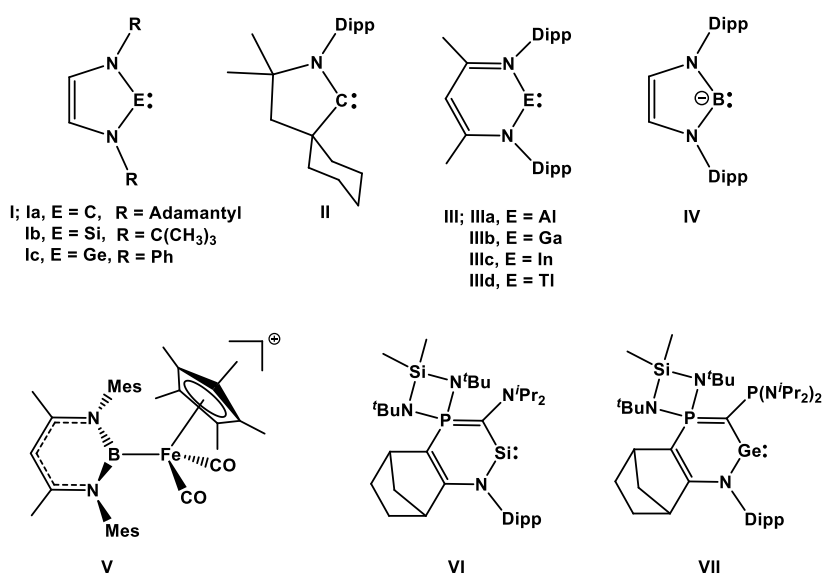
Abstract: In the first part of this chapter, we present the results of our computational studies on the stabilization of neutral, monomeric five-membered boron(I) carbenoids by employing two different ylide functionalities, viz., a conventional carbon-based phosphorous ylide and a zwitterionic four-membered cyclic ylide. The boron(I) carbenoids proposed in this study possess the highest singlet-triplet energy separation values (ΔE_{S-T} = 25.5–42.3 kcal mol^{-1}) known to date and are strongly nucleophilic in nature. In addition, the majority of these borylenes are found to be capable of activating a variety of enthalpically strong bonds such as C–H and C–F bonds, whose computed relatively lower energy barriers than experimentally evaluated systems such as cAAC confirm their potential in small molecule activation. In addition, combined Activation Strain Model-Energy Decomposition Analysis (ASM-EDA) methodology was applied to quantitatively rationalize the different reactivity trends exhibited by the proposed borylenes.

In the second part of this chapter, we have shown computationally the remarkable ability of strongly electron donating ylidic functionalities in stabilizing singlet group 13 carbenoids with promising ligand properties. All the proposed carbenoids are found to be considerably nucleophilic and possess significant singlet-triplet energy separation values. The calculated activation barriers and reaction free energies obtained for the cleavage of different enthalpically strong bonds by these carbenoids are found to be either comparable or lower to those of the experimentally evaluated aluminium and gallium carbenoids thereby indicating their potential in small molecule activation.

[4.1] Stable *N*-Heterocyclic Borylenes with Promising Ligand Properties: A Contribution from Theory

[4.1.1] Introduction

The ground-breaking discovery of a bottleable and crystalline singlet *N*-heterocyclic carbene (NHC, **Ia**, Scheme 4.1.1) [1] by Arduengo in 1991 as well as the isolation of the game-changing cyclic alkyl amino carbene (cAAC, **II**) [2] by Bertrand in 2005 brought a paradigm shift in both main-group and transition metal chemistry. Owing to the availability of high-lying donor and low-lying acceptor orbitals of appropriate symmetry, they could mimic the behaviour of transition metals [3] and are extensively used in several key areas such as in the stabilization of unusual or reactive species [4–8], small molecule activation [9–11] and transition metal catalysis etc [12]. The heavier analogues of NHC, viz., *N*-heterocyclic silylene (NHSi, **Ib**) and germylene (NHGe, **Ic**) are also known and they too are explored comprehensively [11,13]. The monovalent group 13 carbenoids, which are isoelectronic to divalent group 14 compounds (e.g. NHC), are also known for the heavier Al–Tl(III) [14–17] derivatives and are found to be capable of exhibiting metallomimetic behaviour such as small molecule activation [11]. The first addition to this class of compounds came from Roesky and coworkers with the isolation of a neutral six membered Al(I) carbenoid (**IIIa**) supported by a bulky β-diketiminate (NacNac) ligand framework [14]. This was followed by the synthesis of its gallium analogue (**IIIb**) by Power and coworkers [15]. However, the synthesis and isolation of a


I; Ia, E = C, R = Adamantyl
Ib, E = Si, R = C(CH₃)₃
Ic, E = Ge, R = Ph

II

III; IIIa, E = Al
IIIb, E = Ga
IIIc, E = In
IIId, E = Tl

IV

V

VI

VII

Scheme 4.1.1: Schematic representation of some of the experimentally known group 13 and group 14 bases discussed in this study.

neutral monomeric cyclic boron(I) carbenoid has remained elusive to date; this may be attributed to smaller energetic separation between the valence s and p orbitals as well as low singlet–triplet (ΔE_{S-T}) separation [13,18]. In this context, it is pertinent to mention the existence of mono- and bis(Lewis base) stabilized borylenes that have been synthesized by various groups over the years and interestingly, some of them are capable of activating different enthalpically strong bonds (C–H, C–C and B–H) and small molecules like H_2 and N_2 [19]. Similarly, efforts made towards the isolation of a B(I) carbenoid, however, resulted in the formation of either an anionic species (**IV**) [20] or a transition metal complex (**V**) [21]. Recently, based on computational studies, we proposed a couple of B(I) carbenoids having considerable ΔE_{S-T} values [22]. Phosphorous ylides are found to be useful in stabilizing group 14 bases as exemplified by the isolation of **VI** and **VII** [23–29]. By virtue of the presence of a pseudo lone pair at the carbon atom, these ylides can function as strong π-donating substituents that can be employed towards the stabilization of reactive low-valent main-group species [30]. Based on these reports, we envisage that phosphorous ylides could be promising systems for the stabilization and isolation of the hitherto unknown cyclic boron(I) carbenoids. Herein, we present the results of our computational studies on the stabilization of neutral, monomeric five-membered boron(I) carbenoids by employing two different ylide functionalities, viz., a conventional carbon-based phosphorous ylide and a zwitterionic four-membered cyclic ylide [31] (Scheme 4.1.2) and their potential in small molecule activation. Furthermore, in order to make our study meaningful to synthetic chemists, the various electronic, thermodynamic and kinetic parameters of these proposed molecules are compared to those of synthetically amenable compounds such as cAAC (**II**) and Roesky's Al(I) carbenoid (**IIIa**) [32].

[4.1.2] Computational Details

      Density functional theory calculations were carried out to optimize all the molecules without any symmetry constraints by employing the meta-GGA M06 exchange–correlation functional [33] in combination with the valence polarized def2-TZVP basis set for all the elements [34, 35]. Frequency calculations were carried out at the same level of theory to check the nature of the stationary points and all the molecules were found to be minima with real vibrational frequencies. The transition states were characterized by the presence of only one imaginary frequency, which was further
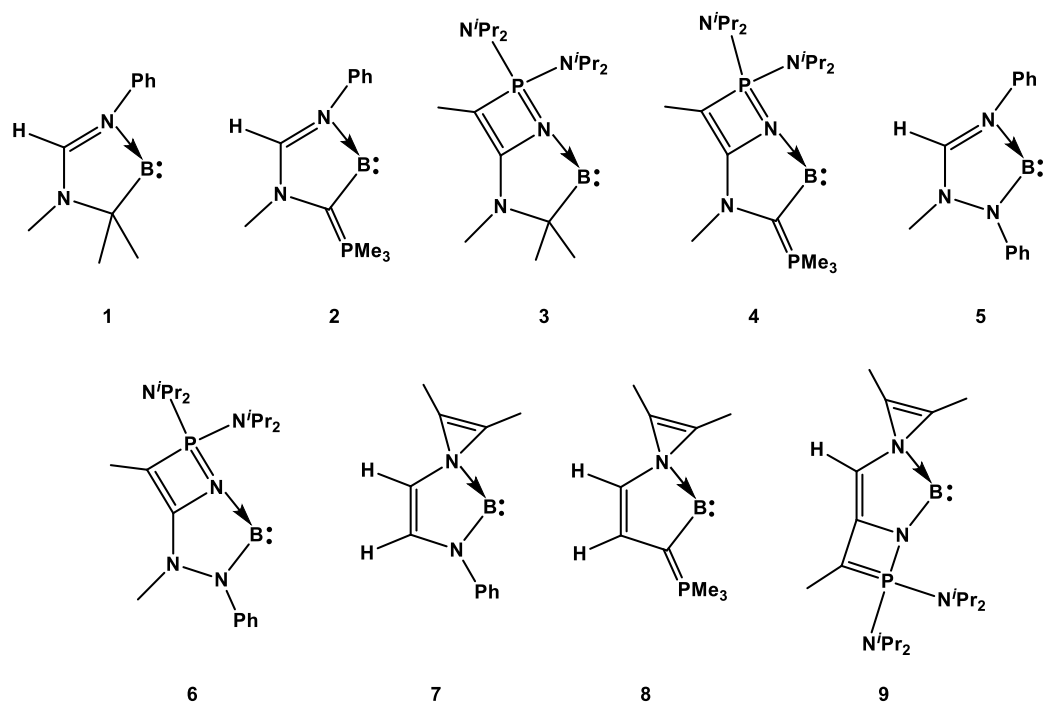
Scheme 4.1.2: Schematic representation of the cyclic five-membered boron(I) carbenoids considered in this study.

confirmed by performing intrinsic reaction coordinate (IRC) calculations at the same level of theory. Dispersion effects were incorporated by using the D3 version of Grimme's dispersion correction coupled with the original D3 damping function with the keyword Empiricaldispersion = GD3 [36]. Solvent effects (Toluene) were incorporated by using the polarizable continuum model (PCM) [37]. The ultrafine grid was used throughout the calculations. Bonding analyses were performed with the help of the NBO routine [38,39] as implemented in the Gaussian 09 suite of programs [40]. The reliability of the calculated ΔE_{S-T} values were checked by recalculating them with three different functionals: PBE0 [41], ωB97XD [42] and B3PW91 [43]. Furthermore, to check the presence of any internal instability in **1–9**, we performed stability tests on the single-determinant wave functions of the optimized geometries of **1–9** (both singlet and triplet states) [44,45]. The activation energy barriers for all the bond splitting processes were evaluated with respect to the sum of the energies of the separated reactants. Furthermore, to check the reliability of the calculated energetics of the different reactions considered in this study, we recalculated a few of them by employing different functionals (PBE0 [41] and ωB97XD [42]). The energetics for all the calculations were evaluated in terms

of change in Gibbs free energies at 1 atm pressure and 298 K temperature unless otherwise specified.

Activation strain model of reactivity and energy decomposition analysis

Within the ASM method [46], also known as the *distortion/interaction model* [46c], the potential energy surface $\Delta E(\zeta)$ is decomposed along the reaction coordinate, ζ, into two contributions, namely the strain $\Delta E_{strain}(\zeta)$ associated with the deformation (or distortion) required by the individual reactants during the process and the interaction $\Delta E_{int}(\zeta)$ between these increasingly deformed reactants:

$$\Delta E(\zeta) = \Delta E_{strain}(\zeta) + \Delta E_{int}(\zeta)$$

Within the EDA method [47], the interaction energy can be further decomposed into the following chemically meaningful terms:

$$\Delta E_{int}(\zeta) = \Delta V_{elstat}(\zeta) + \Delta E_{Pauli}(\zeta) + \Delta E_{orb}(\zeta) + \Delta E_{disp}(\zeta)$$

The term ΔV_{elstat} corresponds to the classical electrostatic interaction between the unperturbed charge distributions of the deformed reactants and is usually attractive. The Pauli repulsion ΔE_{Pauli} comprises the destabilizing interactions between occupied orbitals and is responsible for any steric repulsion. The orbital interaction ΔE_{orb} accounts for bond pair formation, charge transfer (interaction between occupied orbitals on one moiety with unoccupied orbitals on the other, including HOMO-LUMO interactions), and polarization (empty-occupied orbital mixing on one fragment due to the presence of another fragment). Moreover, the NOCV (Natural Orbital for Chemical Valence) [48] extension of the EDA method has been also used to further partition the ΔE_{orb} term. The EDA-NOCV approach provides pairwise energy contributions for each pair of interacting orbitals to the total bond energy.

The program package ADF [49] was used for EDA calculations using the optimized PCM-M06-D3/def2-TZVP geometries at the same DFT level in conjunction with a triple-ζ-quality basis set using uncontracted Slater-type orbitals (STOs) augmented by two sets of polarization functions with a frozen-core approximation for the core electrons [50]. Auxiliary sets of s, p, d, f, and g STOs were used to fit the molecular densities and to represent the Coulomb and exchange potentials accurately in each SCF cycle [51]. Scalar relativistic effects were incorporated by applying the zeroth-

order regular approximation (ZORA) [52]. This level of theory is denoted ZORA-M06/TZ2P//PCM(toluene)-M06–D3/def2-TZVP.

[4.1.3] Results and Discussion

The optimized geometries of **1–9** in their singlet states possess a planar five-membered central ring (Figure 4.1.1). All the newly designed B(I) carbenoids exhibit a stable singlet ground state, which is evident from their calculated moderate-to-high ΔE_{S-T} values (Figure 4.1.2). We optimized both the singlet and triplet states of **1–9** to evaluate their ΔE_{S-T} values. Moreover, analysis of the Mulliken spin density values for the triplet states of **1–9** reveals that for molecules **1**, **2**, **5** and **7–9**, the spin is delocalized over the borylene framework while for **3**, **4** and **6**, the spin is mostly localized at the central boron atom (Table 4.1.1). Furthermore, it should be noted that the calculated ΔE_{S-T} values of **1**, **2**, **5** (8.5–15.7 kcal mol^{-1}, Figure 4.1.2) and **8** (19.2 kcal mol^{-1}) are low-to-moderate thereby ruling out their possible experimental realization and hence these molecules are not considered for small molecule activation (vide infra). Interestingly, incorporation of the strongly electron-donating four-membered ylide functionality into the ring framework of **1**, **2**, **5** and **7** dramatically lifts the ΔE_{S-T} values of **3**, **4**, **6** (ΔE_{S-T} = 31.5–42.3 kcal mol^{-1}) and **9** (31.6 kcal mol^{-1}) respectively; this may be attributed to enhanced charge transfer from the α-nitrogen atom (w.r.t. the central boron atom) to the vacant p orbital at the boron atom. This is also evident from the calculated B–N bond lengths, which are found to be considerably shorter in **3**, **4**, **6** and **9** than that in their respective parent B(I) carbenoids. It is encouraging to note that the ΔE_{S-T} values of **4** and **6** are very high and especially, the ΔE_{S-T} value of **6** is comparable to that of synthetically accessible cAAC (42.7 kcal mol^{-1}, calculated at the same level of theory). To the best of our knowledge, except **3**, **4**, **6**, **7** and **9** no other neutral monomeric cyclic B(I) carbenoids are known to date with such large singlet–triplet separations. The higher singlet state stability of **4** and **6** may be attributed to the presence of two strongly π-donating groups close to the B(I) center that significantly stabilizes the π-symmetric occupied orbital compared to that in either **2** or **3**, which is decorated with only one π-donating group (Figure 4.1.3). Also, we argue that the presence of thermodynamically strong exocyclic P–N bonds further contribute towards the improvement of the singlet state stability of **3**, **4**, **6** and **9**.
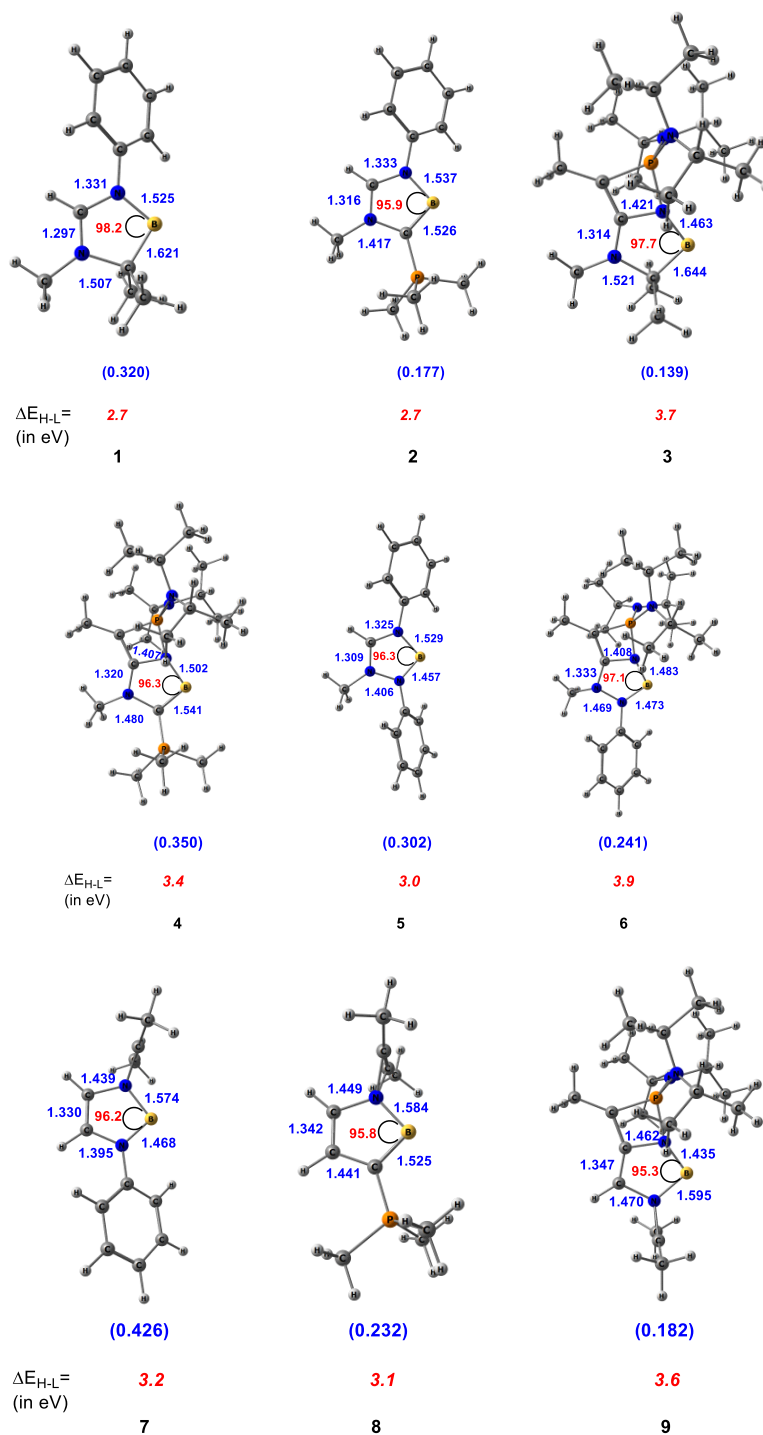
Figure 4.1.1: Pictorial representation of the singlet state optimized geometries of **1-9** calculated at M06-D3/def2-TZVP (Toluene) level of theory. The occupancy of the formally vacant p_π orbital centered at the boron atom for **1-9** are given within parenthesis. Bond lengths and bond angles are given in Å and degree (°) respectively. The HOMO-LUMO (ΔE_{H-L}, in eV) gap values for **1-9** are given in *italics*.
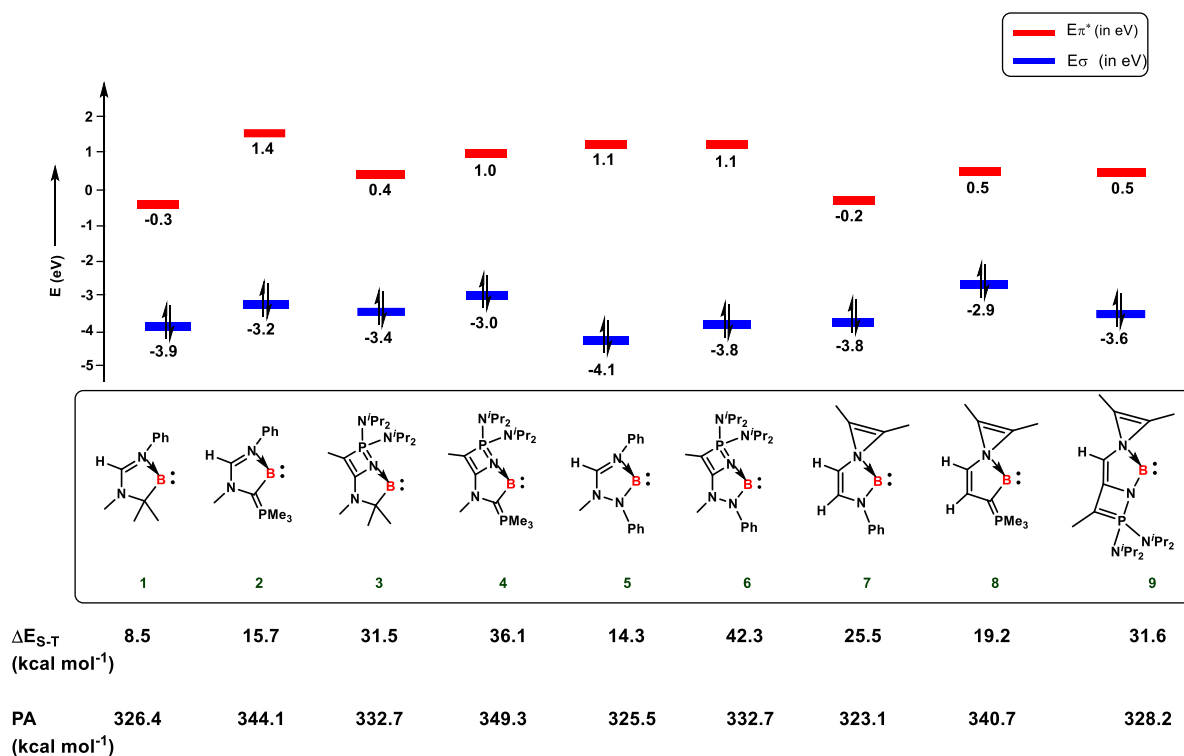
Figure 4.1.2: Calculated (M06-D3/def2-TZVP (Toluene)) energies (in eV) of the donor (E_σ) and acceptor orbitals ($E_\pi*$) concentrated at the boron atom for **1-9** in their singlet state. Also given are the singlet–triplet energy separations (ΔE_{S-T}) and proton affinities (PA).

Table 4.1.1: Calculated (M06-D3/def2-TZVP (Toluene)) Mulliken spin densities at the central boron atom and α-nitrogen and carbon atoms (w.r.t. the central boron atom) of the triplet states for **1-9**.

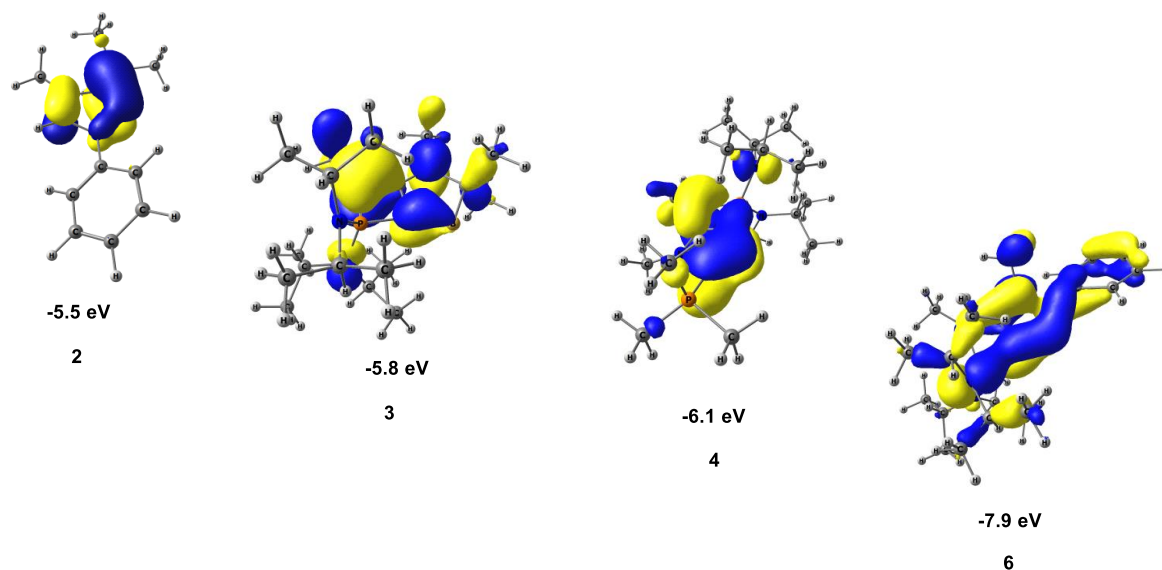| Molecules	B	N_α	C_α/N_α
1	1.056	-0.050	0.002
2	0.586	0.058	0.259
3	1.675	-0.018	0.086
4	1.675	0.015	0.123
5	1.061	-0.068	0.049
6	1.613	-0.057	-0.015
7	1.270	-0.024	-0.087
8	1.003	-0.007	-0.042
9	1.036	-0.056	-0.035

Figure 4.1.3: Pictorial representation of the occupied π-symmetric molecular orbitals (along with their energies in eV) for **2**, **3, 4** and **6** calculated at the M06-D3/def2-TZVP (Toluene) level of theory.

Furthermore, it is evident from Figure 4.1.2 that substitution of the amino group in **7** by an ylidic moiety yielded structure **8** with a considerably lower singlet–triplet energy separation value (19.2 kcal mol^{-1}). Such a reduction in the ΔE_{S-T} value of **8** may be attributed to the inductive destabilization of its singlet state. Calculations at different levels of theory provide similar ΔE_{S-T} values (Table 4.1.2) thereby supporting the level of theory used in this study. In addition, the thermodynamic stabilities of **1–9** were further judged by separately calculating the hydrogenation energies of their singlet and triplet states (Table 4.1.3). Interestingly, the differences in the calculated hydrogenation energies for the singlet and triplet states (ΔE_{Hydro}) of **1–9** are found to be in excellent agreement with their respective ΔE_{S-T} values. In addition, the calculated ΔE_{S-T} values of **3**, **4**, **6** and **9** are found to be comparable (**3** and **9**) and higher (**4** and **6**) than that of the experimentally determined singlet–triplet energy separation value of the parent B–H ($\Delta E_{S-T} \cong 30$ kcal mol^{-1}) moiety [53]. Furthermore, **3**, **4**, **6**, **7** and **9** also possess significant kinetic stability as evident from the calculated higher HOMO–LUMO gaps (Figure 4.1.1). We did not obtain any internal instability for **1–9**.

The ligand properties of **1–9** were examined by evaluating the energies of their σ-symmetric donor (E_σ, in eV) and π-symmetric acceptor orbitals (E^*_π, in eV) concentrated at the boron atom. It is evident from Figure 4.1.2 that all the newly proposed borylenes exhibit substantially higher electron donation ability (E_σ varies from −2.9 to −4.1 eV)

Table 4.1.2: Calculated singlet-triplet energy separation values (ΔE_{S-T}, in kcal mol^{-1}) for **1-9** with different functionals.

Molecules	ΔE_{S-T}			
	M06	**PBE0**	**ωB97XD**	**B3PW91**
1	8.5	4.0	8.5	4.4
2	15.7	13.0	16.1	13.3
3	31.5	25.8	31.8	26.4
4	36.1	30.7	40.2	30.3
5	14.3	11.0	14.7	11.8
6	42.3	37.8	43.6	38.1
7	25.5	21.9	25.4	21.7
8	19.2	15.2	17.9	15.1
9	31.6	28.1	31.2	27.9

Table 4.1.3: Calculated (M06-D3/def2-TZVP (Toluene)) hydrogenation energy values (in kcal mol^{-1}) for **1-9** in their singlet and triplet states. The difference in the calculated hydrogenation energy values for the singlet and triplet states (ΔE_{Hydro}) of **1-9** are given in kcal mol^{-1}.

Molecule	Hydrogenation Energy		ΔE_{Hydro}
	Singlet	**Triplet**	
1	29.8	21.3	8.5
2	53.9	38.2	15.7
3	38.8	7.3	31.5
4	51.8	15.6	36.2
5	48.3	33.9	14.4
6	46.9	4.5	42.4
7	39.8	14.3	25.5
8	46.6	27.4	19.2
9	44.6	13.0	31.6

than that of either NHC **Ia** (−6.5 eV) or cAAC **II** (−5.8 eV) although all of them possess low π-acidity (E^*_π = −0.3 to 1.4 eV). Furthermore, it should be noted that **3**, **4**, **6** and **9**,

which are decorated with a four-membered ylidic moiety, exhibit superior electron donation ability compared to their parent analogs; this may be attributed to the inductive destabilization of the boronic lone pair as the valence shell of the ylidic nitrogen atom gets saturated by withdrawing electron density from the electron-rich $P(N^iPr_2)_2$ fragment. Thus, **1–9** may be considered as strongly nucleophilic ligands and their nucleophilicity is probed by evaluating their proton affinities (PAs). As expected, all these molecules possess very high PA values (323–349 kcal mol^{-1}, Figure 4.1.2) and are appreciably higher than those calculated for either NHC (255.0 kcal mol^{-1}) or cAAC (287.6 kcal mol^{-1}). The calculated PA values of **1–9** are in good agreement with their respective E_σ values and indeed, we obtained a good linear relationship ($R^2 = 0.84$, omitting the point corresponding to **8**, Figure 4.1.4) when plotting the calculated PA vs. the E_σ values. The
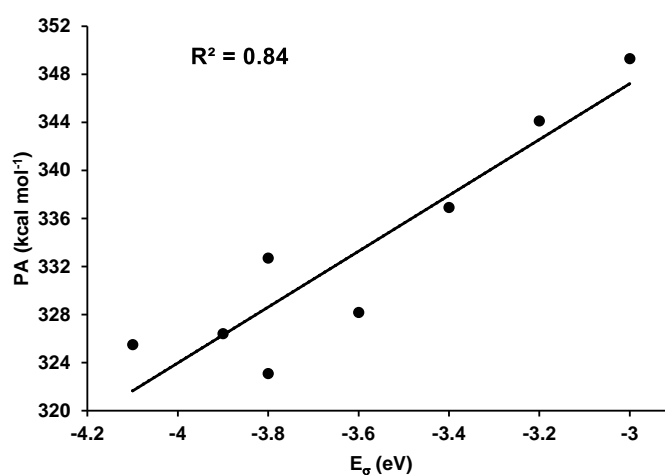

Figure 4.1.4: Correlation plot between proton affinity (PA, in kcal mol^{-1}) and E_σ (in eV) values for **1-9** (omitting the point corresponding to **8**).

significant singlet state stability of **3**, **4**, **6**, **7** and **9** coupled with promising ligand properties make them interesting synthetic targets and this motivated us to undertake a comprehensive study towards probing their potential in small molecule activation.

We began our reactivity study of the proposed borylenes by considering the activation of dihydrogen and methane as these are some of the most widely investigated reactions. Interest in the activation of H_2 stems from the fact that it is a key step in various reaction processes such as hydroformylation and hydrogenation [54,55]. On the other hand, C–H activation helps in the functionalization of hydrocarbons as value added products. Earlier, the splitting of the enthalpically strong H–H and C–H bonds (bond dissociation energies of H–H and C–H bonds are 104.2 and 105.0 kcal mol^{-1}

respectively) [56] was carried out by transition metal (TM) complexes and are well documented [57]. However, TM complexes are generally not only expensive but also toxic and hence, alternatives were sought. Environmentally benign single-site main group systems that can exhibit metallomimetic behavior are ideal candidates for such a task [3,11]. A number of main group systems are known to activate dihydrogen and methane under ambient reaction conditions [9a,e,11,58,59]. For example, in 2007, Bertrand and coworkers reported the facile splitting of dihydrogen by employing a strongly nucleophilic cAAC ligand [9a]. Similarly, in a recent study, Wang and coworkers reported the oxidation of methane under mild conditions by a carbene stabilized hydroborenium complex yielding the corresponding methylborenium complex [60]. Prompted by these reports, we decided to investigate the potential of **3**, **4**, **6**, **7** and **9** towards the activation of these enthalpically strong bonds.

[4.1.3.1] Activation of Dihydrogen

The mechanism of activation of H_2 by **3**, **4**, **6**, **7** and **9** is envisioned to be similar to that for activation by cAAC (**II**) [9], i.e., the interaction of the lone pair at boron with the σ^*_{H-H} orbital generates a hydridic hydrogen that is captured by the positively polarized boron center. The overall process proceeds via a transition state (TS) featuring a substantially elongated and polarized H–H bond. We searched for the probable TSs and the optimized geometries of all the TSs involved in the activation of dihydrogen by **3**, **4**, **6**, **7**, **9**, **II**, **IIIa** and **IIIb** is shown in Figure 4.1.5. Some of the computed structures along the reaction pathway for the activation of H_2 by **3** are shown in Figure 4.1.6 as an illustrative example. All the computed TSs (**3TS**$^{H-H}$, **4TS**$^{H-H}$–**7TS**$^{H-H}$ and **9TS**$^{H-H}$) exhibit substantially elongated (0.894–1.073 Å) and polarized H–H bonds (Table 4.1.4) with the positively polarized hydrogen atom being strongly bonded to the boron center (Wiberg Bond Index (WBI) = 0.499–0.628) whereas the hydridic hydrogen remains detached from it (B–H$^{\delta-}$ bond length = 1.865–2.494 Å). Nonetheless, the calculated WBI values between the central boron and the hydridic hydrogen atoms (WBI = 0.324–0.518) indicate the presence of considerable bonding interactions between them. This is further corroborated by a comparison of the occupancies of the vacant p orbital at boron in the TS and the parent compounds (Table 4.1.4 and Figure 4.1.1).
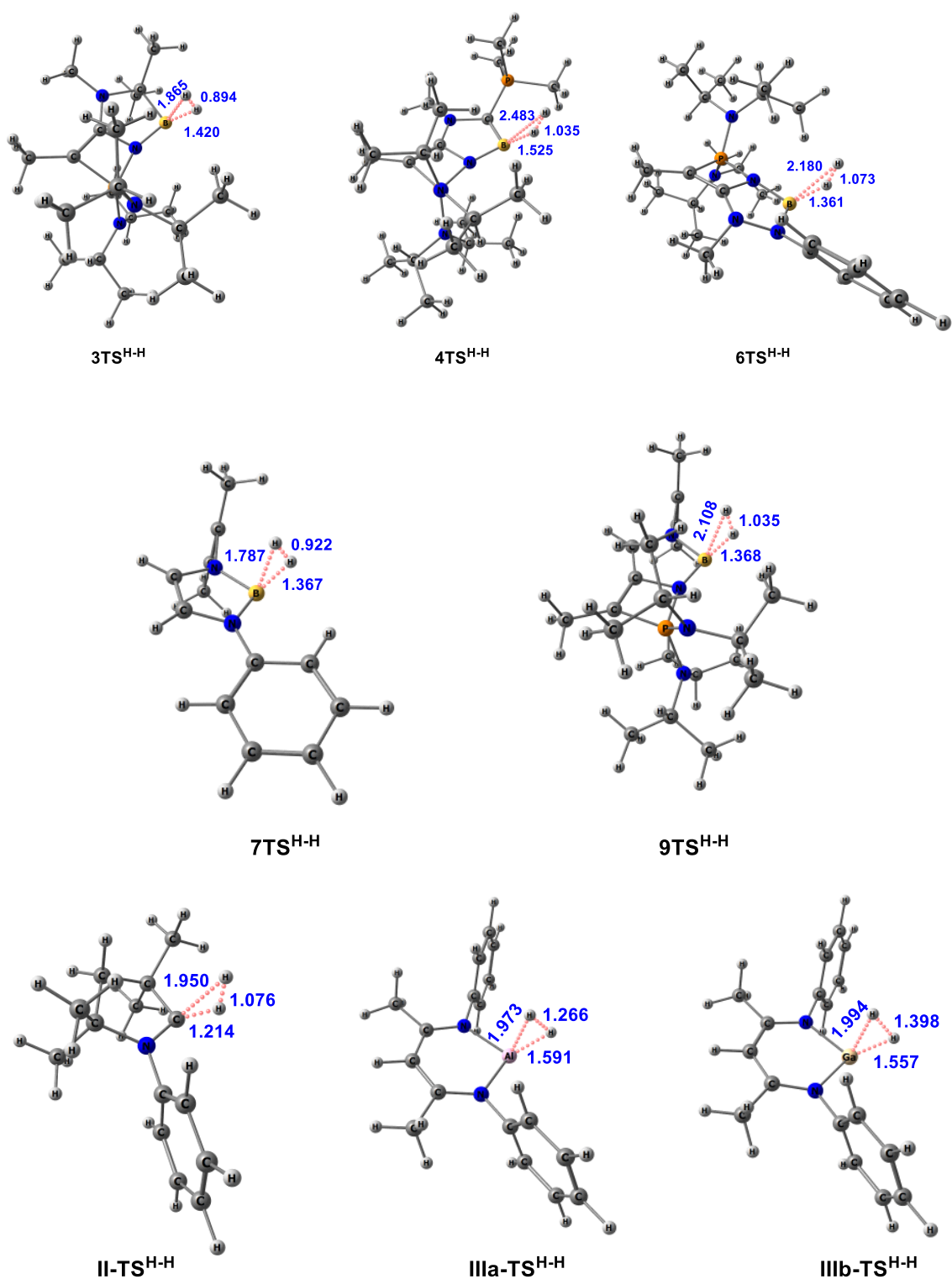
Figure 4.1.5: Optimized geometries of the transition states (TS) involved in the activation of dihydrogen by **3**, **4**, **6**, **7**, **9**, **II**, **IIIa** and **IIIb** (bond lengths are given in Å) at M06-D3/def2-TZVP (Toluene) level of theory.
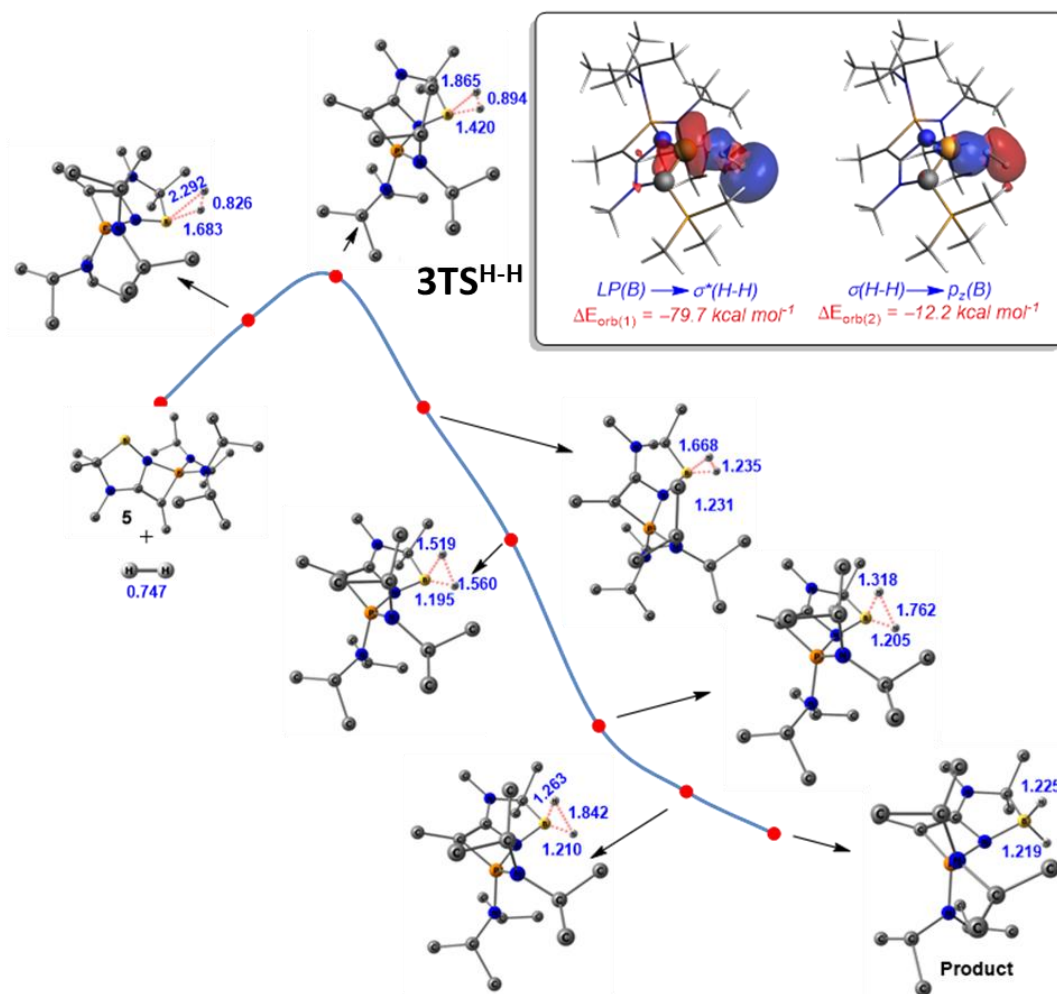
Figure 4.1.6: Some representative structures along the reaction pathway obtained from IRC calculations (PCM(toluene-)M06-D3/def2-TZVP) for the activation of dihydrogen by **3** (bond lengths are given in Å). The hydrogen atoms of the methyl groups are omitted for clarity. Inset: deformation densities of the dominant orbital interactions in complex **4TS$^{H\text{-}H}$**. The colour code used to represent the flow of charge is red→blue.

These results are in line with the bonding analysis provided by the EDA-NOCV method. According to this approach, two main orbital interactions dominate the borylene-mediated dihydrogen activation reactions, namely donation from the LP(B) to the σ*(H–H) molecular orbital and reverse donation from the doubly-occupied σ(H–H) molecular orbital to the vacant p$_z$ atomic orbital of the boron atom (see inset in Figure 4.1.6). Not surprisingly, the LP(B) → σ*(H–H) interaction is much stronger than the reverse σ(H–H)→p$_z$(B), which confirms the high nucleophilicity of the considered borylenes. This is also consistent with the asymmetric nature of the located transition states (i.e. the formation of both B–H bonds does not occur simultaneously but at rather different stages of the transformation, Figure 4.1.6).

Table 4.1.4: Calculated (M06-D3/def2-TZVP (Toluene)) important geometrical parameters, natural charges at the pseudo hydridic hydrogen ($H^{\delta-}$) and positively polarized hydrogen atom ($H^{\delta+}$) and occupancies of the formally vacant p_π orbital centered at the central E atom (E = B, Al, Ga and C) for the transition state involved in the activation of H_2 by **3**, **4**, **6**, **7**, **9**, **II**, **IIIa** and **IIIb**. The bond lengths are given in Å. The Wiberg Bond Index values (WBI) are given within parenthesis.

Molecules	$H^{\delta+}$–$H^{\delta-}$	E–$H^{\delta-}$	E–$H^{\delta+}$	$q_H{}^{\delta-}$	$q_H{}^{\delta+}$	Occ_{p_π}
II-TS^{H-H}	1.076 (0.315)	1.950 (0.465)	1.213 (0.621)	-0.196	0.185	0.756
IIIa-TS^{H-H}	1.266 (0.228)	1.973 (0.689)	1.591 (0.721)	-0.250	-0.159	0.511
IIIb-TS^{H-H}	1.398 (0.167)	1.994 (0.727)	1.556 (0.773)	-0.269	-0.097	0.552
3TS^{H-H}	0.894 (0.480)	1.865 (0.468)	1.420 (0.499)	-0.046	0.021	0.452
4TS^{H-H}	1.035 (0.457)	2.482 (0.324)	1.525 (0.523)	-0.380	-0.030	0.404
6TS^{H-H}	1.073 (0.349)	2.180 (0.467)	1.361 (0.628)	-0.269	-0.019	0.425
7TS^{H-H}	0.922 (0.422)	1.787 (0.518)	1.367 (0.561)	-0.034	0.034	0.497
9TS^{H-H}	1.035 (0.365)	2.108 (0.505)	1.368 (0.615)	-0.217	-0.023	0.462

The free energy barriers for the activation of H_2 ($\Delta G°_{TS}{}^{H-H\ddagger}$) lie within 14.4−18.5 kcal mol^{-1} (Table 4.1.5) with the highest barrier height being computed for **6**. In addition, it is inspiring to note that the computed $\Delta G°_{TS}{}^{H-H\ddagger}$ values are appreciably lower (two times lower for H_2 activation by **3** and **4**) than those computed for the experimentally evaluated cAAC (**II**) which is known to activate H_2 under ambient reaction conditions. The calculated $\Delta G°_{TS}{}^{H-H\ddagger}$ values are also found to be substantially lower (*two-to-four* times) than those calculated for the heavier group 13 carbenoids **IIIa** and **IIIb** at the same level of theory ($\Delta G°_{TS}{}^{H-H\ddagger}$ = 39.9 and 56.4 kcal mol^{-1} for **IIIa** and **IIIb** respectively). Moreover, the calculated reaction free energies ($\Delta G°_{Total}{}^{H-H}$) for **3**, **4**, **6**, **7** and **9** are found to be substantially exergonic (-48.8 to -61.4 kcal mol^{-1}) indicating the feasibility of the reactions. The relative ease of activation by **3**, **4**, **6**, **7** and **9** than that by **II** may be attributed to the substantially higher nucleophilicity of the former (*vide supra*). Therefore, from the calculated free energy barriers as well as reaction free

energies, the computationally discovered borylenes **3**, **4**, **6**, **7** and **9** may be considered as promising candidates for the activation of dihydrogen under ambient reaction conditions.

Table 4.1.5: Calculated activation energy barriers and reaction free energies for the formation of the E–H (E = H and N) and C–F bond splitting products obtained for **3**, **4**, **6**, **7** and **9** at the M06-D3/def2-TZVP (Toluene) level of theory. The energetics for the activation of H_2 and NH_3 by the experimentally evaluated cAAC (**II**) is also given for comparison. The energies are given in kcal mol^{-1}.

Entry	$\Delta G^{\circ}_{TS}{}^{H\text{-}H\ddagger}$	$\Delta G^{\circ}_{Total}{}^{H\text{-}H}$	$\Delta G^{\circ}_{TS}{}^{N\text{-}H\ddagger}$	$\Delta G^{\circ}_{Total}{}^{N\text{-}H}$	$\Delta G^{\circ}_{TS}{}^{C\text{-}F\ddagger}$	$\Delta G^{\circ}_{Total}{}^{C\text{-}F}$
3	14.4	-61.1	16.4	-63.4	20.0	-99.9
4	14.4	-48.8	11.9	-50.5	20.6	-92.0
6	18.5	-53.9	19.5	-58.8	22.9	-96.2
7	18.1	-61.4	19.4	-67.4	22.7	-103.8
9	17.3	-56.1	18.5	-63.1	20.6	-99.2
II	28.7	-43.0	30.5	-26.4		

[4.1.3.2] Activation of Ammonia

Another molecule of interest is ammonia as it prefers to form classical Werner-type amine complexes with transition metal compounds over the N–H bond splitting product [61]. This prompted us to further probe the potential of **3**, **4**, **6**, **7** and **9** towards the activation of NH_3 and compare it with cAAC (**II**), which is known to cleave the N–H bond under ambient reaction conditions [9]. Since **3**, **4**, **6**, **7** and **9** are strongly nucleophilic in nature, therefore, activation of the N–H bond by them is envisioned to occur in a similar fashion to that for H–H activation mentioned earlier. In other words, the reaction process is initiated by the transfer of electron density from the boron lone pair of electrons to one of the N–H antibonding orbitals thereby yielding a pseudo-amide ($NH_2{}^{\delta-}$) fragment, which is captured by the vacant p orbital at boron to produce the desired N–H bond splitting product. All the TSs exhibit substantially elongated (1.397–1.490 Å) and polarized N–H bonds (Figure 4.1.7 and Table 4.1.6) with the positively polarized hydrogen atom being strongly bonded to boron (WBI = 0.660–0.712) while the

$NH_2^{\delta-}$ fragment remains away from it (B–$NH_2^{\delta-}$ bond distance =2.700–2.833 Å). The substantial polarization of the elongated N–H bond can be corroborated by the NBO-based natural charge values, which indicate the presence of considerable positive and negative charges at the hydrogen (0.147 to 0.166) and nitrogen atoms (−1.222 to −1.277) of the pseudo-amide fragment respectively. In all the TSs, the lone pair at the nitrogen atom is directed away from the boron center thereby supporting the nucleophilic mode of activation (Figure 4.1.8) [9a]. Furthermore, the occupancy of the vacant p orbital at boron increases considerably in $3TS^{N-H}$, $4TS^{N-H}$, $6TS^{N-H}$, $7TS^{N-H}$ and $9TS^{N-H}$ compared to that in **3**, **4**, **6**, **7** and **9** respectively indicating the presence of considerable bonding interactions between the pseudoamide fragment and boron (Table 4.1.6 and Figure 4.1.1).

Table 4.1.6: Calculated (M06-D3/def2-TZVP (Toluene)) important geometrical parameters, natural charges at the nitrogen atom of the pseudo amide fragment ($NH_2^{\delta-}$), positively polarized hydrogen atom ($H^{\delta+}$) and occupancies of the formally vacant p_π orbital centered at the central E (E = B and C) atom for the transition state involved in the activation of NH_3 by **3**, **4**, **6**, **7**, **9** and **II**. The bond lengths are given in Å. The Wiberg Bond Index values (WBI) are given within parenthesis.

Molecules	$H^{\delta+}$–$H_2N^{\delta-}$	E–$NH_2^{\delta-}$	E–$H^{\delta+}$	$q_{NH_2}{}^{\delta-}$	$q_H{}^{\delta+}$	Occ_{p_π}
II-TS^{N-H}	1.542 (0.177)	2.428 (0.401)	1.156 (0.695)	-1.165	0.324	0.792
$3TS^{N-H}$	1.416 (0.277)	2.731 (0.301)	1.406 (0.678)	-1.224	0.155	0.275
$4TS^{N-H}$	1.397 (0.286)	2.833 (0.190)	1.495 (0.660)	-1.277	0.166	0.586
$6TS^{N-H}$	1.490 (0.242)	2.745 (0.290)	1.490 (0.712)	-1.241	0.148	0.445
$7TS^{N-H}$	1.446 (0.256)	2.700 (0.320)	1.364 (0.709)	-1.222	0.153	0.608
$9TS^{N-H}$	1.453 (0.253)	2.743 (0.290)	1.376 (0.707)	-1.236	0.147	0.312

The activation barrier ($\Delta G°_{TS^{N-H}}{}^{\ddagger}$) lies within 11.9-19.5 kcal mol^{-1} with the highest and lowest barrier being computed for **6** and **4** respectively (Table 4.1.5). Furthermore, it is encouraging to note that once again all the newly designed ylide anchored B(I) carbenoids outperform the experimentally evaluated **II** in the N–H bond
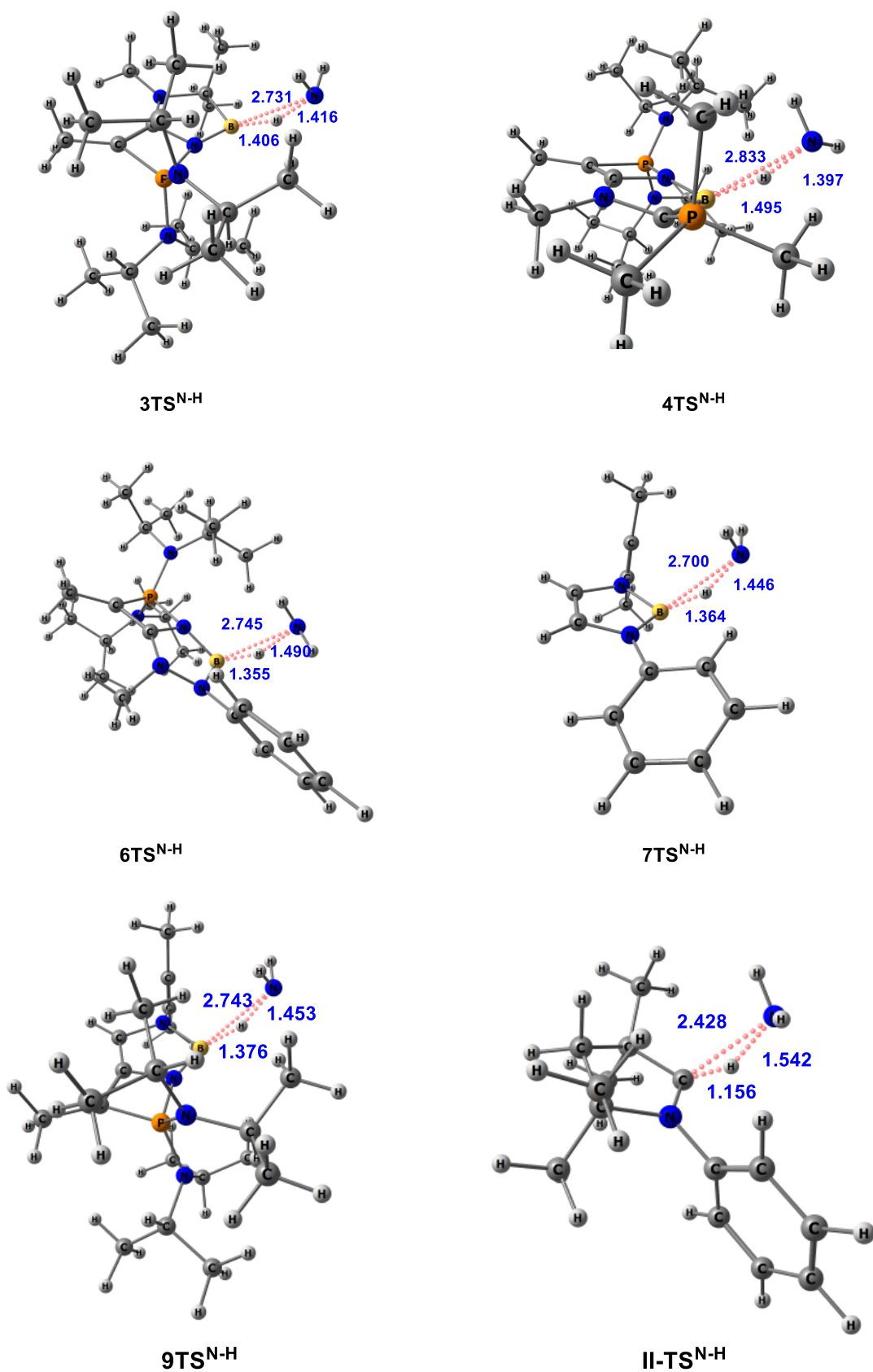
3TS^{N-H}

4TS^{N-H}

6TS^{N-H}

7TS^{N-H}

9TS^{N-H}

II-TS^{N-H}

Figure 4.1.7: Optimized geometries of the TSs involved in the activation of NH$_3$ by **3**, **4**, **6**, **7**, **9** and **II** (bond lengths are given in Å) at M06-D3/def2-TZVP (Toluene) level of theory.
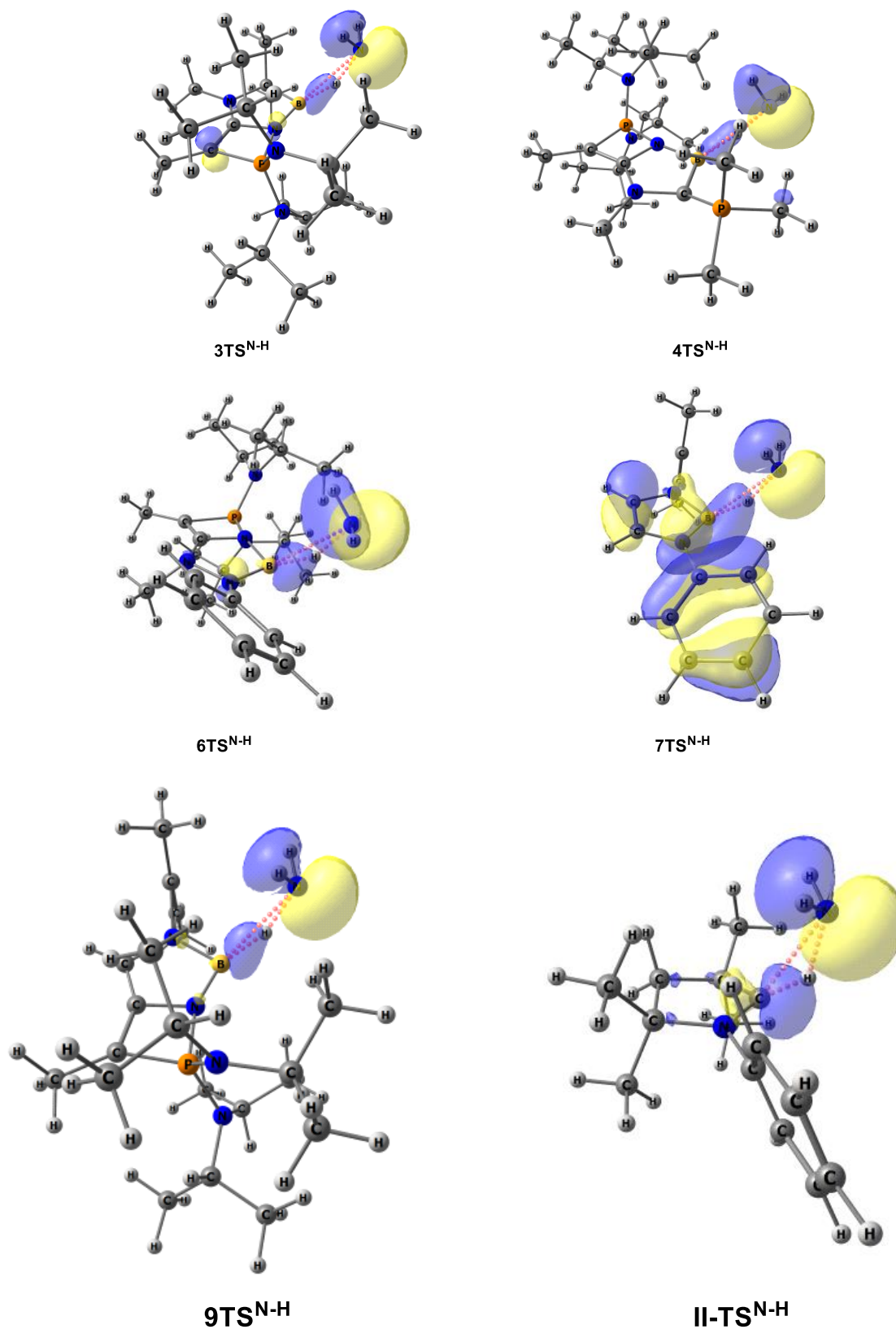
Figure 4.1.8: Pictorial representation of the molecular orbital showing the orientation of the amino lone pair for the transition states (TS) involved in the activation of NH₃ by **3**, **4**, **6**, **7**, **9** and **II** at M06-D3/def2-TZVP (Toluene) level of theory.

activation process which computes considerably higher $\Delta G°_{TS^{N-H}}^{\ddagger}$ value (30.5 kcal mol^{-1}) than those obtained for **3**, **4**, **6**, **7** and **9**. In fact, the computed barrier height for activation by **4** is less than half that for activation by **II**. In addition, the calculated reaction free energies for **3**, **4**, **6**, **7** and **9** are considerably exergonic (-50.5 to -67.4 kcal mol^{-1}) thus indicating the feasibility of the reaction.

To quantitatively understand the enhanced reactivity of borylenes over the parent cAAC (**II**) towards the ammonia activation reaction, the activation strain model (ASM) of reactivity was applied next. Figure 4.1.9 shows the corresponding activation strain diagrams (ASDs) of the **4 + NH₃** and **II + NH₃** reactions from the initial stages of the process up to the corresponding transition states and projected onto the N···H bond-breaking distance. From data in Figure 4.1.9, the process involving **4** benefits from a slightly lower destabilizing strain energy (ΔE_{strain}), which indicates that **4** requires less deformation to adopt the geometry of the corresponding transition state than carbene **II**. This is also related to the fact that **4TS^{N-H}** is reached earlier than **IITS^{N-H}** and therefore the reaction **4** + NH₃ requires less deformation. In addition, the interaction between the increasingly deformed reactants (ΔE_{int}) is clearly much stronger for the activation reaction mediated by **4** along the entire reaction coordinate. For instance, at the same consistent N···H bond-breaking distance of *ca.* 1.4 Å, ΔE_{int} = -33.0 kcal mol^{-1} for the **4** +
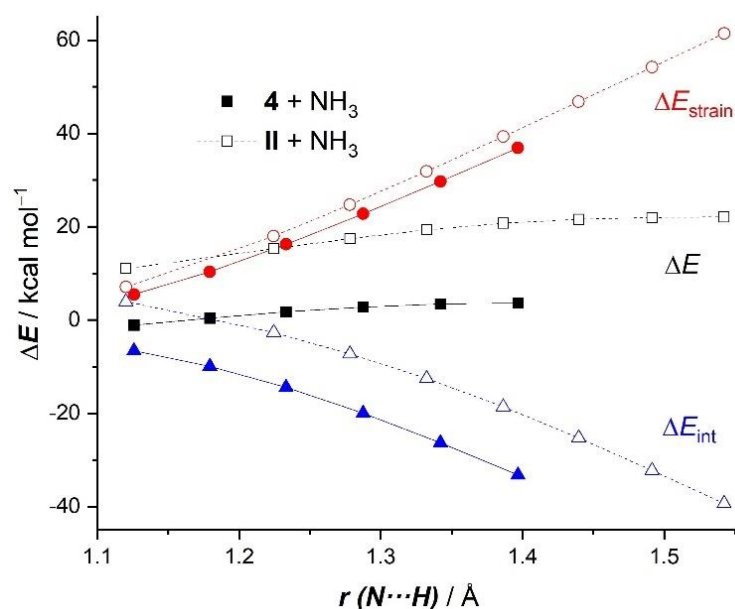

Figure 4.1.9: Comparative activation strain diagrams for the NH₃-activation reactions mediated by **4** (solid lines) and **II** (dotted lines) along the reaction coordinate projected onto the breaking N···H bond distance. All data have been computed at the PCM(toluene)-M06–D3/def2-TZVP level.

NH$_3$ reaction whereas a lower (less stabilizing) value of -19.8 kcal mol^{-1} was computed for the analogous process mediated by **II**. This difference in the interaction energy, $\Delta\Delta E_{int}$ = 13.2 kcal mol^{-1}, roughly matches the difference in the total energy, $\Delta\Delta E$ = 17.2 kcal mol^{-1}. Therefore, the predicted enhanced reactivity of borylenes with respect to cAAC (**II)** in their ammonia activation reactions finds its origin mainly in the enhanced interaction between the reactants and, albeit to a much lesser extent, in a less destabilizing deformation energy. A rather similar ASDs were found for the dihydrogen activation reactions mediated by **4** and **II** (Figure 4.1.10), thus confirming the key role of the interaction between the reactants on the enhanced reactivity of borylenes.

The Energy Decomposition Analysis (EDA) method was used next to understand the factors leading to the stronger ΔE_{int} for the transformation involving **4**. Initially, this can be ascribed to the higher nucleophilicity of the LP(B) as compared to LP(C) (see above). However, our EDA calculations (see Figure 4.1.11 for the evolution of the EDA terms along the reaction coordinate) indicate that the total orbital interactions, ΔE_{orb} (which are dominated by the LP(B/C)→σ*(N-H)) are stronger for the process involving the cAAC (**II**). In addition, the latter process also benefits from stronger electrostatic attractions (ΔV_{elstat}), which suggests that none of these attractive interactions are at all responsible for the higher interaction computed for the reaction involving **4**. At variance,
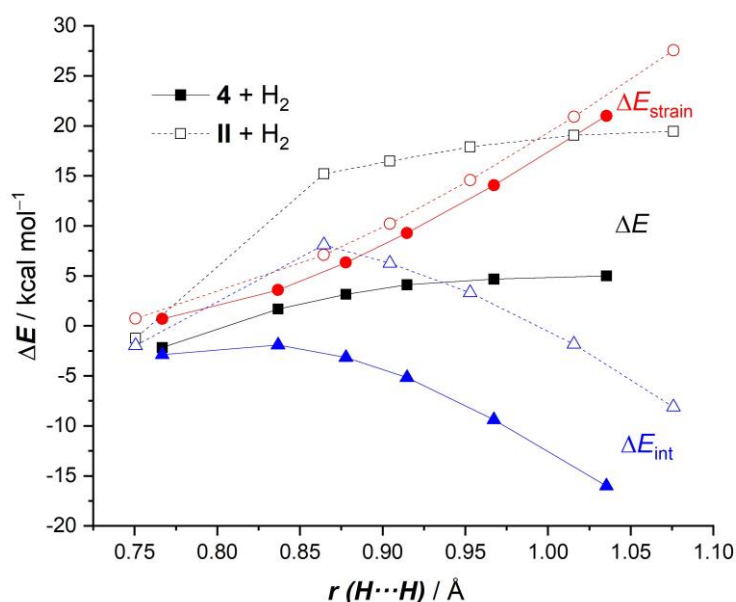

Figure **4.1.10**: Comparative activation strain diagrams for the H$_2$-activation reactions mediated by **4** (solid lines) and **II** (dotted lines) along the reaction coordinate projected onto the breaking H···H bond distance. All data have been computed at the PCM(toluene)-M06–D3/def2-TZVP level.
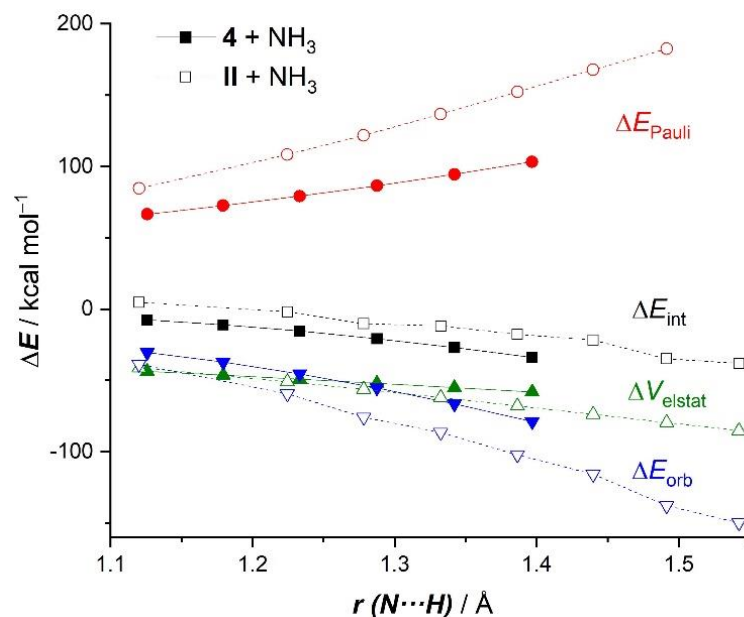
Figure 4.1.11: Comparative energy decomposition analysis for the NH_3-activation reactions mediated by **4** (solid lines) and **II** (dotted lines) along the reaction coordinate projected onto the breaking N···H bond distance. All data have been computed at the ZORA-M06/TZ2P//PCM(toluene)-M06–D3/def2-TZVP level.

the borylene-mediated reaction benefits from a much less destabilizing Pauli repulsion (ΔE_{Pauli}), which efficiently offsets the less favourable orbital and electrostatic attractions and leads to the observed stronger interaction.

The origin of the lower (i.e. less destabilizing) Pauli repulsion in the **4** + NH_3 reaction was investigated by performing a Kohn–Sham molecular orbital (KS-MO) analysis. It is found that the computed reduction in the Pauli repulsion results from a less destabilizing four-electron interaction involving the LP(B) and the key doubly-occupied σ(N-H) molecular orbital as compared to the same interaction involving the LP(C) of the carbene **II**. This is reflected in a significant reduction in the overlap involving these orbitals: at the same consistent N···H bond-breaking distance of *ca.* 1.4 Å, the computed <LP(B)|σ(N-H)> overlap for the reaction involving **4** is lower ($S = 0.32$) than that (<LP(C)|σ(N-H)>) for the analogous NH_3-activation involving **II** ($S = 0.34$). A similar reduction in the overlap was computed for the analogous four-electron interaction involving the adjacent (i.e. not activated) N-H bond ($S = 0.11$ vs $S = 0.15$, for the reactions involving **4** and **II**, respectively). This result resembles that reported for different cycloaddition reactions where, despite exhibiting favourable HOMO(donor)-

LUMO(acceptor) interactions, are controlled by a significant reduction of the involved Pauli repulsion, which is also reflected in a lower overlap [62].

A closer inspection of the data gathered in Table 4.1.5 indicates that the barrier for the activation of NH_3 mediated by **3** is kinetically more difficult ($\Delta G^\circ{}_{TS}^{N-H\ddagger}$ = 16.4 kcal mol^{-1}) than the analogous process involving **4** ($\Delta G^\circ{}_{TS}^{N-H\ddagger}$ = 11.9 kcal mol^{-1}). To understand the reasons behind this markedly different reactivity between these strongly related borylenes, we applied once again the ASM of reactivity for the NH_3 activation reactions involving **3** and **4**.

Figure 4.1.12 shows the corresponding ASDs for both transformations from their initial stages up to the corresponding transition states and projected onto the B⋯H bond-forming distance. From the data in Figure 4.1.12, it becomes clear that the reaction involving **3** benefits from a lower strain energy along the entire reaction coordinate. Despite that, the analogous NH_3 activation promoted by **4** proceeds with a lower barrier because the interaction between the deformed reactants is clearly much more stabilizing. This stronger interaction compensates for the more destabilizing ΔE_{strain} term and is therefore solely responsible for the enhanced reactivity of this species as compared to **3** in the NH_3-activation.
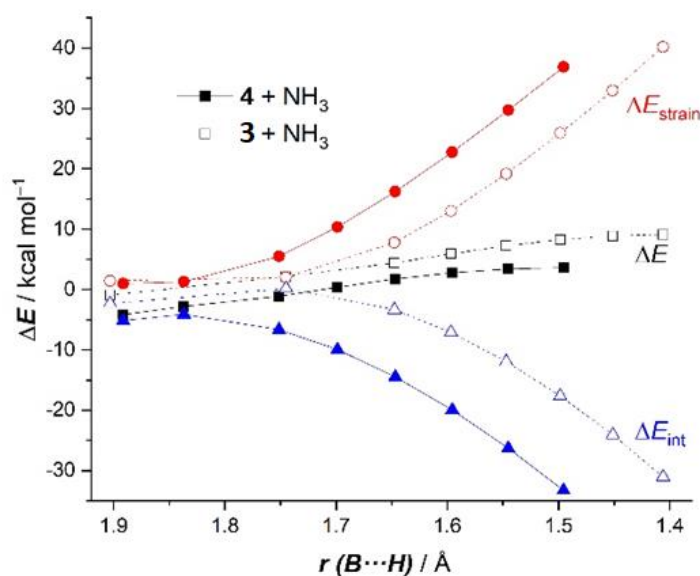

Figure 4.1.12: Comparative activation strain diagrams for the NH_3-activation reactions mediated by **3** (dotted lines) and **4** (solid lines) along the reaction coordinate projected onto the forming B⋯H bond distance. All data have been computed at the PCM(toluene)-M06–D3/def2-TZVP level.

According to the EDA method, the stronger interaction computed for the **4** + NH$_3$ reaction results from stronger electrostatic and orbital interactions along the entire reaction coordinate (Figure 4.1.13). Both attractive terms compensate for the less destabilizing Pauli repulsion computed for the analogous activation reaction involving **3**. For instance, at the same consistent B$\cdots$H bond-forming distance of 1.5 Å, $\Delta\Delta E_{\mathrm{orb}} = 16.1$ kcal mol^{-1} and $\Delta\Delta V_{\mathrm{elstat}} = 9.4$ kcal mol^{-1} favouring the reaction involving **4**, whereas $\Delta\Delta E_{\mathrm{Pauli}} = -9.4$ kcal mol^{-1} favouring the process mediated by **3**, which results in a stronger interaction for former reaction ($\Delta\Delta E_{\mathrm{int}} = 16.1$ kcal mol^{-1}).
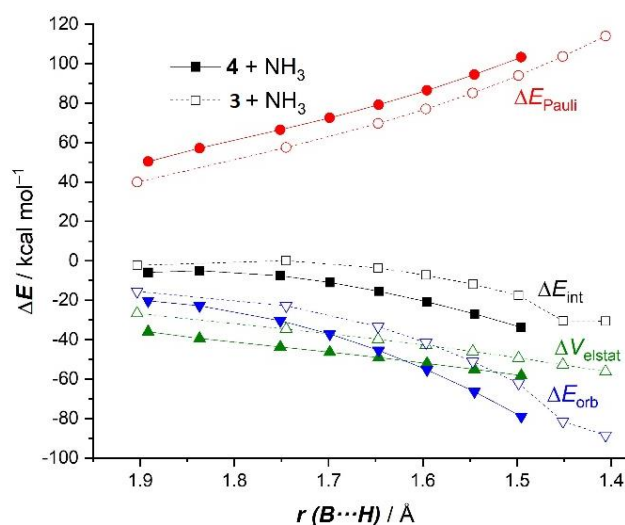

Figure 4.**1**.**13**: Comparative energy decomposition analysis for the NH$_3$-activation reactions mediated by **3** (dotted lines) and **4** (solid lines) along the reaction coordinate projected onto the forming B$\cdots$H bond distance. All data have been computed at the ZORA-M06/TZ2P//PCM(toluene)-M06–D3/def2-TZVP level.

The NOCV extension of the EDA method was applied next to gain further insight into the orbital interactions leading to the stronger ΔE_{orb} computed for the **4** + NH$_3$ reaction. The NOCV identifies the donation from the LP(B) to the σ*(N-H) molecular orbital as the main orbital interaction in the process (Figure 4.1.14). Interestingly, this LP(B)$\rightarrow\sigma$*(N-H) interaction is significantly stronger for the **4** + NH$_3$ reaction than for the analogous reaction involving **3**, which is translated into the computed higher ΔE_{orb} and stronger ΔE_{int}, ultimately leading to the observed lower barrier. For instance, at the same consistent B$\cdots$H bond-forming distance of 1.5 Å, the stabilizing energy associated with this orbital interaction is -57.9 kcal mol^{-1} for the **4** + NH$_3$ reaction, whereas a much lower value of -45.2 kcal mol^{-1} was computed for the **3** + NH$_3$ reaction (Figure 4.1.14).

Therefore, the replacement of the methyl groups in the carbon atom adjacent to the boron atom in borylene **3** by the PMe$_3$ group in **4** further enhances the nucleophilicity of the borylene leading to a stronger LP(B)→σ*(N-H) molecular orbital interaction.

$\Delta E_{orb(1)} = -57.9$ kcal mol^{-1} $\Delta E_{orb(1)} = -45.2$ kcal mol^{-1}
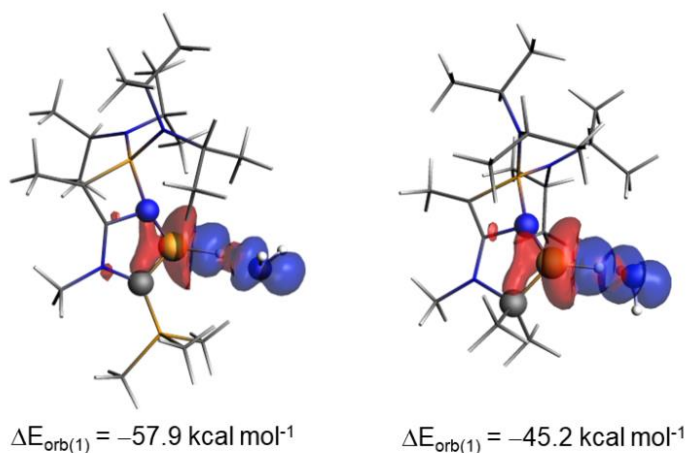
**Figure 4**.**1**.**14**: Plot of the deformation densities of the pairwise orbital interactions in the NH$_3$ activation reactions mediated by **4** (left) and **3** (right), and associated stabilization energies $\Delta E_{orb(1)}$ computed at the same consistent B···H bond-forming distance of 1.5 Å. The color code of the charge flow is red → blue. All data have been computed at the ZORA-M06/TZ2P// PCM(toluene)-M06–D3/def2-TZVP level.

[4.**1**.**3.3] Activation of Methane**

Based on frontier molecular orbital theory (FMO), Bach and coworkers proposed two different approaches viz., σ$_{CH2}$ and π$_{CH2}$ (Scheme 4.1.3) via which a singlet methylene (:CH$_2$) can insert itself across the C–H bond of methane [63]. In the σ$_{CH2}$ approach, the vacant p orbital of the carbene molecule interacts with a filled σ$_{CH2}$ fragment orbital of methane while in the π$_{CH2}$ approach, it interacts with a π-symmetric filled orbital (Scheme 4.1.3). Furthermore, the addition of carbene across the C–H bond
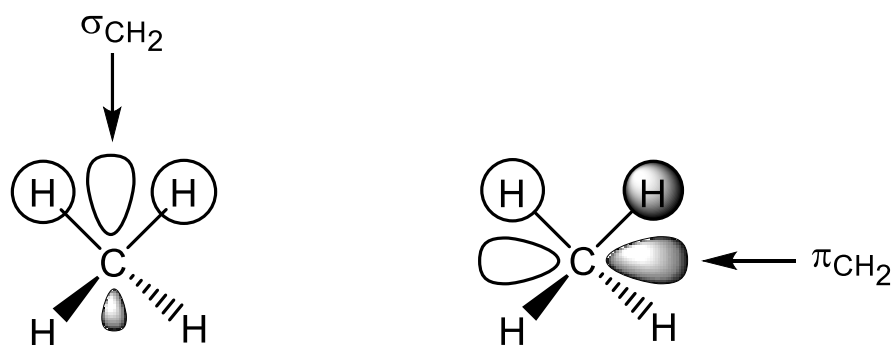
Scheme 4.**1**.**3**: Schematic representation of σ$_{CH2}$ and π$_{CH2}$ mode of carbene insertion into the C–H bond of methane proposed by Bach and coworkers [63].

via π_{CH2} mode may proceed via two different paths as shown in Scheme 4.1.4. Approach **A** represents the carbene insertion via π_{CH2} mode, while approach **B** denotes the inverted π_{CH2}. Bettinger and coworkers employed the same methodology to investigate the addition reaction of acyclic borylenes (:B–R) across the C–H bond of methane [64]. Accordingly, we have considered all the possible approaches while studying the reactivity of **3**, **4**, **6**, **7** and **9** towards the C–H bond activation of methane.
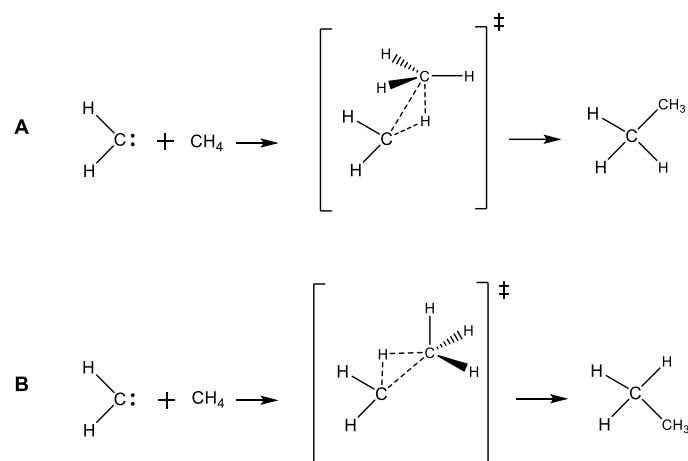
Scheme 4.1.4: Schematic representation of two different π_{CH2} approaches for the carbene insertion into the C–H bond of methane.

The TSs located for the different approaches (σ_{CH2} and inverted π_{CH2}) are shown in Figure 4.1.15 for molecule **3** as a representative example (for others, see Figure 4.1.16 and Figure 4.1.17). The important geometrical parameters for the TSs obtained for **3**, **4**, **6**, **7** and **9** via different approaches are given in Table 4.1.7 and Table 4.1.8. The TSs obtained for **3**, **4**, **6**, **7** and **9** via the σ_{CH2} approach exhibit significantly elongated and polarized C–H bond (1.436–1.624 Å) with the hydrogen atom strongly bonded to the central boron atom (WBI = 0.626–0.729) while the CH_3 fragment remains detached from it (B–CH_3 bond distance = 2.339–2.959 Å, Figure 4.1.15 and Table 4.1.7). However, the calculated WBI values between the central boron atom and the methyl carbon atom (WBI = 0.271–0.538) indicate the presence of considerable bonding interaction between them. The reaction finally gets completed by the eventual migration of the methyl fragment towards the boron atom to yield the desired C–H oxidative addition product. Despite our best efforts, we could not locate the probable TS for pathway **A** but could obtain the same for pathway **B** (Figure 4.1.15 and Figure 4.1.17). Akin to the σ_{CH2} approach, the TS obtained for the inverted π_{CH2} approach exhibits a significantly

elongated and polarized C–H bond (Table 4.1.8). However, the TS involved in the inverted π_{CH_2} approach exhibits a somewhat shorter C–H bond distance than the one obtained for the σ_{CH_2} approach (Table 4.1.7 and Table 4.1.8). Finally, the simultaneous addition of the hydrogen and CH_3 fragment to the central boron atom yields the desired C–H bond splitting product.
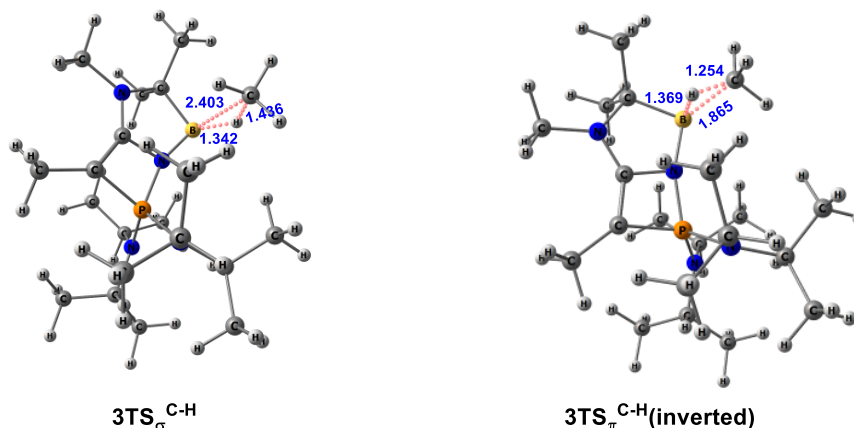

Figure 4.1.15: Optimized geometries of the transition states located for the activation of methane by **3** via σ_{CH_2} and inverted π_{CH_2} approaches (bond lengths are given in Å) at PCM(toluene)-M06-D3/def2-TZVP level.

Table 4.1.7: Calculated (M06-D3/def2-TZVP (Toluene)) important geometrical parameters, natural charges at the carbon atom of the $CH_3^{\delta-}$ fragment, positively polarized hydrogen atom ($H^{\delta+}$) and occupancies of the formally vacant p_π orbital centered at the central E (E = B and C) atom for the transition state involved in the activation of CH_4 by **3**, **4**, **6**, **7**, **9** and **II** via σ_{CH_2} approach. The bond lengths are given in Å. The Wiberg Bond Index values (WBI) are given within parenthesis (X = C and N).

Molecules	$H^{\delta+}$–$H_3C^{\delta-}$	E–$CH_3^{\delta-}$	E–$H^{\delta+}$	$q_{CH_3}^{\delta-}$	$q_H^{\delta+}$	Occ_{p_π}
II-TS^{C-H}	1.557	2.343	1.167	-0.827	0.277	0.832
	(0.224)	(0.518)	(0.674)			
3TS^{C-H}	1.436	2.402	1.342	-0.862	0.112	0.374
	(0.336)	(0.510)	(0.633)			
4TS^{C-H}	1.540	2.959	1.484	-1.062	0.100	0.542
	(0.339)	(0.271)	(0.626)			
6TS^{C-H}	1.624	2.633	1.302	-0.948	0.081	0.448
	(0.239)	(0.460)	(0.729)			
7TS^{C-H}	1.439	2.339	1.319	-0.834	0.116	0.439
	(0.325)	(0.538)	(0.650)			
9TS^{C-H}	1.509	2.482	1.318	-0.894	0.092	0.438
	(0.288)	(0.496)	(0.685)			

3TS$_\sigma^{C-H}$

4TS$_\sigma^{C-H}$

6TS$_\sigma^{C-H}$

7TS$_\sigma^{C-H}$
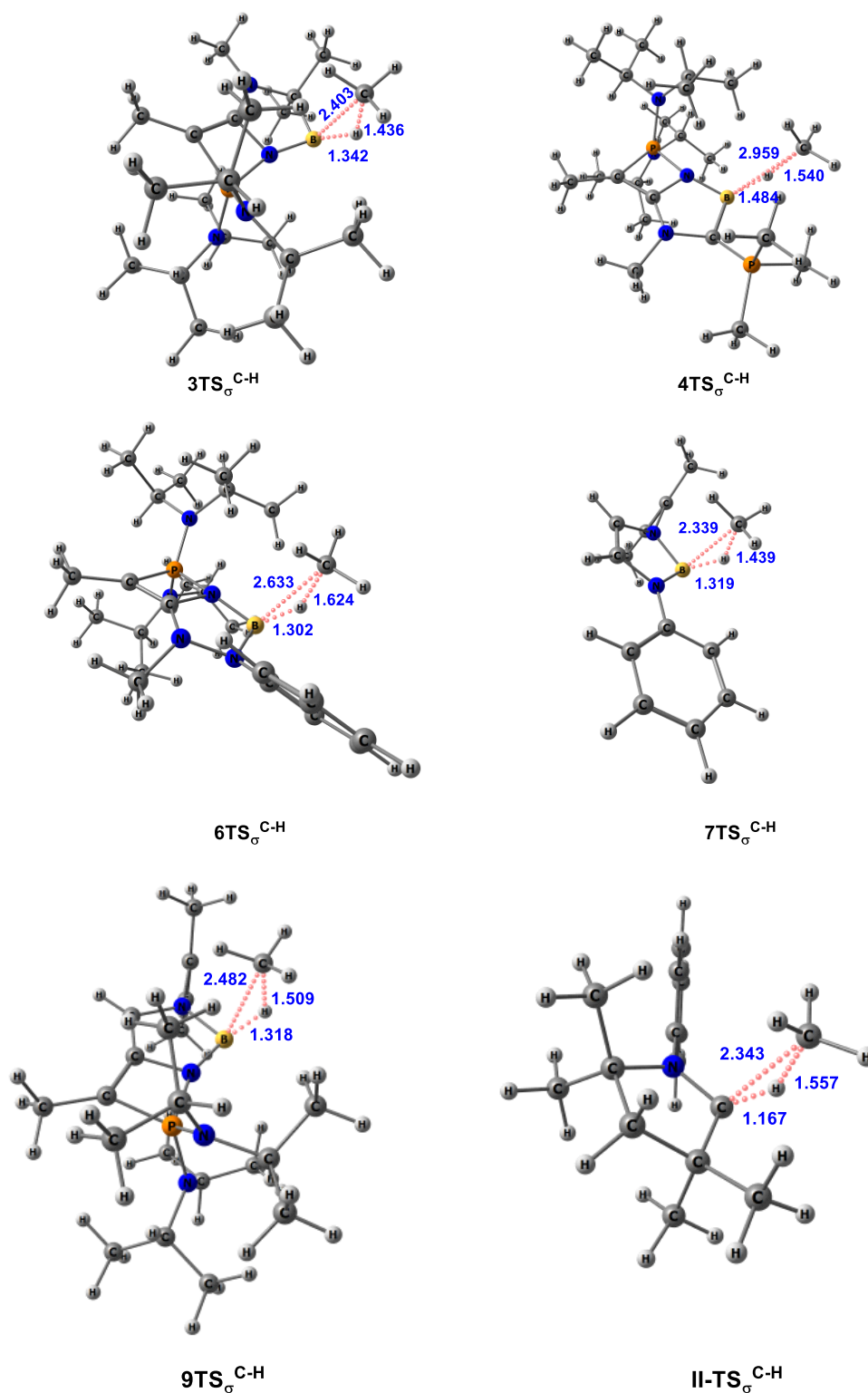
9TS$_\sigma^{C-H}$

II-TS$_\sigma^{C-H}$

Figure 4.1.16: Optimized geometries of the transition states (TS) involved in the activation of C–H bond of CH$_4$ by **3**, **4**, **6**, **7**, **9** and **II** (bond lengths are given in Å) via σ$_{CH_2}$ approach at M06-D3/def2-TZVP (Toluene) level of theory.
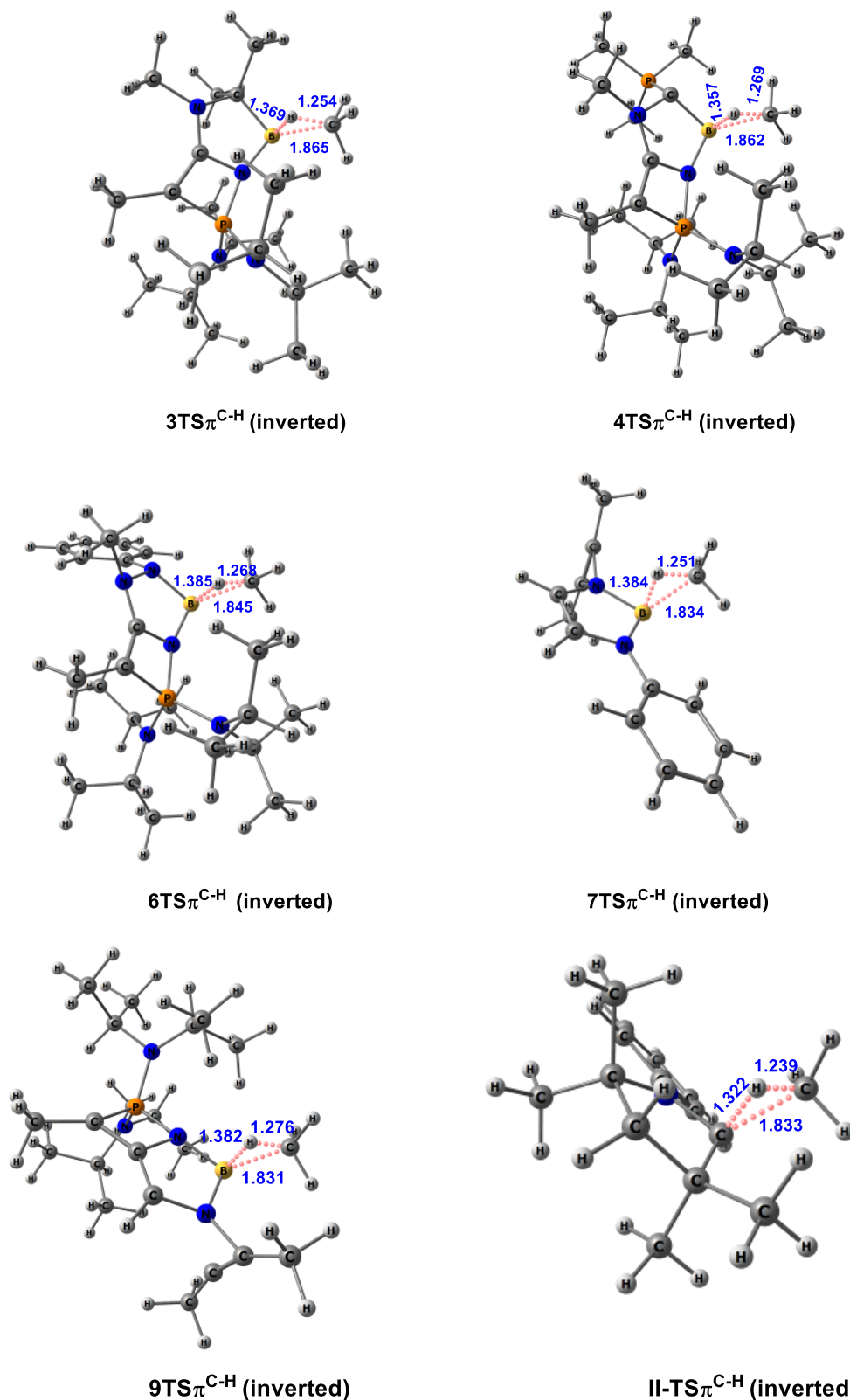
3TSπ^{C-H} (inverted)

4TSπ^{C-H} (inverted)

6TSπ^{C-H} (inverted)

7TSπ^{C-H} (inverted)

9TSπ^{C-H} (inverted)

II-TSπ^{C-H} (inverted)

Figure 4.1.17: Optimized geometries of the transition states (TS) involved in the activation of C–H bond of CH_4 by **3**, **4**, **6**, **7**, **9** and **II** (bond lengths are given in Å) via inverted π_{CH_2} approach at M06-D3/def2-TZVP (Toluene) level of theory.

Table 4.1.8: Calculated (M06-D3/def2-TZVP (Toluene)) important geometrical parameters, natural charges at the carbon atom of the $CH_3^{\delta-}$ fragment, positively polarized hydrogen atom ($H^{\delta+}$) and occupancies of the formally vacant p_π orbital centered at the central E (E = B and C) atom for the transition state involved in the activation of CH_4 by **3**, **4**, **6**, **7**, **9** and **II** via inverted π_{CH_2} approach. The bond lengths are given in Å. The Wiberg Bond Index values (WBI) are given within parenthesis.

Molecules	$H^{\delta+}$–$H_3C^{\delta-}$	E–$CH_3^{\delta-}$	E–$H^{\delta+}$	$q_{CH_3}^{\delta-}$	$q_H^{\delta+}$	Occ_{p_π}
II-TS^{C-H}	1.238	1.833	1.322	-0.649	0.298	0.740
	(0.468)	(0.551)	(0.401)			
3TS^{C-H}	1.254	1.865	1.369	-0.781	0.237	0.637
	(0.582)	(0.582)	(0.403)			
4TS^{C-H}	1.268	1.862	1.357	-0.783	0.257	0.606
	(0.474)	(0.584)	(0.404)			
6TS^{C-H}	1.267	1.844	1.385	-0.779	0.212	0.579
	(0.483)	(0.601)	(0.430)			
7TS^{C-H}	1.251	1.834	1.384	-0.796	0.240	0.488
	(0.501)	(0.604)	(0.397)			
9TS^{C-H}	1.276	1.831	1.382	-0.799	0.233	0.635
	(0.474)	(0.623)	(0.425)			

Furthermore, it should be noted that in the σ_{CH_2} approach, the hydrogen atom of the activated C–H bond can readily move towards the boron center whereas in the inverted π_{CH_2} approach, the migration of the hydrogen atom takes place from the backside of the boronic lone pair [63]. Therefore, a relatively higher barrier height can be anticipated for the inverted π_{CH_2} approach than that of the σ_{CH_2} one. As expected, the barrier heights obtained for activation via the inverted π_{CH_2} approach are computed to be considerably higher (almost two times) compared to the one obtained for σ_{CH_2} approach (Table 4.1.9). Therefore, it can be concluded that all the newly proposed borylenes will favor the σ_{CH_2} approach over the inverted π_{CH_2} one. In addition, the reaction free energies for **3**, **4**, **6**, **7** and **9** are considerably exergonic (-37.2 to -53.5 kcal mol^{-1}) implying the feasibility of the reaction. Further, it is encouraging to note that the barrier heights obtained for **3**, **4**, **6**, **7** and **9** via σ_{CH_2} approach are comparable to that obtained recently for the activation of methane by a carbene-stabilized hydroborenium complex [60]. Similarly, the barrier heights obtained for the newly proposed borylenes via inverted π_{CH_2} approach are found to be comparable to those reported by Bettinger and

coworkers for a series of acyclic borylenes (:B–R) [64]. In addition, the much higher barrier obtained for activation by **II** (40.1 kcal mol^{-1}) is consistent with the lack of methane activation promoted by cAAC.

Table 4.1.9: Calculated activation energy barriers and reaction free energies for the formation of the C–H bond splitting products obtained for **3**, **4**, **6**, **7**, **9** and **II** via σ_{CH2} and inverted π_{CH2} approach at the M06-D3/def2-TZVP (Toluene) level of theory.

Entry	$\Delta G°_{TS\pi_{CH2}}{}^{C\text{-}H\ddagger}$ (inverted)	$\Delta G°_{TS\sigma_{CH2}}{}^{C\text{-}H\ddagger}$	$\Delta G°_{Total}{}^{C\text{-}H}$
3	50.8	29.1	-52.3
4	58.3	28.0	-37.2
6	59.7	31.7	-45.0
7	52.0	29.0	-53.5
9	59.7	29.9	-49.2
II	62.7	40.1	-28.2

The combined ASM-EDA methodology was also applied to rationalize, in a quantitative manner, the strong preference for the σ_{CH2} approach over the alternative π_{CH2} activation. From the data in Figure 4.1.18, the preference for the former approach results almost exclusively from a much stronger interaction between the deformed reactants along the reaction coordinate. This, in turn, derives, according to the EDA method (Figure 4.1.19) exclusively from a much less destabilizing Pauli repulsion and not from the orbital or electrostatic attractions which are stronger for the π_{CH2} activation. Our calculations therefore suggest that the origin of the preferred σ_{CH2} pathway results from a less destabilizing four-electron interaction between the LP(B) of the borylenes and the closest doubly occupied σ(C–H) molecular orbitals of methane. In other words, the steric repulsion is the sole factor controlling the approach of the borylene to the methane molecule.
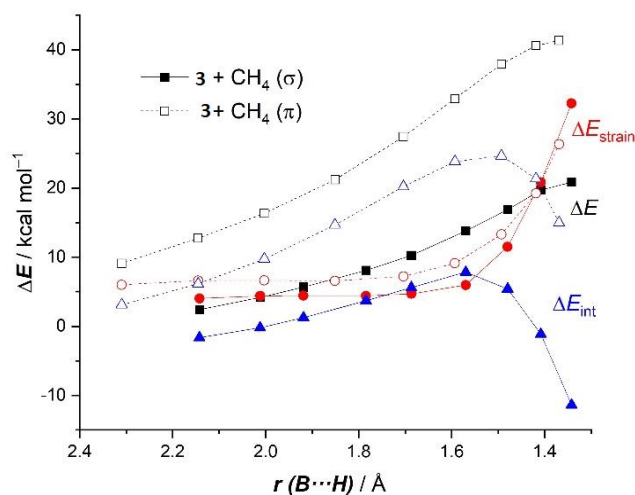
Figure 4.1.18: Comparative activation strain diagrams for the CH_4-activation reactions mediated by **3** in the σ-approach (solid lines) and inverted π-approach (dotted lines) along the reaction coordinate projected onto the forming B···H bond distance. All data have been computed at the PCM(toluene)-M06–D3/def2-TZVP level.

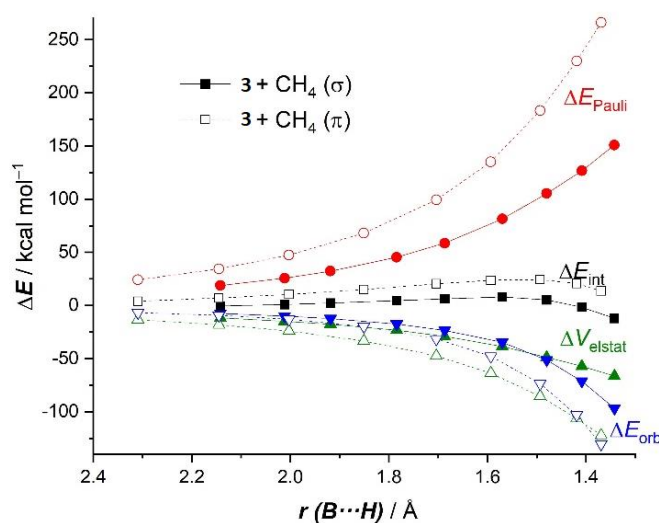**Figure 4.1.19**: Comparative energy decomposition analysis for the CH_4-activation reactions mediated by **3** in the σ-approach (solid lines) and inverted π-approach (dotted lines) along the reaction coordinate projected onto the forming B···H bond distance. All data have been computed at the ZORA-M06/TZ2P//PCM(toluene)-M06–D3/def2-TZVP level.

[4.1.3.4] Activation of Fluorobenzene

Inspired by the ease with which **3**, **4**, **6**, **7** and **9** activate dihydrogen, methane and ammonia, we finally decided to check the ability of these borylenes in the activation of the C–F bond of fluorobenzene. C–F bond activation is one of the most demanding

reaction processes (C–F bond dissociation energy of C_6H_5F is 127.2 kcal mol^{-1}) [56] in materials, agrochemical and pharmaceutical industry [65,66] that often needs drastic reaction conditions or specially designed TM catalysts [67,68]. However, there is precedence in the literature about the use of main group compounds which are capable of activating robust C–F bonds under ambient reaction conditions [11,69]. For example, in a recent study, Nikonov and coworkers reported the facile splitting of the C–F bond for a couple of fluoroarene molecules with the assistance of the NacNac ligand supported Al(I) carbenoid (**IIIa**) [70]. However, **IIIa** was unable to cleave the C–F bond of fluorobenzene even at higher temperatures (100°C). In this context, it is pertinent to mention the recent DFT study by Wang and coworkers who have highlighted the fact that activation of the C–F bond by **IIIa** computes a very high barrier and this could be one of the reasons why **IIIa** failed to activate the C–F bond even under elevated reaction conditions [71].

The mechanism involved in the activation of $C(sp^2)$–F bond by **3**, **4**, **6**, **7** and **9** is similar to that described for the activation of H_2 and NH_3 and hence won't be repeated here. The transitions states (**3TS^{C-F}**, **4TS^{C-F}**, **6TS^{C-F}**, **7TS^{C-F}** and **9TS^{C-F}**) feature the fluorine atom in a bridging position between boron and the C_6H_5 fragment (Figure 4.1.20). The calculated barrier heights lie within 20.0-22.9 kcal mol^{-1} (Table 4.1.5) that should be easily surmounted thermally while **IIIa** computes a relatively higher barrier (29.2 kcal mol^{-1}). Our results indicate that, unlike **IIIa** which could not activate the C–F bond even at higher temperature, **3**, **4**, **6**, **7** and **9** should be able to activate the same under mild conditions. Furthermore, the calculated reaction free energies ($\Delta G°_{Total}^{C-F}$) are computed to be remarkably exergonic (-92.0 to -103.8 kcal mol^{-1}). From the calculated $\Delta G°_{TS}^{C-F\ddagger}$ and $\Delta G°_{Total}^{C-F}$ values, it can be envisioned that the cyclic borylenes proposed in this study may be considered as suitable candidates for the activation of C–F bond.

Furthermore, we have also investigated the possibility of the activation of C–H bonds (*para*, *meta* and *ortho*) of fluorobenzene by employing **3**, **4**, **6**, **7** and **9**. The reaction free energies for the splitting of all three kinds of C–H bonds by **3**, **4**, **6**, **7** and **9** are found to be exergonic thereby indicating the feasibility of the reaction. However, it should be noted that the barrier heights obtained for C–H activation by the proposed borylenes are found to be comparable to that of the C–F bond activation process (Table 4.1.5 and Table 4.1.10). Thus both the C–H and C–F bond activated product may be expected upon reaction of fluorobenzene with **3**, **4**, **6**, **7** and **9**. The optimized geometries
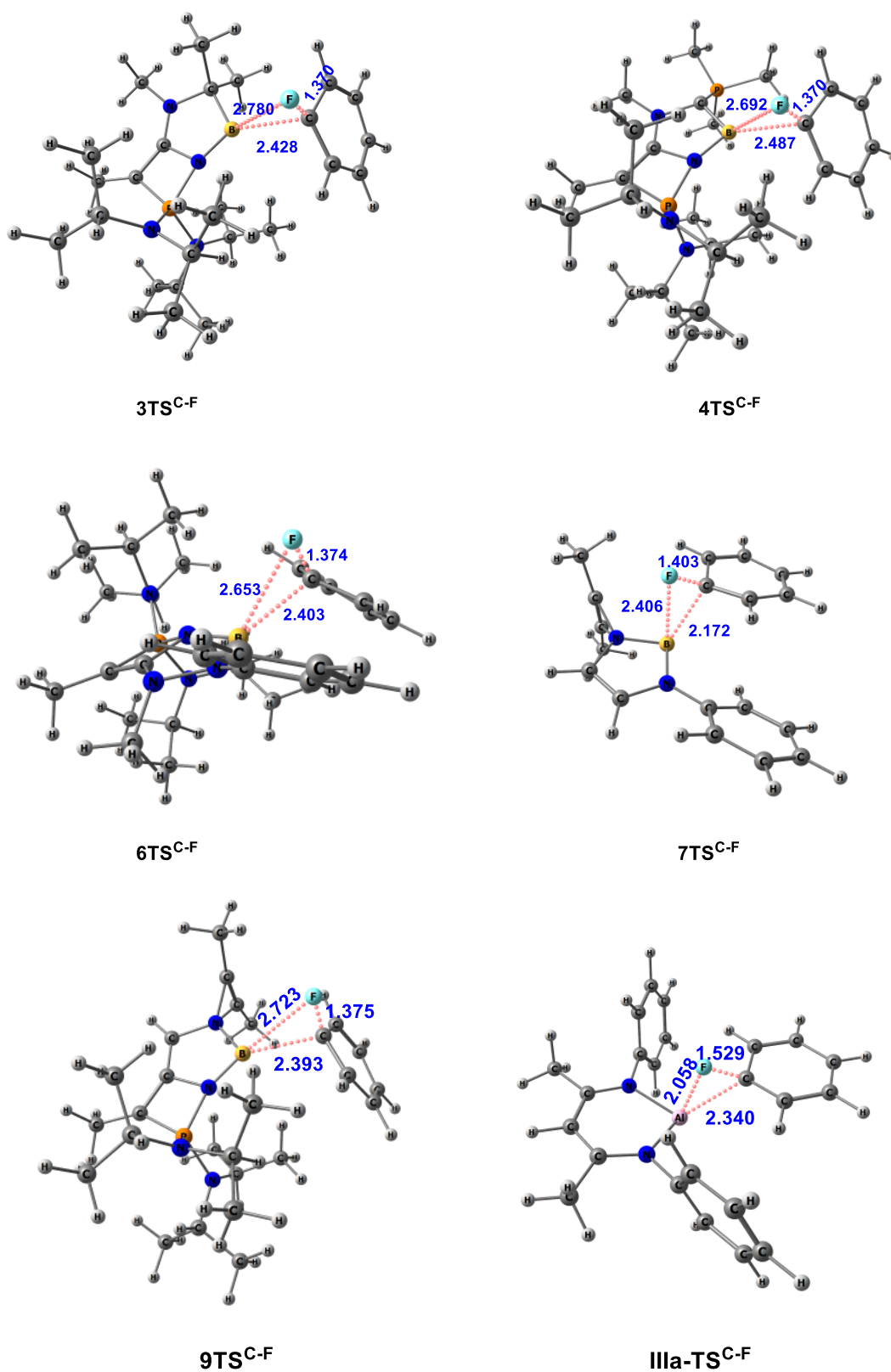
3TS^{C-F}

4TS^{C-F}

6TS^{C-F}

7TS^{C-F}

9TS^{C-F}

IIIa-TS^{C-F}

Figure 4.1.20: Optimized geometries of the transition states (TS) involved in the activation of C–F bond of C_6H_5F by **3**, **4**, **6**, **7**, **9** and **IIIa** (bond lengths are given in Å) at M06-D3/def2-TZVP (Toluene) level of theory.

of all the TS involved in the activation of C–H bond by **3**, **4**, **6**, **7** and **9** are given in Figures 4.1.21–4.1.23.

Table 4.1.10: Calculated (M06-D3/def2-TZVP(toluene)) activation energy barriers and reaction free energies (in kcal mol^{-1}) for the activation of the C–H (*para*, *meta* and *ortho*) bond of C_6H_5F by **3**, **4**, **6**, **7** and **9**.

Molecules	*para*		*meta*		*ortho*	
	$\Delta G°_{TS}{}^{\ddagger}$	$\Delta G°_{Total}$	$\Delta G°_{TS}{}^{\ddagger}$	$\Delta G°_{Total}$	$\Delta G°_{TS}{}^{\ddagger}$	$\Delta G°_{Total}$
3	22.7	-57.7	20.0	-58.6	17.4	-58.0
4	18.3	-48.0	16.6	-48.4	14.7	-48.8
6	25.0	-50.8	22.8	-51.3	20.8	-49.5
7	25.1	-60.1	23.8	-60.7	21.6	-61.0
9	24.8	-54.2	23.5	-55.8	20.6	-54.8

We finally explore the factors behind the observed reactivity trends involving the activation of the different C–H bonds with the help of the ASM approach. To this end, we selected the C–H activation reactions involving borylene **3**. From the computed activation strain values (see Table 4.1.11), it becomes evident that the lower barriers for the activation of the C–H bonds in C_6H_5F as compared to CH_4 mainly result from a much stronger interaction between the deformed reactants despite the activation strain energies being more destabilizing for the reactions involving the aromatic system. The higher reactivity (i.e. lower barrier) of the *ortho*-C–H bonds as compared to the analogous *met*a- and *para*-counterparts finds its origin not only in a slightly higher interaction but mainly in a less destabilizing activation strain.

Table 4.1.11: Computed ASM values (in kcal mol^{-1}) for the C–H activation reactions involving borylene **5**. All data have been computed at the PCM(toluene)-M06-D3/def2-TZVP level.

reaction	$\Delta E^{\ddagger}$	$\Delta E_{strain}{}^{\ddagger}$	$\Delta E_{int}{}^{\ddagger}$
3 + CH₄ (σ)	20.8	32.2	-11.4
3 + C₆H₅F *(ortho)*	8.2	33.6	-25.4
3 + C₆H₅F *(meta)*	12.0	36.3	-24.3
3 + C₆H₅F *(para)*	13.3	37.5	-24.3

3TS$^{p(C-H)}$

4TS$^{p(C-H)}$

6TS$^{p(C-H)}$
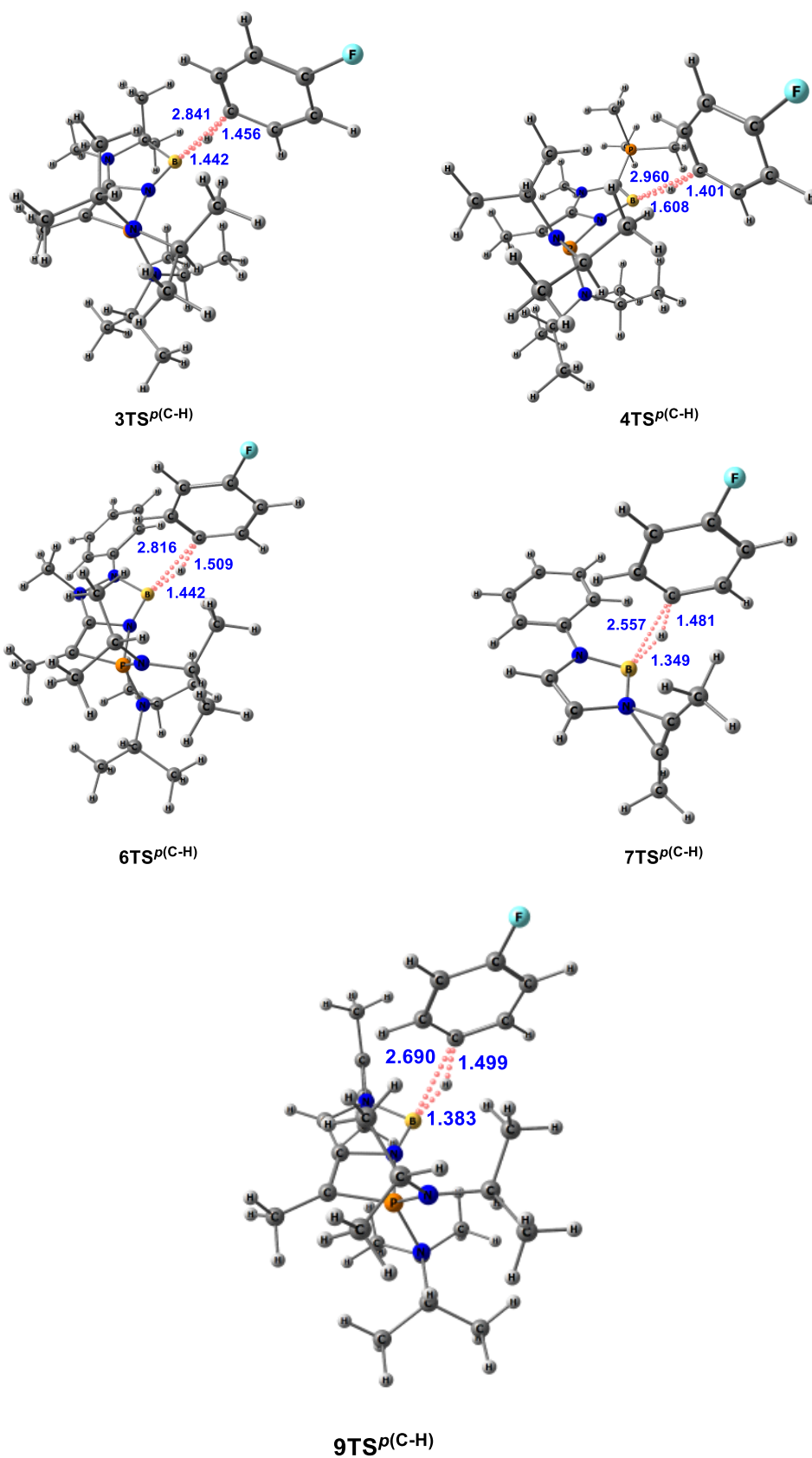

7TS$^{p(C-H)}$

9TS$^{p(C-H)}$

Figure 4.1.21: Optimized geometries of the transition states (TS) involved in the activation of *para* C–H bond of C_6H_5F by **3**, **4**, **6**, **7** and **9** (bond lengths are given in Å) at M06-D3/def2-TZVP (Toluene) level of theory.
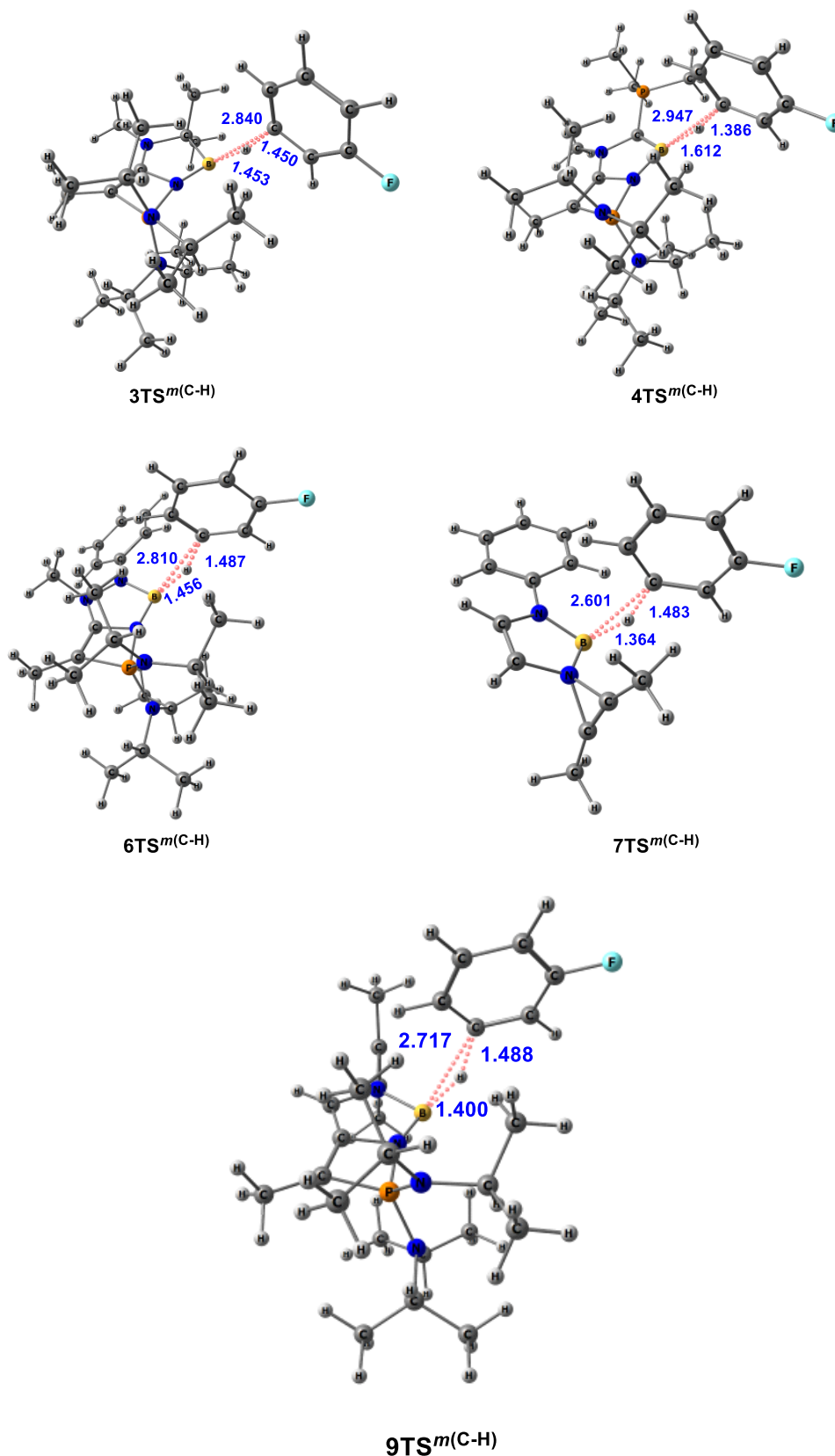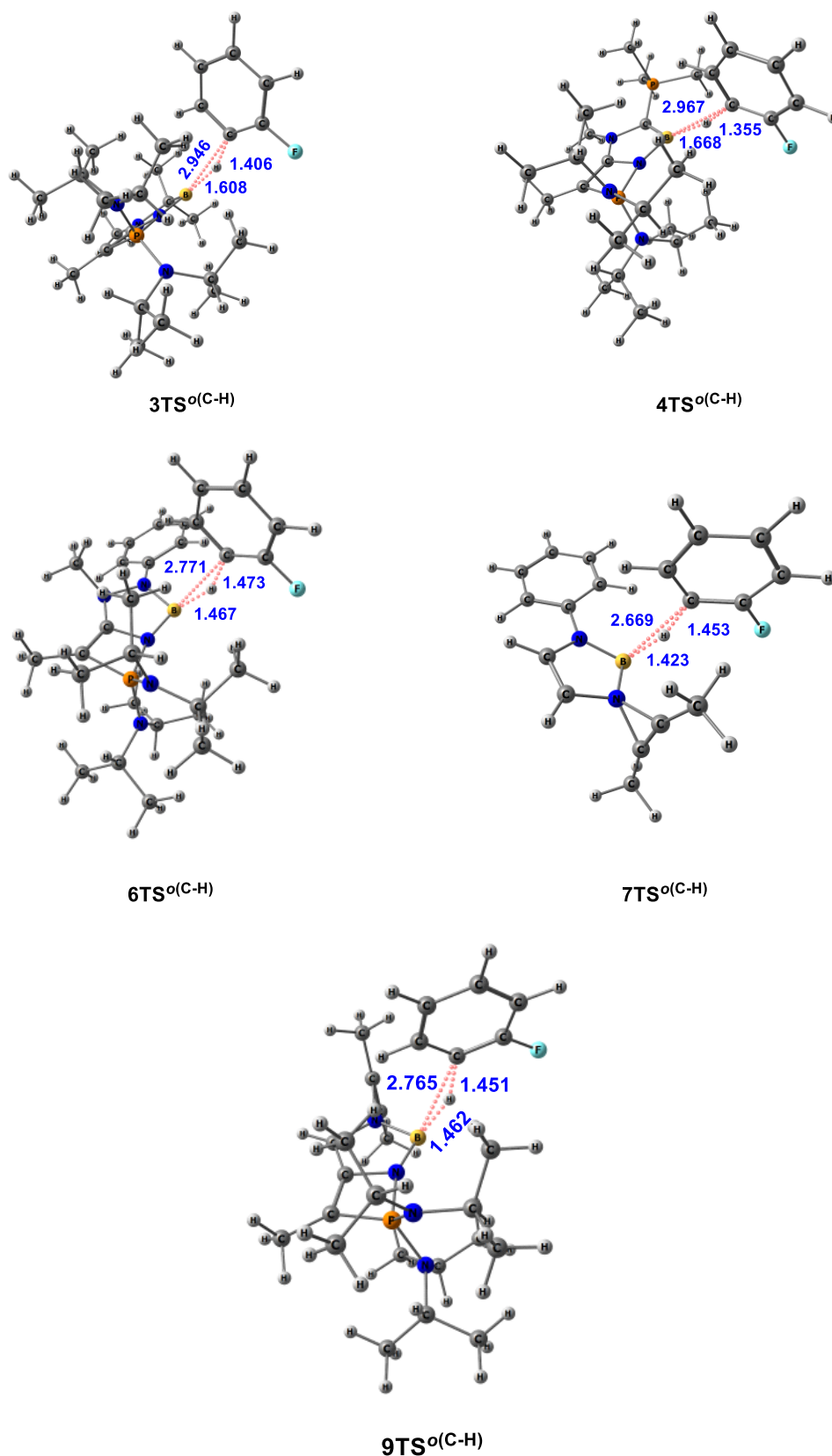
Figure 4.1.22: Optimized geometries of the transition states (TS) involved in the activation of *meta* C–H bond of C_6H_5F by **3**, **4**, **6**, **7** and **9** (bond lengths are given in Å) at M06-D3/def2-TZVP (Toluene) level of theory.

3TS$^{o(C-H)}$

4TS$^{o(C-H)}$

6TS$^{o(C-H)}$

7TS$^{o(C-H)}$

9TS$^{o(C-H)}$

Figure 4.1.23: Optimized geometries of the transition states (TS) involved in the activation of *ortho* C–H bond of C_6H_5F by **3**, **4**, **6**, **7** and **9** (bond lengths are given in Å) at M06-D3/def2-TZVP (Toluene) level of theory.

Further, we have recalculated reaction free energies and barrier heights for some of the representative calculations considered in this study by employing PBE0 and ωB97XD functionals and obtained comparable values to those obtained at M06 level of theory (Table 4.1.12) thereby lending credence to the level of theory used in this study.

Table 4.1.12: Calculated activation energy barriers and reaction free energies (in kcal mol^{-1}) for the formation of the E–H (E = H, N and C) splitting products obtained for **3**, **4**, **6**, **7** with different functionals.

Molecules	M06		PBE0		ωB97XD	
	$\Delta G°_{TS}{}^{\ddagger}$	$\Delta G°_{Total}$	$\Delta G°_{TS}{}^{\ddagger}$	$\Delta G°_{Total}$	$\Delta G°_{TS}{}^{\ddagger}$	$\Delta G°_{Total}$
4 + H₂	14.4	-48.8	11.6	-47.0	14.7	-46.9
7 + H₂	18.1	-61.4	14.5	-62.8	18.8	-60.7
3 + NH₃	16.4	-63.4	14.0	-63.6	15.9	-62.7
7 + NH₃	19.4	-67.4	17.1	-68.1	20.2	-65.8
6 + CH₄	31.7	-45.0	31.8	-44.6	35.6	-44.0
9 + CH₄	29.9	-49.2	29.4	-49.2	33.3	-48.4

[4.1.4] Conclusions

Density functional theory calculations suggest that strongly π-electron donating groups such as amino or ylides may be used for the stabilization of neutral monomeric five-membered boron(I) carbenoids (**1**–**9**, Scheme 4.1.2). It is encouraging to note that the molecules **3**, **4**, **6**, **7** and **9** compute the highest singlet-triplet separation values (ΔE_{S-T} = 25.5–42.3 kcal mol^{-1}) known to date, and to the best of our knowledge, no other cyclic borylenes are known with such large values thus highlighting the remarkable power of ylides in stabilizing unusual species. In addition, the calculated ΔE_{S-T} values are found to be either comparable or higher than that of the synthetically amenable Roesky's Al(I) carbenoid (34.1 kcal mol^{-1}) or cAAC (42.7 kcal mol^{-1}) further providing a hint towards their possible isolation. In addition, **3**, **4**, **6**, **7** and **9** are remarkably nucleophilic and compute considerably lower barrier heights for the activation of E–H (E = H, C and N) and C–F bonds compared to that of the experimentally evaluated systems. According to our ASM-EDA(NOCV) calculations, the enhanced reactivity of the proposed borylenes as compared to the parent cAAC (**II**) finds its origin in a lower Pauli repulsion of the

LP(B) with the key σ-(E–H) molecular orbital ultimately leading to a much stronger interaction between the deformed reactants. Our findings clearly confirm the potential of these proposed cyclic borylenes in small molecule activation and call for sustained synthetic efforts toward their synthesis and isolation.

[4.1.5] Bibliography

[1]   Arduengo III, A. J., Harlow, R. L., and Kline, M. A Stable Crystalline Carbene. *Journal of the American Chemical Society*, 113(1):361-363, 1991.

[2]   Lavallo, V., Canac, Y., Präsang, C., Donnadieu, B., and Bertrand, G. Stable Cyclic (Alkyl)(Amino) Carbenes as Rigid or Flexible, Bulky, Electron-Rich Ligands for Transition-Metal Catalysts: A Quaternary Carbon Atom Makes the Difference. *Angewandte Chemie International Edition*, 44(35):5705-5709, 2005.

[3]   (a) Power, P. P. Main-group elements as transition metals. *Nature*, 463(7278):171-177, 2010; (b) Légaré, M. A., Pranckevicius, C., and Braunschweig, H. Metallomimetic Chemistry of Boron. *Chemical Reviews*, 119(14):8231-8261, 2019.

[4]   Nesterov, V., Reiter, D., Bag, P., Frisch, P., Holzner, R., Porzelt, A., and Inoue, S. NHCs in Main Group Chemistry. *Chemical Reviews*, 118(19):9678-9842, 2018.

[5]   Borthakur, B., Ghosh, B., and Phukan, A. K. The flourishing chemistry of carbene stabilized compounds of group 13 and 14 elements. *Polyhedron*, 197:115049, 2021.

[6]   Doddi, A., Peters, M., and Tamm, M. N-Heterocyclic Carbene Adducts of Main Group Elements and Their Use as Ligands in Transition Metal Chemistry. *Chemical Reviews*, 119(12):6994-7112, 2019.

[7]   Melaimi, M., Jazzar, R., Soleilhavoup, M., and Bertrand, G. Cyclic (Alkyl)(amino) Carbenes (CAACs): Recent Developments. *Angewandte Chemie International Edition*, 56(34):10046-10068, 2017.

[8]   Soleilhavoup, M., and Bertrand, G. Cyclic (Alkyl)(Amino) Carbenes (CAACs): Stable Carbenes on The Rise. *Accounts of Chemical Research*, 48(2):256-266, 2015.

[9]   (a) Frey, G. D., Lavallo, V., Donnadieu, B., Schoeller, W. W., and Bertrand, G. Facile Splitting of Hydrogen and Ammonia by Nucleophilic Activation at a Single Carbon Center. *Science*, 316(5823):439-441, 2007; (b) Devarajan, D., Doubleday, C. E., and Ess, D. H. Theory of Divalent Main Group H_2 Activation: Electronics and Quasiclassical Trajectories. *Inorganic Chemistry*, 52(15):8820-8833, 2013; (c)

Vermeeren, P., Doppert, M. T., Bickelhaupt, F. M., and Hamlin, T. A. How metallylenes activate small molecules. *Chemical Science*, 12(12):4526-4535, 2021; (d) Steinert, H., Löffler, J., and Gessner, V. H. Single-Site and Cooperative Bond Activation Reactions with Ylide-Functionalized Tetrylenes: A Computational Study. *European Journal of Inorganic Chemistry*, 2021(47):5004-5013, 2021; (e) Fujimori, S., and Inoue, S. Small Molecule Activation by Two-Coordinate Acyclic Silylenes. *European Journal of Inorganic Chemistry*, 2020(33):3131-3142, 2022; (f) Rullich, M., Tonner, R., and Frenking, G. P-Heterocyclic carbenes as effective catalysts for the activation of single and multiple bonds. A theoretical study. *New Journal of Chemistry*, 34(8):1760-1773, 2010.

[10]   Martin, D., Soleilhavoup, M., and Bertrand, G. Stable singlet carbenes as mimics for transition metal centers. *Chemical Science*, 2(3):389-399, 2011.

[11]   Chu, T., and Nikonov, G. I. Oxidative Addition and Reductive Elimination at Main-Group Element Centers. *Chemical Reviews*, 118(7):3608-3680, 2018.

[12]   Paul, U. S., and Radius, U. What Wanzlick Did Not Dare To Dream: Cyclic (Alkyl)(amino) carbenes (CAACs) as New Key Players in Transition-Metal Chemistry. *European Journal of Inorganic Chemistry*, 2017(28):3362-3375, 2017.

[13]   Asay, M., Jones, C., and Driess, M. *N*-Heterocyclic Carbene Analogues with Low-Valent Group 13 and Group 14 Elements: Syntheses, Structures, and Reactivities of a New Generation of Multitalented Ligands. *Chemical Reviews*, 111(2):354-396, 2011.

[14]   Cui, C., Roesky, H. W., Schmidt, H. G., Noltemeyer, M., Hao, H., and Cimpoesu, F. Synthesis and Structure of a Monomeric Aluminum(I) Compound [{HC(CMeNAr)$_2$}Al](Ar= 2,6–^{i}Pr$_2$C$_6$H$_3$): A Stable Aluminum Analogue of a Carbene. *Angewandte Chemie International Edition*, 39(23):4274-4276, 2000.

[15]   Hardman, N. J., Eichler, B. E., and Power, P. P. Synthesis and characterization of the monomer Ga{(NDippCMe)$_2$CH}(Dipp=C$_6$H$_3$Pr$^{i}_2$-2,6): a low valent gallium(I) carbene analogue. *Chemical Communications*, (20):1991-1992, 2000.

[16]   Hill, M. S., and Hitchcock, P. B. A mononuclear indium(I) carbene analogue. *Chemical Communications*, (16):1818-1819, 2004.

[17]   Hill, M. S., Hitchcock, P. B., and Pongtavornpinyo, R. Neutral carbene analogues of the heaviest Group 13 elements: Consideration of electronic and steric effects on structure and stability. *Dalton Transactions*, (2):273-277, 2005.

[18]   Chang, M. C., and Otten, E. Reduction of (Formazanate) boron Difluoride Provides Evidence for an *N*-Heterocyclic B(I) Carbenoid Intermediate. *Inorganic Chemistry*, 54(17):8656-8664, 2015.

[19]   (a) Kinjo, R., Donnadieu, B., Celik, M. A., Frenking, G., and Bertrand, G. Synthesis and Characterization of a Neutral Tricoordinate Organoboron Isoelectronic with Amines. *Science*, 333(6042):610-613, 2011; (b) Soleilhavoup, M., and Bertrand, G. Borylenes: an Emerging Class of Compounds. *Angewandte Chemie International Edition*, 56(35):10282-10292, 2017; (c) Légaré, M. A., Bélanger-Chabot, G., Dewhurst, R. D., Welz, E., Krummenacher, I., Engels, B., and Braunschweig, H. Nitrogen Fixation and Reduction at Boron. *Science*, 359(6378):896-900, 2018; (d) Soleilhavoup, M., and Bertrand, G. Stable Carbenes, Nitrenes, Phosphinidenes, and Borylenes: Past and Future. *Chem*, 6(6):1275-1282, 2020; (e) Légaré, M. A., Bélanger-Chabot, G., Rang, M., Dewhurst, R. D., Krummenacher, I., Bertermann, R., and Braunschweig, H. One-pot, room-temperature conversion of dinitrogen to ammonium chloride at a main-group element. *Nature Chemistry*, 12(11):1076-1080, 2020; (f) Kong, L., and Cui, C. Perspective on Organoboron Chemistry. *Synlett*, 32(13):1316-1322, 2021; (g) Dahcheh, F., Martin, D., Stephan, D. W., and Bertrand, G. Synthesis and Reactivity of a CAAC–Aminoborylene Adduct: A Hetero-Allene or an Organoboron Isoelectronic with Singlet Carbenes. *Angewandte Chemie International Edition*, 53(48):13159-13163, 2014; (h) Bissinger, P., Braunschweig, H., Damme, A., Dewhurst, R. D., Kupfer, T., Radacki, K., and Wagner, K. Generation of a Carbene-Stabilized Bora-Borylene and its Insertion into a C–H Bond. *Journal of the American Chemical Society*, 133(47):19044-19047, 2011; (i) Curran, D. P., Boussonnière, A., Geib, S. J., and Lacôte, E. The Parent Borylene: Betwixt and Between. *Angewandte Chemie International Edition*, 51(7):1602-1605, 2012; (j) Arrowsmith, M., Böhnke, J., Braunschweig, H., Gao, H., Légaré, M. A., Paprocki, V., and Seufert, J. Synthesis and Reduction of Sterically Encumbered Mesoionic Carbene-Stabilized Aryldihaloboranes. *Chemistry–A European Journal*, 23(50):12210-12217, 2017; (k) Braunschweig, H., Dewhurst, R. D., Hupp, F., Nutz, M., Radacki, K., Tate, C. W., Vargas, A., and Ye, Q. Multiple complexation of CO and related ligands to a main-group element. *Nature*, 522(7556):327-330, 2015; (l) Pranckevicius, C., Jimenéz-Halla, J. O. C., Kirsch, M., Krummenacher, I., and Braunschweig, H. Complexation and Release of N-Heterocyclic Carbene-Aminoborylene Ligands from Group VI and VIII Metals. *Journal of the American*

Chemical Society, 140(33):10524-10529, 2018; (m) Wang, H., Zhang, J., Lee, H. K., and Xie, Z. Borylene Insertion into Cage B–H Bond: A Route to Electron-Precise B–B Single Bond. *Journal of the American Chemical Society*, 140(11):3888-3891, 2018; (n) Wu, L., Dewhurst, R. D., Braunschweig, H., and Lin, Z. C–C versus C–H Activation: Understanding How the Carbene π-Accepting Ability Controls the Intramolecular Reactivities of Mono (carbene)-Stabilized Borylenes. *Organometallics*, 40(6):766-775, 2021.

[20] Segawa, Y., Yamashita, M., and Nozaki, K. Boryllithium: Isolation, Characterization, and Reactivity as a Boryl Anion. *Science*, 314(5796):113-115, 2006.

[21] Firinci, E., Bates, J. I., Riddlestone, I. M., Phillips, N., and Aldridge, S. Coordinative trapping of the boron β-diketiminato system [B(NMesCMe)$_2$CH] via metal-templated synthesis. *Chemical Communications*, 49(15):1509-1511, 2013.

[22] Bharadwaz, P., and Phukan, A. K. Introducing *N*-Heterocyclic Borylenes: Theoretical Prediction of Stable, Neutral, Monomeric Boron(I) Carbenoids. *Inorganic Chemistry*, 58(9):5428-5432, 2019.

[23] Nakafuji, S. Y., Kobayashi, J., and Kawashima, T. Generation and Coordinating Properties of a Carbene Bearing a Phosphorus Ylide: An Intensely Electron-Donating Ligand. *Angewandte Chemie International Edition*, 47(6):1141-1144, 2008.

[24] Fürstner, A., Alcarazo, M., Radkowski, K., and Lehmann, C. W. Carbenes Stabilized by Ylides: Pushing the Limits. *Angewandte Chemie International Edition*, 47(43):8302-8306, 2008.

[25] Borthakur, B., and Phukan, A. K. Moving toward Ylide-Stabilized Carbenes. *Chemistry–A European Journal*, 21(32):11603-11609, 2015.

[26] Bharadwaz, P., Chetia, P., and Phukan, A. K. Electronic and Ligand Properties of Skeletally Substituted Cyclic(Alkyl)(Amino)Carbenes (CAACs) and Their Reactivity towards Small Molecule Activation: A Theoretical Study. *Chemistry–A European Journal*, 23(41):9926-9936, 2017.

[27] Asay, M., Inoue, S., and Driess, M. Aromatic Ylide-Stabilized Carbocyclic Silylene. *Angewandte Chemie International Edition*, 50(41):9589-9592, 2011.

[28] Alvarado-Beltran, I., Baceiredo, A., Saffon-Merceron, N., Branchadell, V., and Kato, T. Cyclic Amino(Ylide)Silylene: A Stable Heterocyclic Silylene with Strongly Electron-Donating Character. *Angewandte Chemie International Edition*, 55(52):16141-16144, 2016.

[29]   Berthe, J., Garcia, J. M., Ocando, E., Kato, T., Saffon-Merceron, N., De Cózar, A., Cossío, F. P., and Baceiredo, A. Synthesis and Reactivity of a Phosphine-Stabilized Monogermanium Analogue of Alkynes. *Journal of the American Chemical Society*, 133(40):15930-15933, 2011.

[30]   Sarbajna, A., Swamy, V. S. V. S. N., and Gessner, V. H. Phosphorus-ylides: powerful substituents for the stabilization of reactive main group compounds. *Chemical Science*, 12(6):2016-2024, 2021.

[31]   Tejeda, J., Reau, R., Dahan, F., and Bertrand, G. Synthesis and Molecular Structure of a $1,2\lambda^5$-azaphosphete: A Cyclic 4-π-Electron Ylide. *Journal of the American Chemical Society*, 115(17):7880-7881, 1993.

[32]   To reduce the computational cost, the cyclohexyl and Dipp groups attached to the nitrogen atoms of **II** and **IIIa** were replaced with methyl and phenyl groups respectively.

[33]   Zhao, Y., and Truhlar, D. G. The M06 suite of density functionals for main group thermochemistry, thermochemical kinetics, noncovalent interactions, excited states, and transition elements: two new functionals and systematic testing of four M06-class functionals and 12 other functionals. *Theoretical Chemistry Accounts*, 120(1):215-241, 2008.

[34]   Weigend, F., and Ahlrichs, R. Balanced basis sets of split valence, triple zeta valence and quadruple zeta valence quality for H to Rn: Design and assessment of accuracy. *Physical Chemistry Chemical Physics*, 7(18):3297-3305, 2005.

[35]   Weigend, F. Accurate Coulomb-fitting basis sets for H to Rn. *Physical Chemistry Chemical Physics*, 8(9):1057-1065, 2006.

[36]   Grimme, S., Antony, J., Ehrlich, S., and Krieg, H. A consistent and accurate ab initio parametrization of density functional dispersion correction (DFT-D) for the 94 elements H-Pu. *The Journal of Chemical Physics*, 132(15):154104, 2010.

[37]   Cossi, M., Scalmani, G., Rega, N., and Barone, V. New developments in the polarizable continuum model for quantum mechanical and classical calculations on molecules in solution. *The Journal of Chemical Physics*, 117(1):43-54, 2002.

[38]   Glendening, E. D., Reed, A. E., Carpenter, J. E. and Weinhold, F. NBO Program 3.1, W. T. Madison, 1988.

[39]   Reed, A. E., Curtiss, L. A., and Weinhold, F. Intermolecular Interactions from a Natural Bond Orbital, Donor-Acceptor Viewpoint. *Chemical Reviews*, 88(6):899-926, 1988.

[40]   Frisch, M. J., Trucks, G. W., Schlegel, H. B., Scuseria, G. E., Robb, M. A., Cheeseman, J. R., Montgomery, J. A., Jr., Vreven, T., Kudin, K. N., Burant, J. C., Millam, J. M., Iyengar, S. S., Tomasi, J., Barone, V., Mennucci, B., Cossi, M., Scalmani, G., Rega, N., Petersson, G. A., Nakatsuji, H., Hada, M., Ehara, M., Toyota, K., Fukuda, R., Hasegawa, J., Ishida, M., Nakajima, T., Honda, Y., Kitao, O., Nakai, H., Klene, M., Li, X., Knox, J. E., Hratchian, H. P., Cross, J. B., Bakken, V., Adamo, C., Jaramillo, J., Gomperts, R., Stratmann, R. E., Yazyev, O., Austin, A. J., Cammi, R., Pomelli, C., Ochterski, J. W., Ayala, P. Y., Morokuma, K., Voth, G. A., Salvador, P. J., Dannenberg, J., Zakrzewski, V. G., Dapprich, S., Daniels, A. D., Strain, M. C., Farkas, O., Malick, D. K., Rabuck, A. D., Raghavachari, K., Foresman, J. B., Ortiz, J. V., Cui, Q., Baboul, A. G., Clifford, S., Cioslowski, J., Stefanov, B. B., Liu, G., Liashenko, A., Piskorz, P., Komaromi, I., Martin, R. L., Fox, D. J., Keith, T., Al- Laham, M. A., Peng, C. Y., Nanayakkara, A., Challacombe, M., Gill, P. M. W., Johnson, B., Chen, W., Wong, M. W., Gonzalez, C., and Pople, J. A. *Gaussian 03*, *Revision D.02*; Gaussian, Inc., Pittsburgh, PA, 2003.

[41]   Adamo, C., and Barone, V. Toward reliable density functional methods without adjustable parameters: The PBE0 model. *The Journal of Chemical Physics*, 110(13):6158-6170, 1999.

[42]   Chai, J. D., and Head-Gordon, M. Long-range corrected hybrid density functionals with damped atom–atom dispersion corrections. *Physical Chemistry Chemical Physics*, 10(44):6615-6620, 2008.

[43]   Becke, A. D., Density-functional thermochemistry. III. The role of exact exchange, *The Journal of Chemical Physics*, 98(7):5648-5652, 1993.

[44]   Seeger, R., and Pople, J. A. Self-consistent molecular orbital methods. XVIII. Constraints and stability in Hartree–Fock theory. *The Journal of Chemical Physics*, 66(7):3045-3050, 1977.

[45]   Bauernschmitt, R., and Ahlrichs, R. Stability analysis for solutions of the closed shell Kohn–Sham equation. *The Journal of Chemical Physics*, 104(22):9047-9052, 1996.

[46]   (a) Fernández, I., and Bickelhaupt, F. M. The activation strain model and molecular orbital theory: understanding and designing chemical reactions. *Chemical Society Reviews*, 43(14):4953-4967, 2014; (b) Wolters, L. P., and Bickelhaupt, F. M. The activation strain model and molecular orbital theory. *Wiley Interdisciplinary Reviews: Computational Molecular Science*, 5(4):324-343, 2015; (c) Bickelhaupt, F. M., and

Houk, K. N. Analyzing reaction rates with the distortion/interaction-activation strain model. *Angewandte Chemie International Edition*, 56(34):10070-10086, 2017.

[47]   For reviews on the EDA method, see: a) F. M. Bickelhaupt and E. J. Baerends (2000). *Reviews in Computational Chemistry*. In Lipkowitz, K. B.;. Boyd, D. B, editors, volume 15, pages. 1-86, Wiley-VCH: New York; b) Hopffgarten, M. V., and Frenking, G. Energy decomposition analysis. *Wiley Interdisciplinary Reviews: Computational Molecular Science*, 2(1):43-62, 2012; c) Fernández, I. (2018). *Applied Theoretical Organic Chemistry*. In Tantillo, D. J., editor, World Scientific, pages. 191-226, New Jersey.

[48]   Mitoraj, M. P., Michalak, A., and Ziegler, T. A Combined Charge and Energy Decomposition Scheme for Bond Analysis. *Journal of Chemical Theory and Computation*, 5(4):962-975; 2009.

[49]   (a) Te Velde, G. T., Bickelhaupt, F. M., Baerends, E. J., Fonseca Guerra, C., van Gisbergen, S. J., Snijders, J. G., and Ziegler, T. Chemistry with ADF. *Journal of Computational Chemistry*, 22(9):931-967, 2001; (b) *ADF2020*, SCM, Theoretical Chemistry, Vrije Universiteit, Amsterdam, The Netherlands, http://www.scm.com

[50]   Snijders, J. G., Vernooijs, P., and Baerends, E. J. Roothaan-Hartree-Fock-Slater atomic wave functions: single-zeta, double-zeta, and extended Slater-type basis sets for $_{87}$Fr-$_{103}$Lr. *Atomic Data and Nuclear Data Tables*, 26(6):483-509, 1981.

[51]   Krijn, J., and Baerends, E. J. Fit Functions in the HFS-Method: Internal Report. *Vrije Universiteit: Amsterdam, The Netherlands*, 1984.

[52]   (a) Lenthe, E. V., Baerends, E. J., and Snijders, J. G. Relativistic regular two-component Hamiltonians. *The Journal of Chemical Physics*, 99(6):4597-4610, 1993; (b) van Lenthe, E., Baerends, E. J., and Snijders, J. G. Relativistic total energy using regular approximations. *The Journal of Chemical Physics*, 101(11):9783-9792, 1994; (c) Van Lenthe, E., Ehlers, A., and Baerends, E. J. Geometry optimizations in the zero order regular approximation for relativistic effects. *The Journal of Chemical Physics*, 110(18):8943-8953, 1999.

[53]   Brazier, C. R. Emission spectroscopy of the triplet system of the BH radical. *Journal of Molecular Spectroscopy*, 177(1):90-105, 1996.

[54]   Kubas G. J. (2001). *Metal Dihydrogen and σ-Bond Complexes: Structure, Theory, and Reactivity*; Springer US: New York City, NY.

[55]   R. Mas-Ballesté and A. Lledós (2013). In Editor Poeppelmeier, K., H−H Bond Activation. *Comprehensive Inorganic Chemistry II*, Elsevier: Amsterdam,; Volume 9, pages 727−766.

[56]   Blanksby, S. J., and Ellison, G. B. Bond Dissociation Energies of Organic Molecules. *Accounts of Chemical Research*, 36(4):255-263, 2003.

[57]   (a) Labinger, J. A., and Bercaw, J. E. Understanding and exploiting C–H bond activation. *Nature*, 417(6888):507-514, 2002; (b) Cook, A. K., Schimler, S. D., Matzger, A. J., and Sanford, M. S. Catalyst-controlled selectivity in the C–H borylation of methane and ethane. *Science*, 351(6280):1421-1424, 2016; (c) Smith, K. T., Berritt, S., González-Moreiras, M., Ahn, S., Smith III, M. R., Baik, M. H., and Mindiola, D. J. Catalytic borylation of methane. *Science*, 351(6280):1424-1427, 2016.

[58]   Chu, T., Korobkov, I., and Nikonov, G. I. Oxidative Addition of σ Bonds to an Al(I) Center. *Journal of the American Chemical Society*, 136(25):9195-9202, 2014.

[59]   (a) Seifert, A., Scheid, D., Linti, G., and Zessin, T. Oxidative Addition Reactions of Element–Hydrogen Bonds with Different Polarities to a Gallium(I) Compound. *Chemistry–A European Journal*, 15(44):12114-12120, 2009; (b) Kötting, C., and Sander, W. Insertion of Difluorovinylidene into Hydrogen and Methane. *Journal of the American Chemical Society*, 121(38):8891-8897, 1999; (c) Filthaus, M., Schwertmann, L., Neuhaus, P., Seidel, R. W., Oppel, I. M., and Bettinger, H. F. C–H Bond Amination by Photochemically Generated Transient Borylnitrenes at Room Temperature: A Combined Experimental and Theoretical Investigation of the Insertion Mechanism and Influence of Substituents. *Organometallics*, 31(10):3894-3903, 2012; (d) Bettinger, H. F., Filthaus, M., and Neuhaus, P. Insertion into dihydrogen employing the nitrogen centre of a borylnitrene. *Chemical Communications*, (16):2186-2188, 2009.

[60]   Liu, Y., Dong, W., Li, Z. H., and Wang, H. Methane activation by a borenium complex. *Chem*, 7(7):1843-1851, 2021.

[61]   van der Vlugt, J. I. Advances in selective activation and application of ammonia in homogeneous catalysis. *Chemical Society Reviews*, 39(6):2302-2322, 2010.

[62]   (a) Hamlin, T. A., Fernández, I., and Bickelhaupt, F. M. How Dihalogens Catalyze Michael Addition Reactions. *Angewandte Chemie International Edition*, 58(26):8922-8926, 2019; (b) Vermeeren, P., Hamlin, T. A., Fernández, I., and Bickelhaupt, F. M. How Lewis Acids Catalyze Diels–Alder Reactions. *Angewandte Chemie International Edition*, 59(15): 6201-6206, 2020; (c) Fernández, I. Understanding

the reactivity of polycyclic aromatic hydrocarbons and related compounds. *Chemical Science*, 11(15):3769-3779, 2020; (d) Hamlin, T. A., Bickelhaupt, F. M., and Fernández, I. The Pauli Repulsion-Lowering Concept in Catalysis. *Accounts of Chemical Research*, 54(8):1972-1981, 2021.

[63]   Bach, R. D., Su, M. D., Aldabbagh, E., Andres, J. L., and Schlegel, H. B. A Theoretical Model for the Orientation of Carbene Insertion into Saturated Hydrocarbons and the Origin of the Activation Barrier. *Journal of the American Chemical Society*, 115(22):10237-10246, 1993.

[64]   Krasowska, M., and Bettinger, H. F. Reactivity of Borylenes toward Ethyne, Ethene, and Methane. *Journal of the American Chemical Society*, 134(41):17094-17103, 2012.

[65]   Ameduri, B.; Sawada, H. (2016). *Fluorinated Polymers: Synthesis, Properties, Processing and Simulation*. Volume 1, Royal Society of Chemistry.

[66]   O'Hagan, D. Fluorine in health care: Organofluorine containing blockbuster drugs. *Journal of Fluorine Chemistry*, 131(11):1071-1081, 2010.

[67]   Kuehnel, M. F., Lentz, D., and Braun, T. Synthesis of Fluorinated Building Blocks by Transition-Metal-Mediated Hydrodefluorination Reactions. *Angewandte Chemie International Edition*, 52(12):3328-3348, 2013.

[68]   Amii, H., and Uneyama, K. C−F Bond Activation in Organic Synthesis. *Chemical Reviews*, 109(5):2119-2183, 2009.

[69]   (a) Mandal, D., Gupta, R., and Young, R. D. Selective Monodefluorination and Wittig Functionalization of Gem-Difluoromethyl Groups to Generate Monofluoroalkenes. *Journal of the American Chemical Society*, 140(34):10682-10686, 2018; (b) Mandal, D., Gupta, R., Jaiswal, A. K., and Young, R. D. Frustrated Lewis-Pair-meditated Selective Single Fluoride Substitution in Trifluoromethyl Groups. *Journal of the American Chemical Society*, 142(5):2572-2578, 2020; (c) Cabrera-Trujillo, J. J., and Fernández, I. Understanding the C−F Bond Activation Mediated by Frustrated Lewis Pairs: Crucial Role of Non-covalent Interactions. *Chemistry–A European Journal*, 27(11):3823-3831, 2021.

[70]   Chu, T., Boyko, Y., Korobkov, I., and Nikonov, G. I. Transition Metal-Like Oxidative Addition of C–F and C–O Bonds to an Aluminum(I) center. *Organometallics*, 34(22):5363-5365, 2015.

[71]   Pitsch, C. E., and Wang, X. Aluminum(I) β-diketiminato complexes activate $C(sp^2)$–F and $C(sp^3)$–F bonds by different oxidative addition mechanisms: a DFT study. *Chemical Communications*, 53(58):8196-8198, 2017.

[4.2] Unravelling the Potential of Ylides in Stabilizing Low-Valent Group 13 Compounds: Theoretical Predictions of Stable, Five-membered Group 13 (Al and Ga) Carbenoids Capable of Small Molecule Activation

[4.2.1] Introduction

The synthesis of a "bottleable" singlet cyclic carbene (NHC) [1] and its unmatched potential in several chemical process such as stabilization of highly reactive molecules [2-3], olefin metathesis [4-5] and other catalytic process [6-10] has inspired the synthesis of other potent carbenes such as cyclic(alkyl)(amino)carbene (cAAC) [11] and diamido carbene (DAC) [12]–to name a few. It may be worthwhile to mention that prior to the advent of such strongly nucleophilic and ambiphilic carbenes, it was the transition metal-based systems that enjoyed the monopoly in small molecule activation. While Lewis basic group 14 compounds had already made their mark in coordination and main group chemistry, similar group 13 compounds are yet to achieve that kind of a feat because of the difficulties associated with the isolation of these compounds in low oxidation state (i.e. +1) [13]. The two most celebrated examples of experimentally characterized group 13 carbenoids are [{HC(CMeNAr)$_2$}Al] [14] (**I**, Scheme 4.2.1) and [{HC(CMeNAr)$_2$}Ga] [15] (**II**, Ar = 2,6–^{i}Pr$_2$C$_6$H$_3$) and they are found to be capable of performing various chemical reactions. For example, Nikonov et al. experimentally studied the activation of H–X (X = H, B, C, N, O, Al, P, Si) bonds [16] by **I** while Crimmin et al. reported the reaction of **I** with a series of cyclic and acyclic 1,2-, 1,3- and 1,5-dienes [17]. Furthermore, the heavier analogs of **I** and **II** are also known (**III** and **IV**) [18-19].

Even though it is well established by now that both **I** and **II** are promising ligands for challenging bond cleavage and small molecule activation [16, 20-23], **I** suffers from low yield and reproducibility [24] and hence, it is of interest to develop new robust Al(I) systems. In this regard, seminal contributions came from the group of Inoue with the isolation of the first neutral Al(I) compound containing an Al=Al double bond (dialumene **V**, Scheme 4.2.1) that could fix CO$_2$ as well as undergo cycloaddition reactions with ethylene and phenyl acetylene [25]. In addition, significant advances have been made in the recent years with the isolation of several nucleophilic aluminyl anions [26-34]. In 2018, Aldridge and Goicoechea et al. reported the first isolation of a nucleophilic aluminyl anion ([K{Al(NON)}]$_2$, **VI**) by employing a chelating ligand (NON = 4,5-bis(2,6-diisopropylanilido)-2,7-di-tertbutyl-9,9-dimethylxanthene) [26]. The same group succeeded in isolating a monomeric charge-separated version of **VI** in the
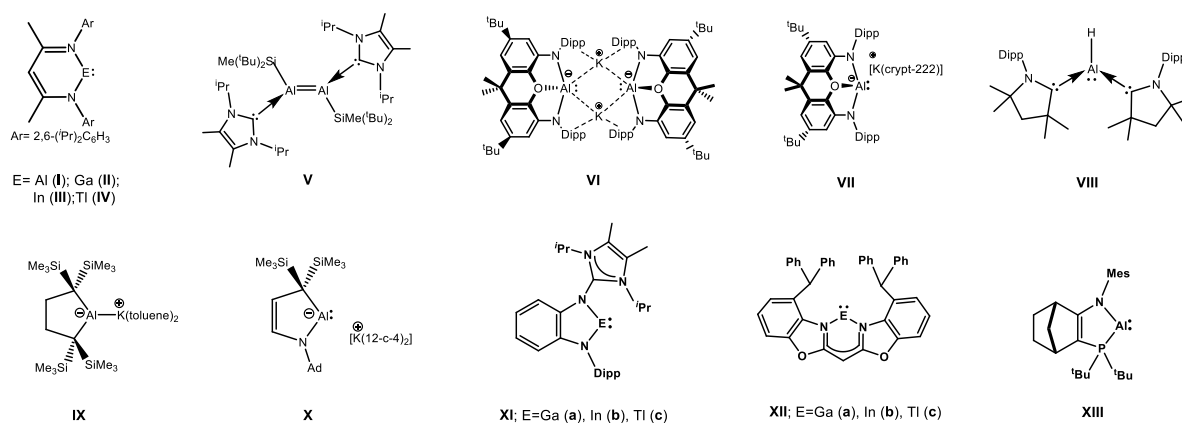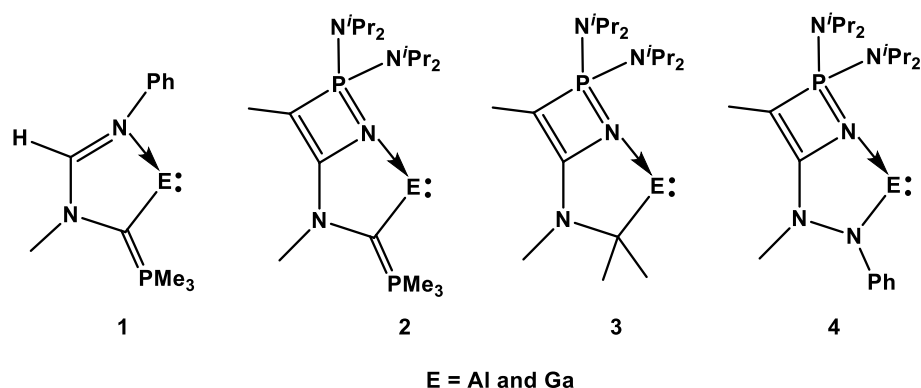
Scheme 4.2.1: Schematic representation of experimentally known group 13 compounds discussed in this study.

following year (**VII**, Scheme 4.2.1) [27]. Another significant contribution came from the group of Braunschweig who reported the isolation of a monomeric Lewis base stabilized Al(I) hydride (**VIII**)- the ground state of which has a non-negligible contribution from Al(III) singlet diradical character [35]. Despite being nucleophilic, the reaction of **VIII** with molecules such as CO, CO_2 and H_2 led to a variety of decomposition products. Very recently, Yamashita's group reported an alkyl substituted aluminium anion (**IX**) that exhibits very strong basicity and nucleophilicity [36]. **IX** was found to undergo [1+2] and [1+4] cycloaddition reactions with unsaturated hydrocarbons and could activate C−F bonds of hexafluorobenzene [37]. Moving a step forward, Kinjo and co-workers succeeded in isolating a bottleable cyclic(alkyl)(amino) alumanyl anion (cAAAl, **X**) that may be considered as an aluminium analogue of cAAC [38]. Similar to cAAC, the Al(I) center of **X** readily cleaves both polar and nonpolar bonds under very mild conditions.

In a recent study, Frank and coworkers used an amino imidazoline-2-imine (HAmIm) framework to stabilize the first neutral five-membered E(I) carbenoids (E = Ga, In and Tl, **XI**). However, attempts to isolate the corresponding Al complex has led to an unexpected Al(III) insertion product [39]. Stalke and coworkers further enriched the library of this class of compounds by isolating a number of neutral six-membered heavier group 13 bases (**XII**) via salt metathesis reactions [40]. More recently, Cowley and coworkers successfully trapped a transient monomeric five-membered aluminyl (**XIII**) (that exist in equilibrium with its dimeric form in solution) by reacting its dimer with Me₃SiC≡CSiMe₃ [41].

Among all the group 13 carbenoids, the Al(I) carbenoid is of special interest due to high abundance, low cost and less toxicity of aluminium. However, the synthesis and isolation of a stable, neutral five–membered aluminium(I) carbenoid remains a tantalizing goal. Compared to the extensive range of carbenes (and their heavier analogs) that are known experimentally – both in terms of structure and reactivity [2-3, 13, 42], the number and variety of stable group 13 carbenoids are very limited and this calls for an in-depth study towards the design and development of novel stable group 13 carbenoids and probing their potential in stabilizing unusual species as well as in reactions such as small molecule activation. In this context, it is pertinent to mention the role of ylidic groups in enhancing the singlet state stability and nucleophilicity of divalent group 14 bases [43-50]. Recently, we have computationally shown that ylidic groups could be used as building blocks for the stabilization of hitherto unknown boron(I) carbenoids [51]. Herein, we present the results of our computational studies towards stabilizing monovalent five-membered group 13 carbenoids (Scheme 4.2.2, E =Al and Ga) by employing strongly electron donating ylidic moieties.

E = Al and Ga

Scheme 4.**2**.**2**: Schematic representation of the group 13 carbenoids considered in this study.

[4.2.2] Computational Details

Density functional theory calculations have been carried out to optimize all the molecules without any geometrical constraints by employing meta-GGA M06 exchange-correlation functional [52] in combination with valence polarized def2-TZVP basis set for all the elements [53-54]. Frequency calculations were carried out at the same level of theory to check the nature of the stationary points. All the molecules were found to be minima with real vibrational frequencies. The transition states were characterized by

only one imaginary frequency which was further confirmed by performing the intrinsic reaction coordinate (IRC) calculations at the same level of theory. The activation energy barriers for all the reaction processes were evaluated with respect to the sum of the energies of the separated reactants. Dispersion effects were incorporated by using D3 version of Grimme's dispersion correction coupled with the original D3 damping function with the keyword Empiricaldispersion=GD3 [55]. Solvent effects (Toluene) were incorporated by using the polarizable continuum model (PCM) [56]. The ultrafine grid was used throughout the calculations. Bonding analysis were performed with the help of NBO routine [57-58] as implemented in the Gaussian 09 suite of programs [59]. The energetics for all the calculations were evaluated in terms of change in Gibbs free energies at 1 atm pressure and 298 K temperature unless otherwise specified.

[4.2.3] Results and Discussion

All the molecules exhibit a planar central ring (see Figure 4.2.1) with two different E–X bond lengths (E = Al, Ga and X = N, C), and the central $\angle$X-E-N bond angle varies from 76.8°–82.1° (Table 4.2.1). The calculated geometrical parameters of the experimentally characterized group 13 bases **I**, **II** [60] and **XIa** are found to be in excellent agreement with the observed values thereby indicating the reliability of the level of theory used in this study. The thermodynamic stability of **1–4** was judged by evaluating their singlet-triplet energy separation (ΔE_{S-T}, in kcal mol^{-1}) values (Figure 4.2.2) and were compared with those of synthetically amenable group 13 carbenoids **I**, **II** and **XIa** (Figure 4.2.2). All the molecules (**1–4**) exhibit a stable singlet ground state which is evident from their calculated highly positive ΔE_{S-T} values (43.5-53.9 kcal mol^{-1}). Furthermore, optimization of the triplet states of **3Ga** and **4Ga** leads to a broken geometry and hence, they were not considered for further study. It is apparent from Figure 4.2.2 that installation of the thermodynamically robust four-membered ylide group considerably raises the ΔE_{S-T} values of **2–4**, i.e., stabilizes the singlet state. Such stabilization of the singlet state may be credited to the enhanced delocalization of electron density from the α-nitrogen (ylidic nitrogen) atom to the vacant p orbital of the central E atom. This is also corroborated from the considerable shortening of the E–Nα bonds of **2–4** than that of **1** (Table 4.2.1). For example, the calculated E–Nα bond lengths for **2Al** (1.958 Å) and **2Ga** (2.101 Å) are found to be considerably shorter than that for **1Al** (2.019 Å) and **1Ga** (2.157Å) respectively. In addition, analysis of the molecular
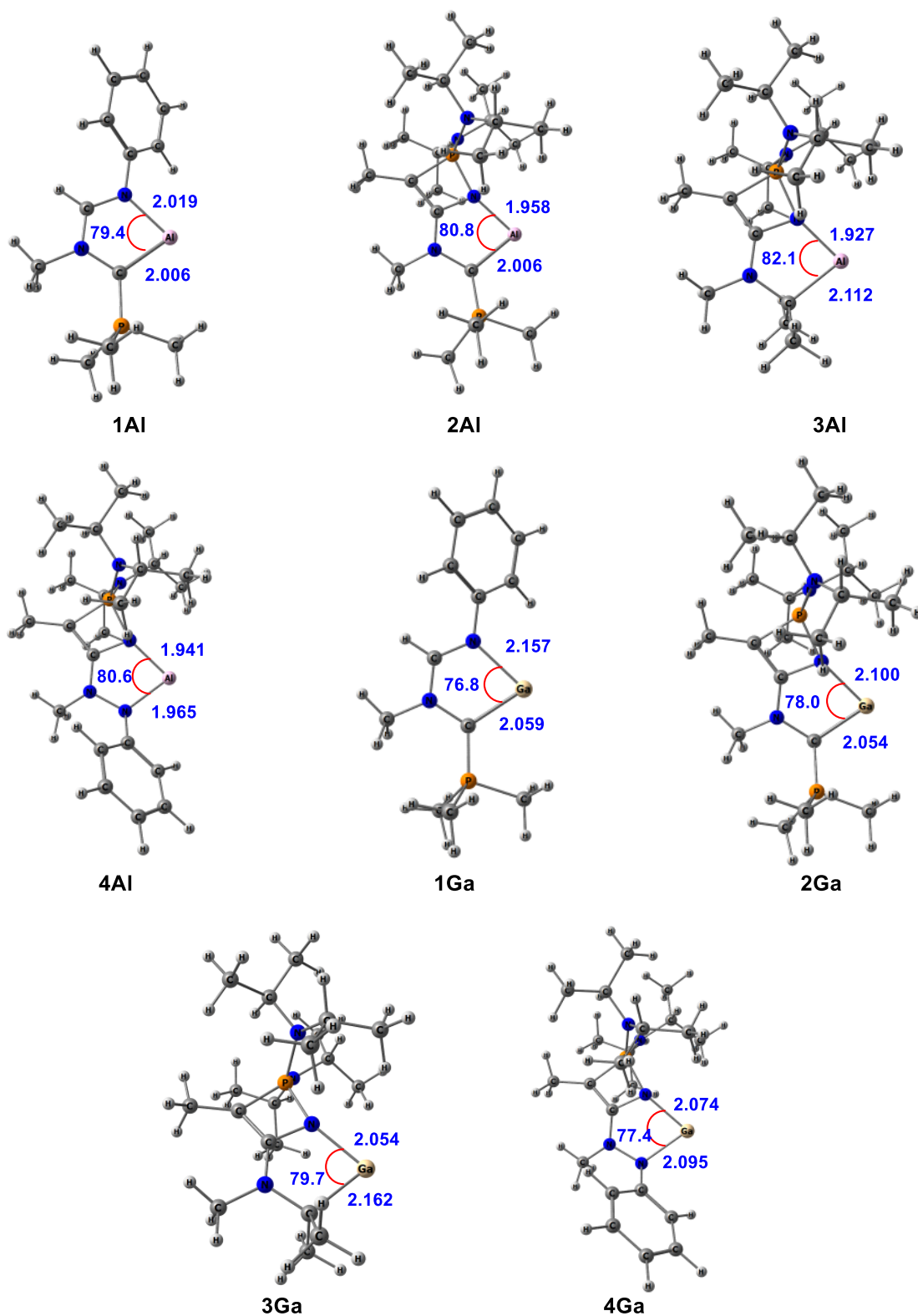
Figure 4.2.1: Singlet state optimized geometries of **1–4** at M06-D3/def2-TZVP(Toluene) level of theory.

Table 4.2.1: Calculated (M06-D3/def2-TZVP(Toluene)) E–X bond lengths (in Å), Wiberg Bond Indices (WBI) values and ∠X–E–N bond angle (in degrees) for the singlet state geometry of **1–4**, **I**, **II** and **XIa**. The experimental values are given in parenthesis (E = Al, Ga and X = C, N).

Molecules	E–X (r_1/r_2)	WBI	∠X-E-N
1Al	2.019/2.005	0.290/0.539	79.4
2Al	1.958/2.006	0.297/0.549	80.8
3Al	1.927/2.112	0.289/0.353	82.1
4Al	1.941/1.965	0.281/0.312	80.6
1Ga	2.157/2.059	0.276/0.586	76.8
2Ga	2.101/2.055	0.295/0.614	78.0
3Ga	2.054/2.162	0.296/0.413	79.7
4Ga	2.104/2.076	0.288/0.273	77.5
I	1.973/1.973 (*1.957/1.957*)	0.261/0.261	89.3 (*89.8*)
II	2.098/2.098 (*2.053/2.056*)	0.254/0.254	85.9 (*87.5*)
XIa	2.152/1.987 (*2.061/1.959*)	0.236/0.3503	78.1 (*79.7*)
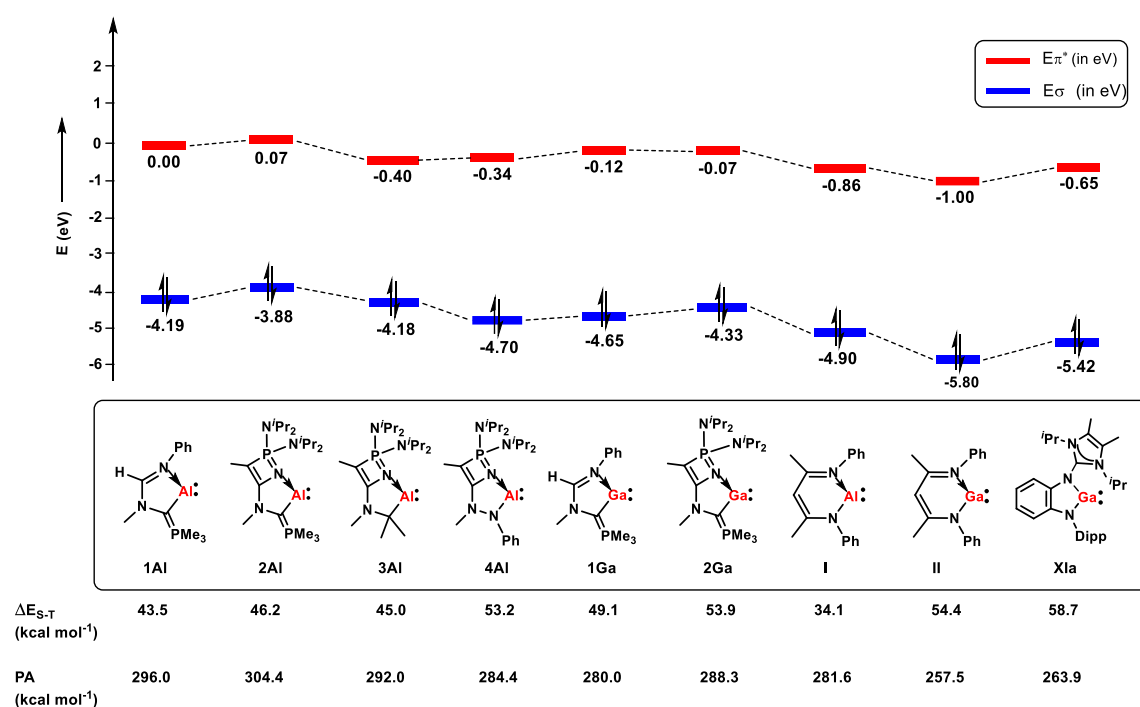
Figure 4.2.2: Calculated (M06-D3/def2-TZVP(Toluene)) energies (in eV) of the σ-symmetric donor (E_σ) and π-symmetric acceptor (E_{π^*}) orbitals concentrated at the Al(I) and Ga(I) center for the molecules **1–4**, **I**, **II** and **XIa** in their singlet state. The singlet-triplet energy separations (ΔE_{S-T}) and proton affinity (PA) values are given in kcal mol^{-1}.

orbitals (MO) also reveals that installation of the four-membered ylide group substantially stabilizes the π-symmetric MOs (Figure 4.2.3). Also, the presence of the thermodynamically robust ylidic P-N fragments further improves the stability of **2–4**. Therefore, it can be inferred that strongly π-electron donating moieties such as ylide and amino groups remarkably stabilize the molecules **1**–**4** in their singlet states and hence, such functionalities may be used as ideal structural motifs for design and synthesis of

1Al
-4.93 eV

2Al
-5.64 eV

3Al
-5.54 eV

4Al
-7.05 eV

(a)

1Ga
-4.78 eV

2Ga
-5.41 eV

(b)
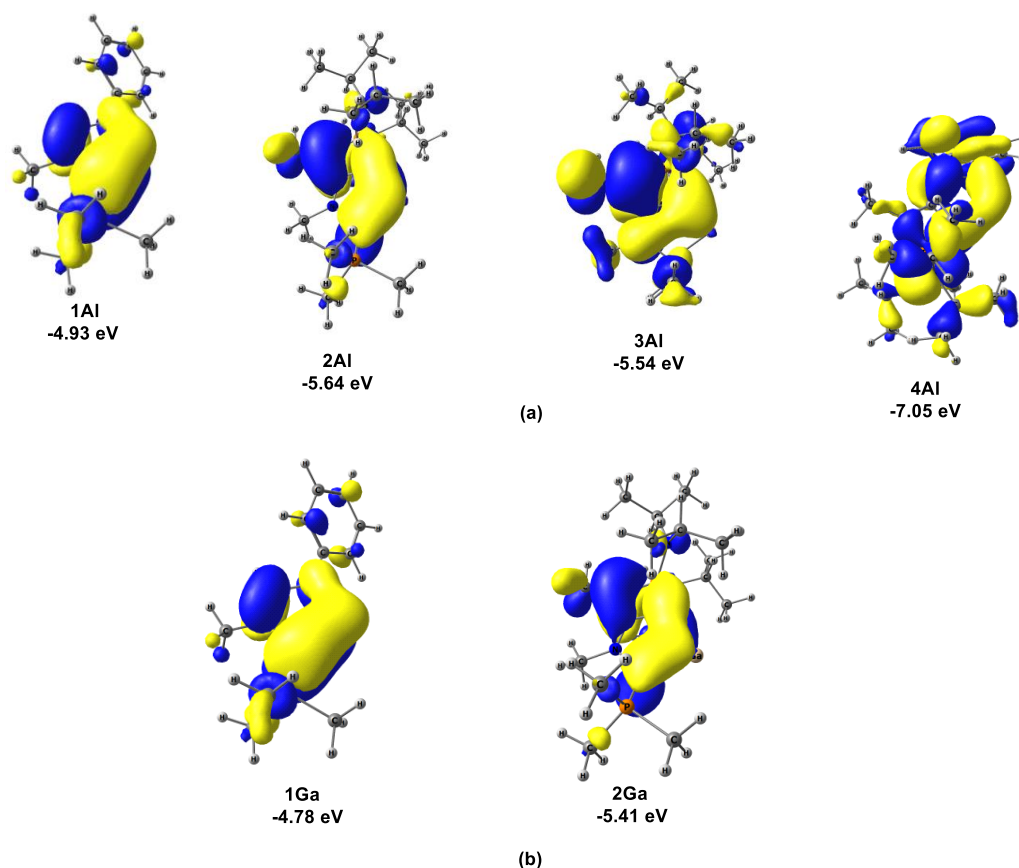
Figure 4.2.3: Pictorial representation of the π-symmetric occupied molecular orbital (along with their energies in eV) for the molecules (a) **1Al–4Al** and (b) **1Ga-2Ga** at M06-D3/def2-TZVP(Toluene) level of theory.

monovalent group 13 carbenoids. Furthermore, the calculated ΔE_{S-T} values for the proposed gallium bases are found to be comparable to those of **II** and **XIa**. On the other hand, all the newly designed aluminium bases (**1Al**–**4Al**) have a significantly higher calculated ΔE_{S-T} values (43.5–53.2 kcal mol^{-1}) than that computed for **I** (34.1 kcal mol^{-1}). The reliability of the calculated singlet-triplet energy separation values of **1**–**4** was checked by recalculating their ΔE_{S-T} values by employing other functionals (PBE0, ωB97XD and B3PW91, Table 4.2.2). Interestingly, the calculated ΔE_{S-T} values for **1**–**4**

with these functionals are found to be comparable to those obtained at M06 thereby indicating the reliability of the level of theory used in this study.

Table 4.2.2: Calculated singlet-triplet energy separation values (ΔE_{S-T}, in kcal mol^{-1}) for **1–4** with different functionals.

Molecules	ΔE_{S-T}			
	M06	**PBE0**	**ωB97XD**	**B3PW91**
1Al	43.5	40.6	43.4	41.0
2Al	46.2	40.2	45.5	40.3
3Al	45.0	36.6	42.4	37.0
4Al	53.2	44.6	50.3	44.9
1Ga	49.1	46.4	48.7	46.6
2Ga	53.9	48.0	56.7	48.5

The ligand properties of the proposed carbenoids are judged by evaluating the energies of their σ-symmetric donor (E_σ) and π-symmetric acceptor orbitals (E_π^*) concentrated at the central group 13 atom (Figure 4.2.2). It is apparent from Figure 4.2.2 that **1–4** possess substantial electron donation abilities (higher E_σ values) compared to that of **I**, **II** and **XIa**. Also, the lone pair centered at the central Al or Ga atoms of **1–4** has less s character than **I**, **II** and **XIa** further implying the higher Lewis basicity of **1–4** (Table 4.2.3). It is to be noted that all the proposed carbenoids possess lower electron

Table 4.2.3: Calculated (M06-D3/def2-TZVP(Toluene)) natural charges (q), occupancies of the formally vacant valence p-orbital (Occ_p) and % s character of the lone pair centered at the central E atom (E = Al and Ga) for **1–4**, **I**, **II** and **XIa**.

Molecules	q	Occ_p	% s
1Al	0.504	0.161	83.1
2Al	0.514	0.151	80.1
3Al	0.623	0.051	84.3
4Al	0.688	0.077	85.9
1Ga	0.470	0.170	89.2
2Ga	0.454	0.164	86.7
I	0.700	0.071	86.9
II	0.697	0.072	93.3
XIa	0.636	0.142	92.2

acceptance abilities (higher E_π^* values) than the experimentally known ones. Furthermore, the electron donation abilities of these group 13 bases were probed by evaluating their proton affinity (PA, in kcal mol^{-1}) values (Figure 4.2.2). In general, the higher the PA value, the higher will be electron donation ability of the molecule under consideration. The calculated PA values for **1–4** lie within 280.0-304.4 kcal mol^{-1} with the highest and the lowest PA values being obtained for **2Al** and **1Ga** respectively. The calculated PA values of **1–4** are considerably higher than that calculated for **I**, **II** and **XIa** further corroborating the higher degree of Lewis basicity of **1–4**. In addition, the calculated PA values are found to be in nice agreement with the E_σ values and indeed, we obtained a good correlation ($R^2 = 0.90$) between the calculated PA and the E_σ values (Figure 4.2.4).
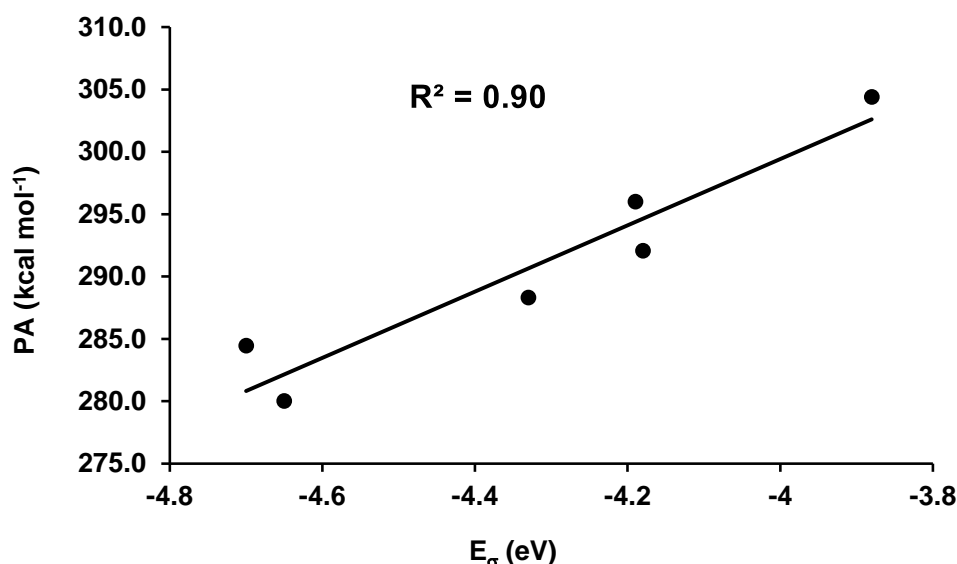
Figure 4.2.4: Correlation plot between the calculated proton affinity (PA, in kcal mol^{-1}) and E_σ (eV) values for **1–4** at M06-D3/def2-TZVP(Toluene) level of theory.

Motivated by the considerable stability (as evident from the calculated ΔE_{S-T} values) and promising ligand properties of the proposed group 13 carbenoids, we decided to probe their potential in the activation of enthalpically strong bonds and compare the energetics with that of **I** and **II** which were documented to perform a variety of bond activations under ambient reaction conditions [16, 20-23]. Herein, we have considered H_2, $PHPh_2$, SiH_3Ph, C_2H_2 and C_6F_6 as some of the substrates that will be subjected to activations by **1–4**.

[4.2.3.1] Activation of Dihydrogen

Activation of dihydrogen remains an area of intense investigation over the years because of its widespread applicability in various industrial as well as biological processes [61-64]. The splitting of the H–H bond by the proposed carbenoids may be thought to proceed via a transition state (TS) that features significantly elongated and polarized H–H bond (Table 4.2.4 and Figure 4.2.5) with the pseudo hydridic hydrogen (H^α) remaining distant from the group 13 (E) center [65]. Thereafter, the eventual migration of the H^α from the activated H–H bond to the vacant p orbital centered at the E center yields the dihydrogen cleaved product.

The calculated activation energy barriers ($\Delta G^\circ_{TS}{}^{H\text{-}H\ddagger}$) obtained for **1Al–4Al** lie within 33.6–40.1 kcal mol^{-1} (Table 4.2.5) with the highest and lowest values being computed for **4Al** and **3Al** respectively. Further, it is encouraging to note that the barrier heights obtained for them are comparable to that obtained for **I** (39.9 kcal mol^{-1}, calculated at the same level of theory) which is known to activate dihydrogen at 70° C.

Table 4.2.4: Calculated (M06-D3/def2-TZVP(Toluene)) important geometrical parameters and natural charges at the hydrogen atoms of dihydrogen molecule and occupancies of the formally vacant p_π orbital at the central atom (E =Al and Ga) (Occ$_{P_\pi}$) of the transition states involved in the activation of hydrogen by **1–4**, **I** and **II**. Bond lengths are given in Å and Wiberg Bond Index (WBI) values are given within parentheses.

Molecules	H–H	E–H$^\alpha$	E–H$^\beta$	$q_H{}^\alpha$	$q_H{}^\beta$	Occ$_{P_\pi}$
I-TS$^{H\text{-}H}$	1.266 (0.228)	1.973 (0.689)	1.591 (0.721)	-0.250	-0.159	0.511
II-TS$^{H\text{-}H}$	1.398 (0.167)	1.994 (0.727)	1.556 (0.773)	-0.269	-0.097	0.552
1Al-TS$^{H\text{-}H}$	1.277 (0.225)	2.101 (0.655)	1.610 (0.704)	-0.317	-0.193	0.568
2Al-TS$^{H\text{-}H}$	1.280 (0.218)	2.180 (0.624)	1.619 (0.699)	-0.347	-0.213	0.345
3Al-TS$^{H\text{-}H}$	1.234 (0.245)	1.936 (0.686)	1.609 (0.688)	-0.229	-0.166	0.481
4Al-TS$^{H\text{-}H}$	1.275 (0.225)	1.963 (0.693)	1.592 (0.714)	-0.258	-0.171	0.370
1Ga-TS$^{H\text{-}H}$	1.404 (0.170)	2.156 (0.654)	1.573 (0.746)	-0.363	-0.318	0.468
2Ga-TS$^{H\text{-}H}$	1.415 (0.162)	2.234 (0.617)	1.579 (0.746)	-0.395	-0.159	0.403

1Al-TS[H-H]

2Al-TS[H-H]

3Al-TS[H-H]

4Al-TS[H-H]

1Ga-TS^{H-H}

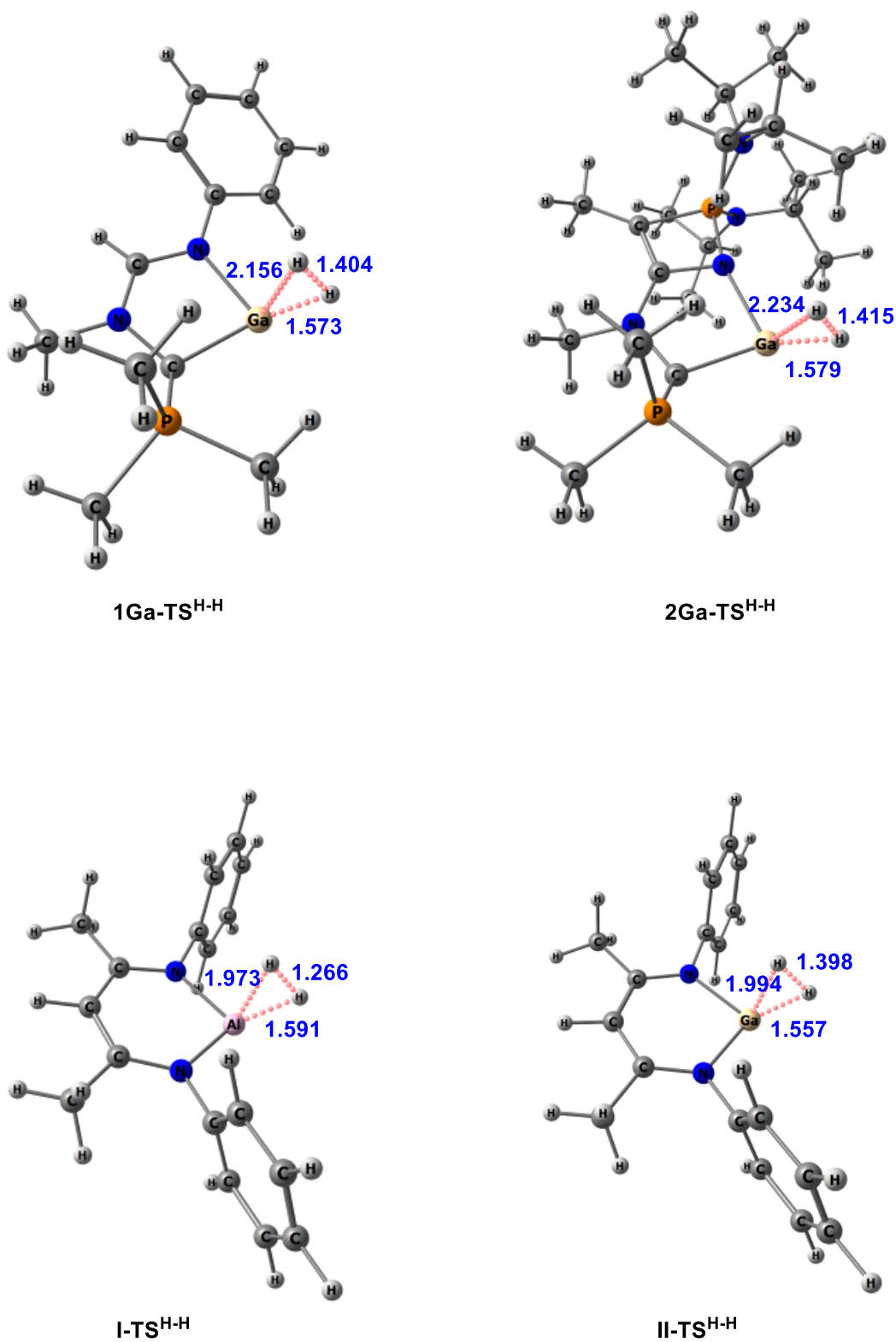**2Ga-TS**$^{H-H}$

I-TS^{H-H}

II-TS^{H-H}
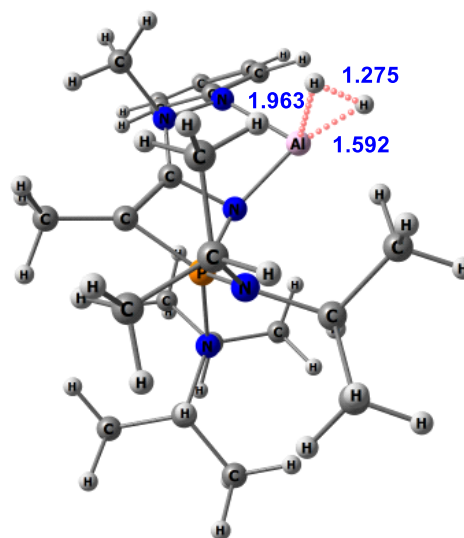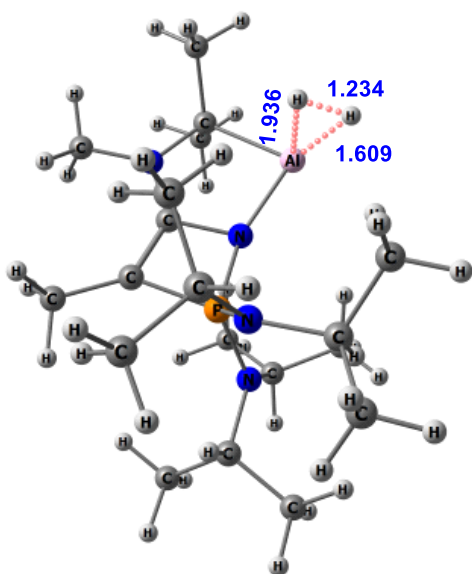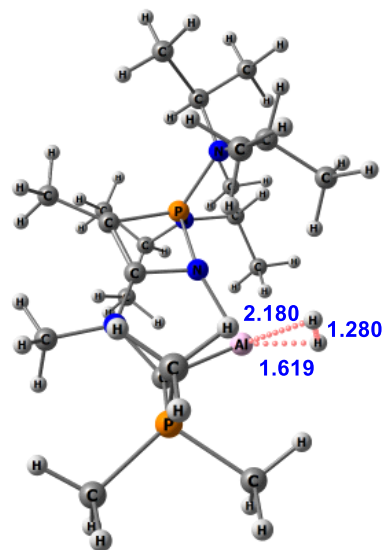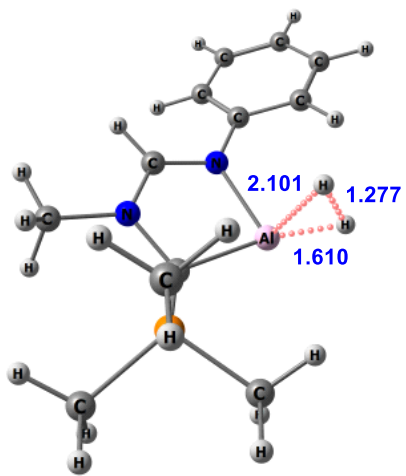
Figure 4.2.5: Optimized geometries of the transition states involved in the activation of dihydrogen by **1–4**, **I** and **II** at M06-D3/def2-TZVP(Toluene) level of theory.

Table 4.2.5: Computed (M06-D3/def2-TZVP (Toluene)) activation energy barriers ($\Delta G^\circ_{TS}{}^{X\text{-}Y\ddagger}$) and reaction free energies for the formation of the intermediates ($\Delta G^\circ_{Int}{}^{X\text{-}Y}$) and X–Y (X =H, P, Si, C; Y = H, F) bond cleaved products ($\Delta G^\circ_{Total}{}^{X\text{-}Y}$) by **1–4**, **I** and **II**. The Energies are given in kcal mol^{-1}.

Entry	$\Delta G^\circ_{TS}{}^{H\text{-}H\ddagger}$	$\Delta G^\circ_{Total}{}^{H\text{-}H}$	$\Delta G^\circ_{Int}{}^{P\text{-}H}$	$\Delta G^\circ_{TS}{}^{P\text{-}H\ddagger}$	$\Delta G^\circ_{Total}{}^{P\text{-}H}$	$\Delta G^\circ_{Int}{}^{Si\text{-}H}$	$\Delta G^\circ_{TS}{}^{Si\text{-}H\ddagger}$	$\Delta G^\circ_{Total}{}^{Si\text{-}H}$	$\Delta G^\circ_{Int}{}^{C\text{-}F}$	$\Delta G^\circ_{TS}{}^{C\text{-}F\ddagger}$	$\Delta G^\circ_{Total}{}^{C\text{-}F}$
1Al	38.5	-25.1	-	9.5	-31.4	2.4	20.3	-22.0	4.1	15.7	-103.0
2Al	35.7	-27.4	-	17.4	-36.3	0.8	19.2	-25.0	3.4	13.8	-105.6
3Al	33.6	-30.4	0.8	22.9	-36.4	3.1	18.4	-25.0	3.7	17.5	-104.0
4Al	40.1	-27.4	-	28.8	-33.9	2.3	23.0	-22.6	7.2	22.2	-102.8
1Ga	50.0	-3.9	-	19.4	-11.7	1.5	26.8	-3.5	-	-	-57.0
2Ga	45.6	-7.7	-	26.2	-16.3	1.2	22.8	-6.7	2.9	18.3	-61.5
I	39.9	-29.2	2.0	26.2	-32.4	5.8	22.6	-24.0	5.1	22.1	-104.6
II	56.4	-4.9	-1.3	39.6	-9.2				6.3	34.2	-54.6

Therefore, it can be anticipated that **1Al–4Al** could be considered as suitable candidates for the activation of dihydrogen. The reaction free energies ($\Delta G°_{Total}{}^{H-H}$) obtained for **1Al–4Al** are comparable to that of **I** (Table 4.2.5) indicating the feasibility of dihydrogen splitting by these group 13 carbenoids. Furthermore, the activation barrier obtained for **I** is found to be comparable to those reported earlier by others [65]. On the other hand, both **1Ga** and **2Ga** compute significantly higher barrier heights than **1Al–2Al** but are considerably lower compared to that obtained for **II** (56.4 kcal mol^{-1}). The lower reactivity of **1Ga** and **2Ga** compared to their aluminium analogs may be attributed to their low nucleophilcity. The high $\Delta G°_{TS}{}^{H-H\ddagger}$ values for **1Ga** and **2Ga** suggest that both the proposed Ga(I) bases may need elevated reaction conditions to carry out the activation process. Our findings are in stark contrast with the experimental observation of the activation of dihydrogen by the gallium carbenoid **II** at room temperature by Linti and coworkers [22].

[4.2.3.2] Activation of Diphenylphosphine

For carbenoids having moderate-to-high electrophilicity, the activation of Ph_2PH can be thought of as initiated by the formation of a loosely bound complex by interaction between the group 13 center (E) and the lone pair at phosphorus (LP_P) while that by nucleophilic carbenoids involve interaction between the lone pair at E and the P–H antibonding orbital (σ^*_{P-H}). In the present study, only **I**, **II** and **3Al** are found to form van der Waals complexes as intermediates while others failed due to their low electrophilicity (higher(E_π^* values). Figure 4.2.6 depicts the energy profile diagram for the activation of Ph_2PH by considering **1Al** and **3Al** as the representative carbenoids (similar energy profiles for activation by the gallium carbenoids are given Figure 4.2.7). The formation of the intermediates is associated with an increase and decrease in the occupancies of the vacant orbital at E and LP_P respectively (Table 4.2.3 and Table 4.2.6). For example, the occupancy of the vacant orbital at Al increases from 0.05 in **3Al** to 0.21 in **3Al-Int^{P-H}**. Consequently, the occupancies of
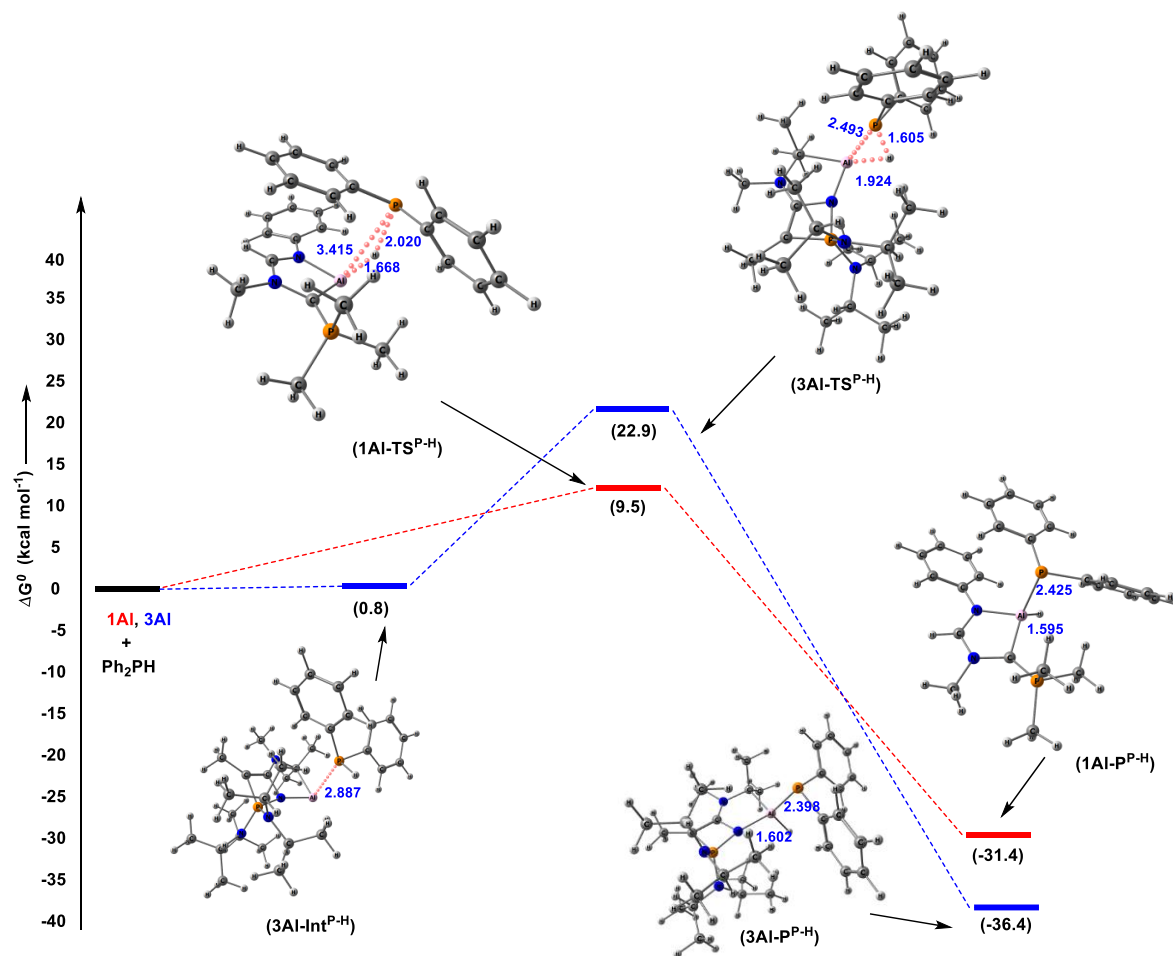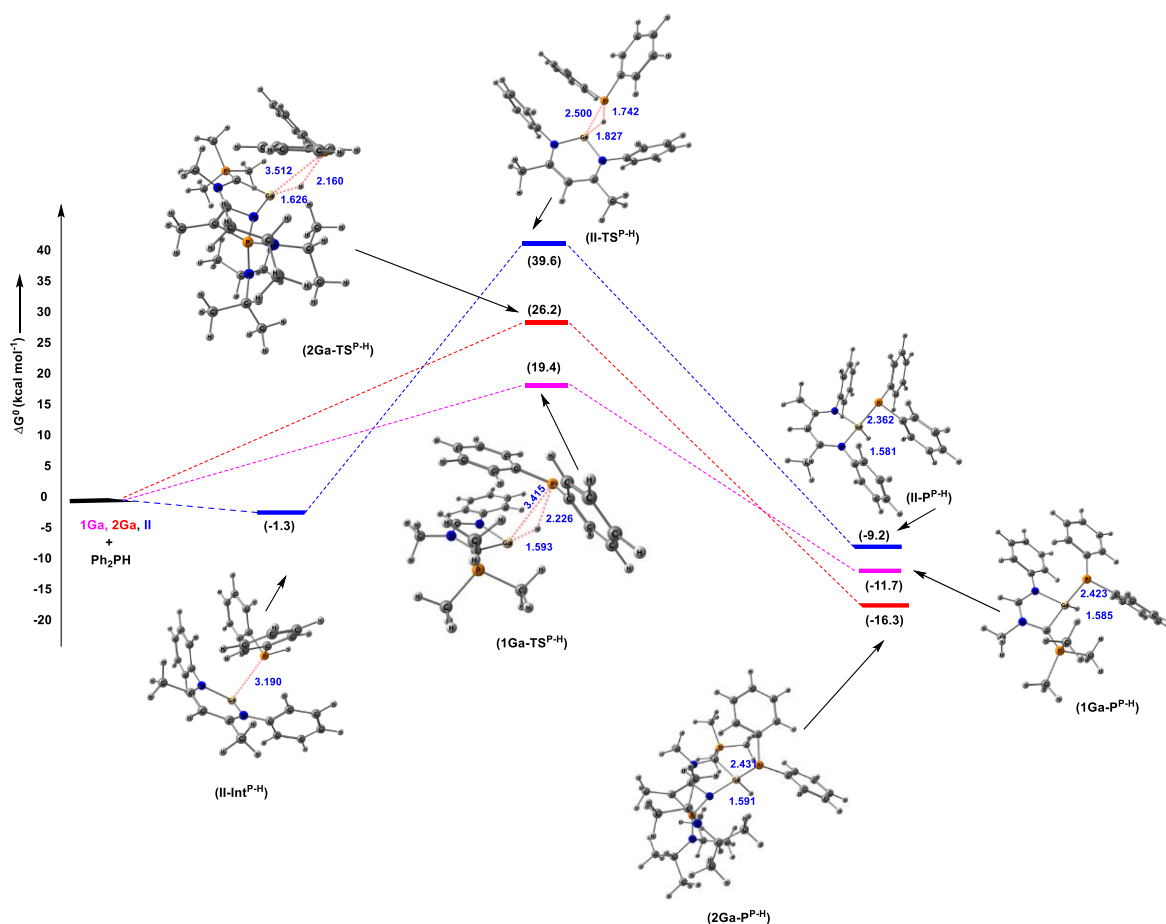
Figure 4.2.6: Energy profile diagram for the activation of P–H bond of Ph$_2$PH by **1Al** and **3Al** at M06-D3/def2-TZVP (Toluene) level of theory.

LP$_P$ decreases from 1.942 in Ph$_2$PH to 1.751 in **3Al-Int^{P-H}**. The formation of the intermediates is followed by interaction of the lone pair at E with the activated P–H bonds generating the P–H splitting products. A closer look at Figure 4.2.6 show that the optimized geometries of the TS obtained for **1Al** and **3Al** differ significantly from each other. For example, the Al–P bond is substantially stretched in **1Al-TS^{P-H}** compared to that in **3Al-TS^{P-H}** while the Al–H bond is shorter in **1Al-TS^{P-H}** than that in **3Al-TS^{P-H}**. The important geometrical parameters for all the TSs involved in the activation of P–H by **1–4**, **I** and **II** are listed in Table 4.2.7.

Figure 4.**2**.**7**: Energy profile diagram for the activation of P–H bond of Ph_2PH by **1Ga, 2Ga** and **II** at M06-D3/def2-TZVP (Toluene) level of theory.

Table 4.**2**.**6**: Calculated (M06-D3/Def2-TZVP(Toluene)) important geometrical parameters and natural charges and occupancies (Occ_{p_π}) at the Al/Ga center for the intermediate (**Int**) involved in the activation of P–H bond of PPh_2H by **3Al**, **I** and **II**. Bond lengths are given in Å and Wiberg Bond Index (WBI) values are given within parentheses.

Molecules	E–PPh$_2$H	q_E	Occ_{p_π}
I-Int^{P-H}	2.753 (0.372)	0.651	0.133
II-Int^{P-H}	3.190 (0.186)	0.635	0.146
3Al-Int^{P-H}	2.887 (0.401)	0.532	0.222

Table 4.2.7: Calculated (M06-D3/Def2-TZVP(Toluene)) important geometrical parameters and natural charges at the phosphorus atom of the pseudo phosphide fragment (q_{PPh_2}) and hydrogen atom (q_H) of the transition states involved in the activation of P-H bond of PPh_2H by **1–4**, **I** and **II**. Bond lengths are given in Å and Wiberg Bond Index (WBI) values are given within parentheses.

Molecules	H–PPh$_2$	Ph$_2$P–E	E–H	q_{PPh_2}	q_H	Occ$_{p_\pi}$
I-TS^{P-H}	1.619	2.451	1.949	0.277	-0.046	0.534
	(0.631)	(0.798)	(0.291)			
II-TS^{P-H}	1.742	2.500	1.827	0.286	-0.078	0.419
	(0.501)	(0.801)	(0.401)			
1Al-TS^{P-H}	2.020	3.415	1.668	0.362	-0.308	0.379
	(0.204)	(0.350)	(0.635)			
2Al-TS^{P-H}	1.955	3.433	1.703	0.379	-0.305	0.227
	(0.238)	(0.348)	(0.599)			
3Al-TS^{P-H}	1.605	2.493	1.924	0.307	-0.068	0.223
	(0.648)	(0.751)	(0.276)			
4Al-TS^{P-H}	2.214	3.461	1.607	0.352	-0.325	0.218
	(0.132)	(0.387)	(0.705)			
1Ga-TS^{P-H}	2.226	3.415	1.593	0.300	-0.239	0.370
	(0.131)	(0.292)	(0.728)			
2Ga-TS^{P-H}	2.160	3.512	1.626	0.293	-0.247	0.273
	(0.152)	(0.266)	(0.698)			

The calculated barrier heights for **1–4** lie within 9.5–28.8 kcal mol^{-1} (Table 4.2.5). It is encouraging to note that **1Al** (9.5 kcal mol^{-1}) computes almost three times less barrier than that obtained for **I** (26.2 kcal mol^{-1}) while the same for **1Ga** (19.4 kcal mol^{-1}) is less than half than that for **II** (39.6 kcal mol^{-1}). Further, the reaction free energies are also substantially exergonic (-11.7 to -36.4 kcal mol^{-1}) indicating the likelihood of facile P–H activation by these proposed carbenoids. The optimized geometries of the intermediates and TSs involved the activation of P–H bond by **1–4**, **I** and **II** are shown in Figures 4.2.8 and Figures 4.2.9 respectively.
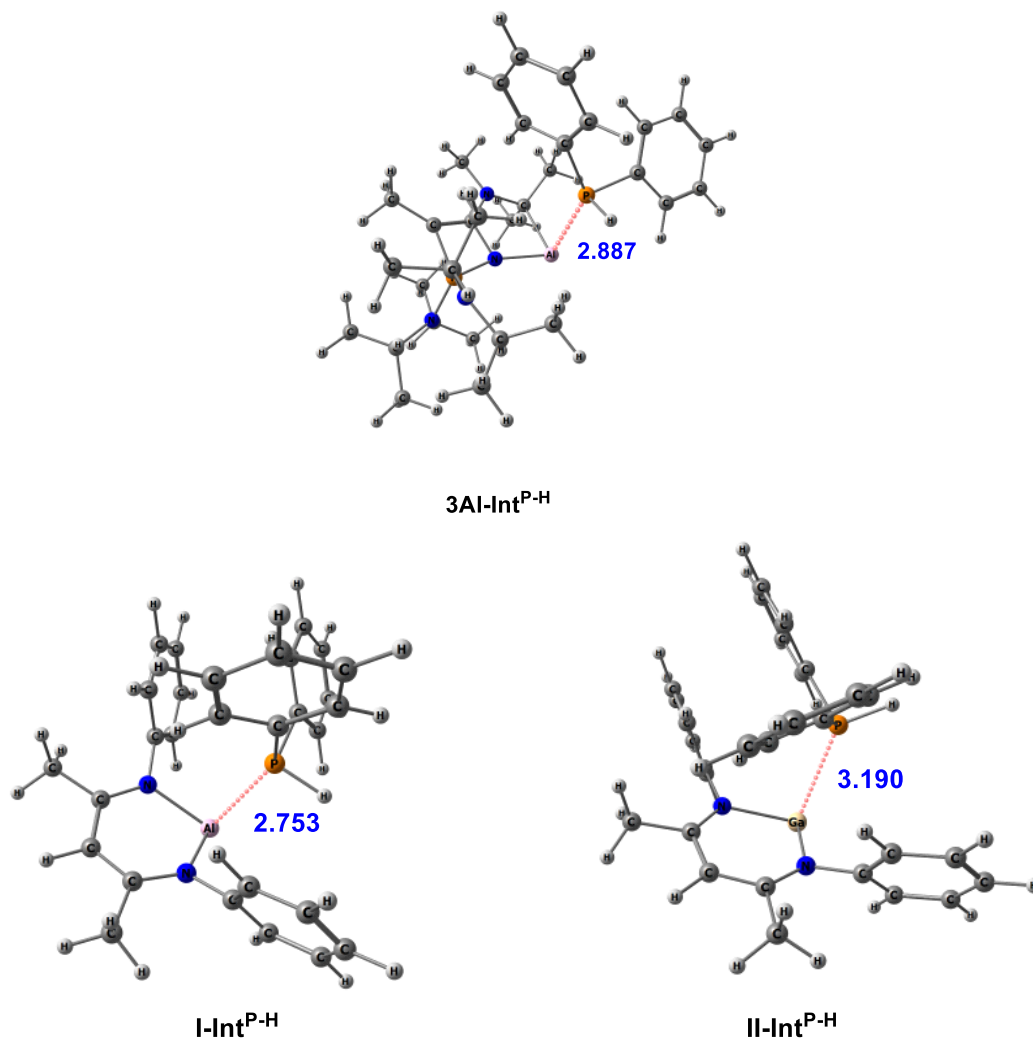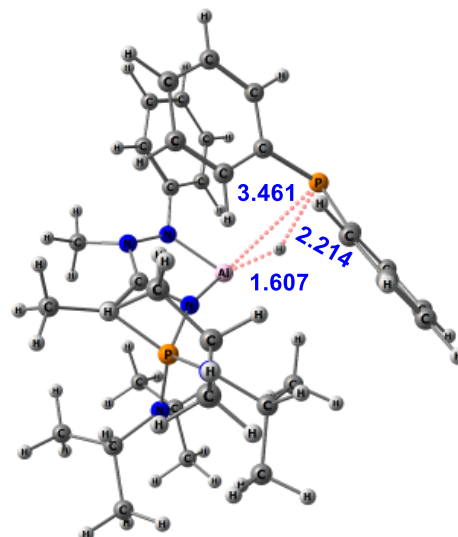
Figure 4.2.8: Optimized geometries of the intermediate involved in the activation of P – H bond of PHPh₂ by **3Al, I** and **II** at M06-D3/def2-TZVP(Toluene) level of theory.

1Al-TS^{P-H}

2Al-TS^{P-H}

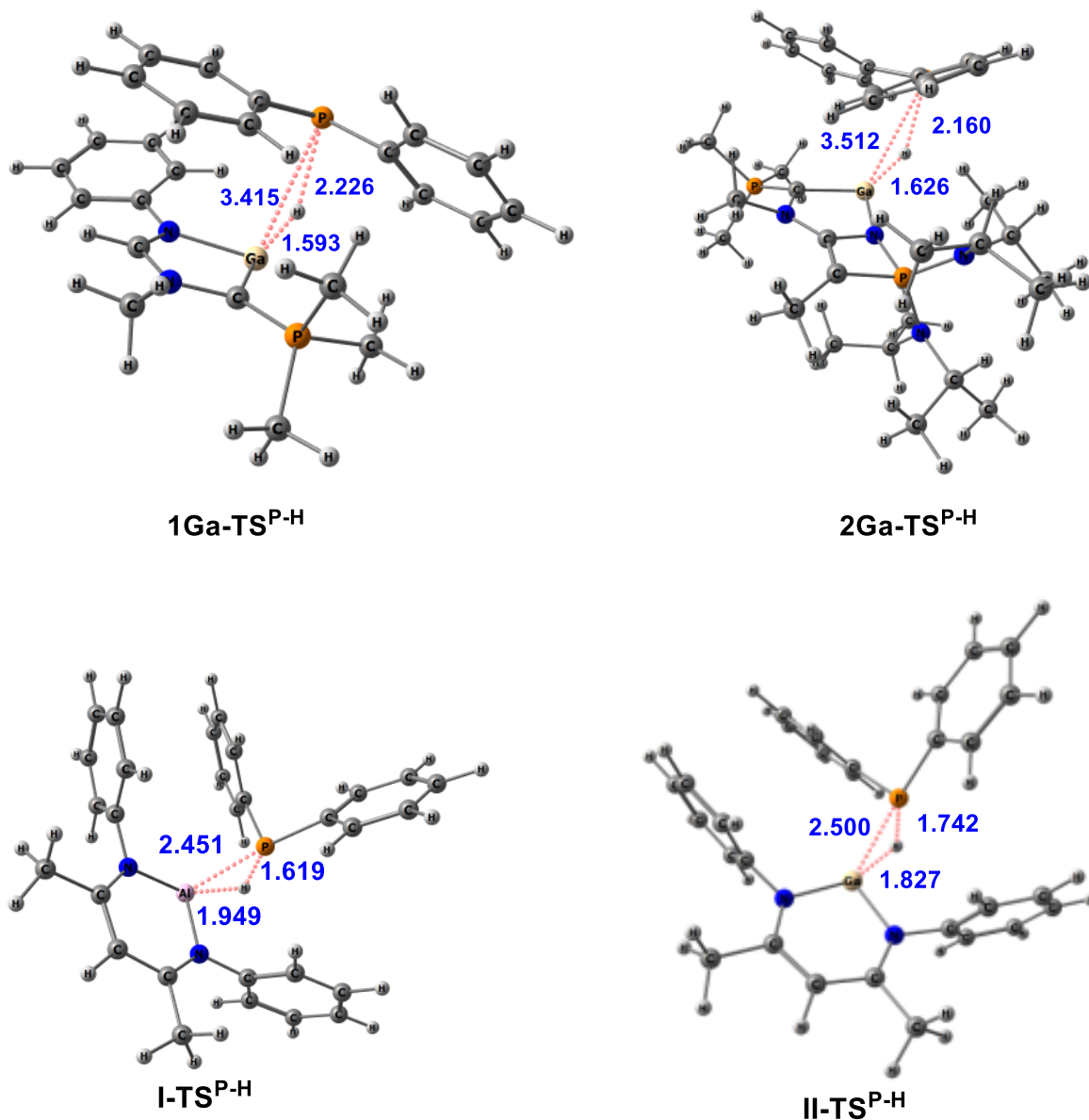**3Al-TS^{P-H}**
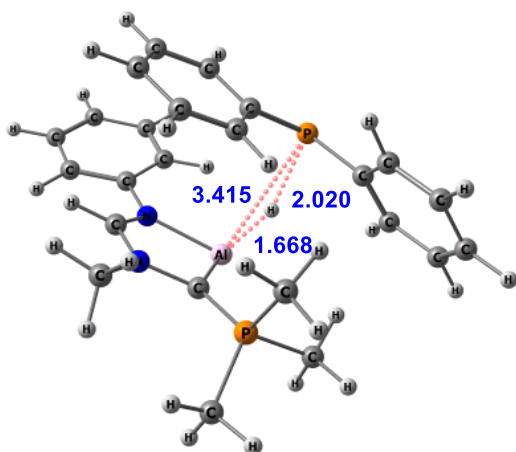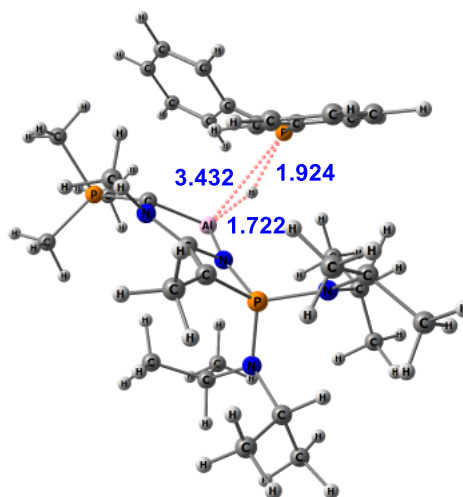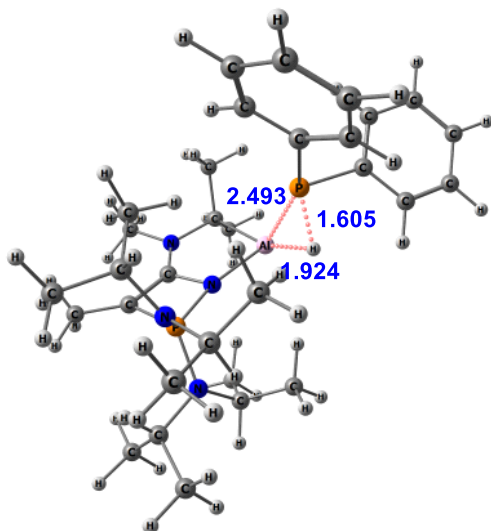
4Al-TS^{P-H}

Figure 4.2.9: Optimized geometries of the transition states involved in the activation of P–H bond of PHPh$_2$ by **1–4**, **I** and **II** at M06-D3/def2-TZVP(Toluene) level of theory.

[4.2.3.3] Activation of Silane (SiH$_3$Ph)

The activation of silane may be envisioned to proceed via two steps as shown in Figure 4.2.10 by considering **1Al** and **4Al** as representative examples. In the first step, one of the Si–H bonds of SiH$_3$PH transfer its electron density to the vacant p orbital located at the Al center to yield the van der Waals complexes **1Al-Int^{Si-H}** and **4Al-Int^{Si-H}**. Thereafter, in the

second step, these complexes pass through TS that feature a 3c-2e interaction between the participating groups to generate the Si–H bond splitting products. The calculated important geometrical parameters for the van der Waals complexes as well as the TSs involved in the activation of Si–H bond by **1**–**4** and **I** are given in Tables 4.2.8-4.2.9 and Figures 4.2.11-4.2.12 respectively.

A closer look at Figure 4.2.10 shows that the geometrical parameters of **1Al-TS^{Si-H}** and **4Al-TS^{Si-H}** differ significantly from each other. For example, the distance between the hydridic hydrogen and the Al center is *ca.* 0.3 Å shorter in **4Al-TS^{Si-H}** compared to that in **1Al-TS^{Si-H}** which may be attributed to better accepting ability of **4Al** than that of **1Al**
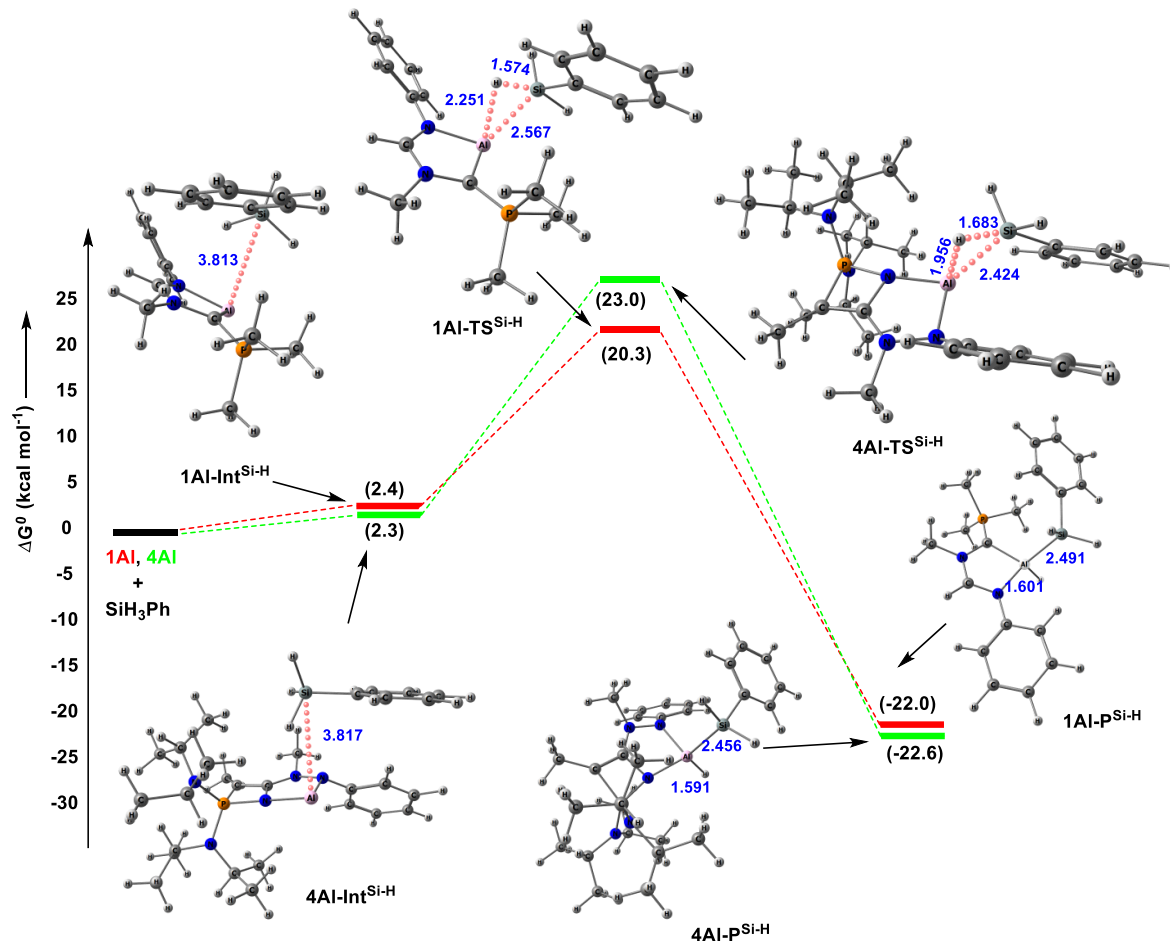
Figure 4.2.10: Energy profile diagram for the activation of Si–H bond of SiH$_3$Ph by **1Al** and **4Al** at M06-D3/def2-TZVP (Toluene) level of theory.

(Figure 4.2.2). The incipient formation of the hydridic hydrogen as well as the substantial polarization of the Si–H bond in all the TSs is also supported by the calculated NBO based natural charge values which reveals the presence of considerable negative (-0.224 to –0.286) and positive (0.453 to 0.607) charges at the hydridic hydrogen and silicon atom of the SiH$_2$Ph fragment respectively.

The activation barriers ($\Delta G^{\circ}{}_{TS}{}^{Si\text{-}H\ddagger}$) obtained for **1Al–4Al** and **1Ga–2Ga** lie within 18.4–26.8 kcal mol^{-1} and are comparable to that obtained for the experimentally evaluated **I** (22.6 kcal mol^{-1}, Table 4.2.5). Furthermore, the calculated free energies ($\Delta G^{\circ}{}_{Total}{}^{Si\text{-}H}$) for the reactions of **1Al–4Al** are comparable to that obtained for **I**. The calculated energetics indicate the potential of the proposed aluminium carbenoids towards facile activation of silane.

Table 4.2.8: Calculated (M06-D3/def2-TZVP(Toluene)) important geometrical parameters and natural charges at the silicon (q_{Si}) atom of the SiH$_3$Ph and at the central atom (q_E, E = Al and Ga) of the van der Waals complexes involved in the activation of Si–H bond of SiH$_3$Ph by **1–4** and **I**. The PhH$_3$Si–E, E-X (E = Al and Ga and X = C, N) bond lengths and ∠X–E–N bond angles are given in Å and in degree (°) respectively.

Molecules	PhH$_3$Si–E	E-X	∠X-E-N	q_E	q_{Si}
I-Int$^{Si\text{-}H}$	3.746 (0.034)	1.971/1.988 (0.241)/(0.241)	89.3	0.737	0.933
1Al-Int$^{Si\text{-}H}$	3.813 (0.016)	2.015/2.011 (0.279)/(0.515)	79.3	0.520	0.941
2Al-Int$^{Si\text{-}H}$	3.797 (0.022)	1.954/2.017 (0.291)/(0.496)	80.9	0.540	0.966
3Al-Int$^{Si\text{-}H}$	3.789 (0.036)	1.932/2.116 (0.275)/(0.337)	82.1	0.645	0.943
4Al-Int$^{Si\text{-}H}$	3.817 (0.024)	1.942/1.974 (0.270)/(0.284)	80.5	0.700	0.966
1Ga-Int$^{Si\text{-}H}$	3.989 (0.010)	2.152/2.060 (0.275)/(0.574)	76.7	0.427	0.945
2Ga-Int$^{Si\text{-}H}$	3.784 (0.019)	2.096/2.067 (0.297)/(0.569)	78.2	0.471	0.965

Table 4.2.9: Calculated (M06-D3/def2-TZVP(Toluene)) important geometrical parameters and natural charges at hydridic ($q_{H^{\delta-}}$) hydrogen and silicon atom of the SiH$_2$Ph fragment ($q_{Si^{\delta+}}$) and occupancies of the formally vacant p$_\pi$ orbital at the E = Al and Ga center (Occ$_{P_\pi}$) of the transition states involved in the activation of Si–H bond of SiH$_3$Ph by **1–4** and **I**. Bond lengths (E–X, E = Al, Ga and X = N, C), bond angles (∠X-E-N) are given in Å and in degree (°) respectively and Wiberg Bond Index (WBI) values are given within parentheses.

Molecules	PhH$_2$Si$^{\delta+}$–H$^{\delta-}$	E–H$^{\delta-}$	PhH$_2$Si$^{\delta+}$–E	E-X	∠X-E-N	$q_{H^{\delta-}}$	$q_{Si^{\delta+}}$	Occ$_{P_\pi}$
I-TS^{Si-H}	1.631	1.988	2.493	1.908/1.915	94.0	-0.245	0.618	0.545
	(0.551)	(0.313)	(0.734)	(0.305)/(0.299)				
1Al-TS^{Si-H}	1.574	2.251	2.567	1.947/1.958	83.2	-0.232	0.575	0.479
	(0.642)	(0.215)	(0.704)	(0.321)/(0.559)				
2Al-TS^{Si-H}	1.590	2.364	2.533	1.895/1.955	85.2	-0.230	0.453	0.237
	(0.672)	(0.197)	(0.735)	(0.313)/(0.543)				
3Al-TS^{Si-H}	1.612	1.988	2.509	1.891/2.053	86.3	-0.224	0.607	0.338
	(0.593)	(0.297)	(0.684)	(0.326)/(0.407)				
4Al-TS^{Si-H}	1.683	1.956	2.424	1.872/1.904	85.7	-0.256	0.550	0.253
	(0.514)	(0.347)	(0.806)	(0.340)/(0.355)				
1Ga-TS^{Si-H}	1.709	2.084	2.376	2.015/1.971	83.2	-0.281	0.558	0.430
	(0.475)	(0.315)	(0.857)	(0.365)/(0.645)				
2Ga-TS^{Si-H}	1.717	2.190	2.375	1.971/1.974	84.6	-0.286	0.489	0.310
	(0.517)	(0.281)	(0.853)	(0.657)/(0.374)				

3.813

3.797

1Al-Int^{Si-H}   **2Al-Int^{Si-H}**

3Al-Int^{Si-H}
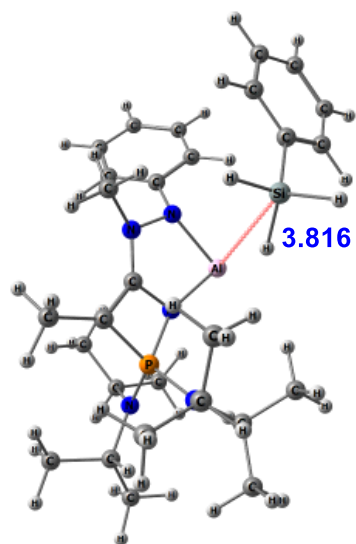
4Al-Int^{Si-H}
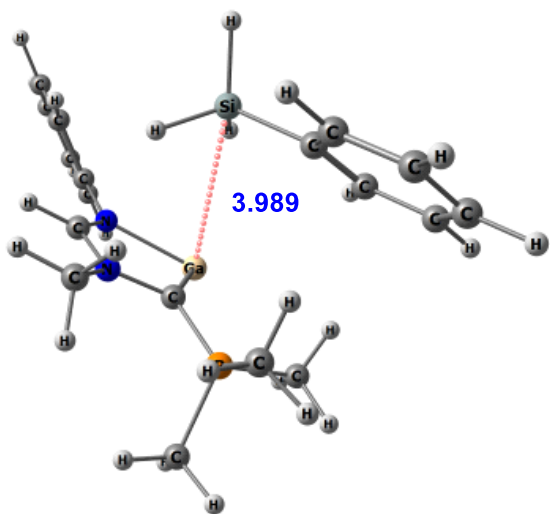
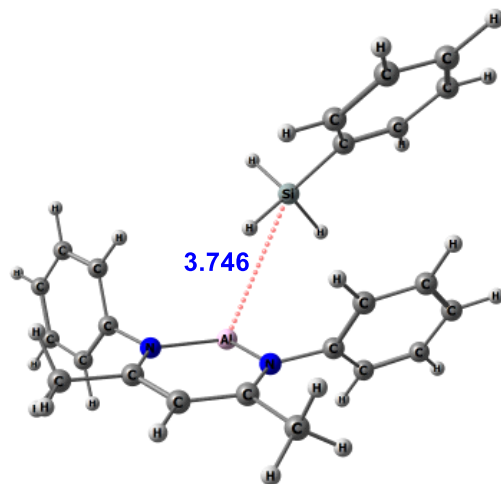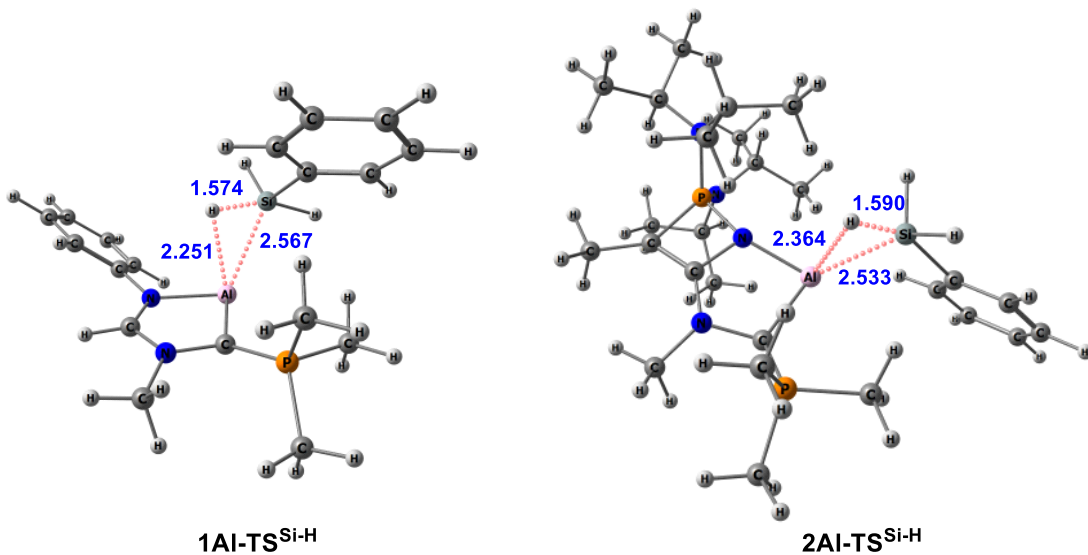**1Ga-Int^{Si-H}**
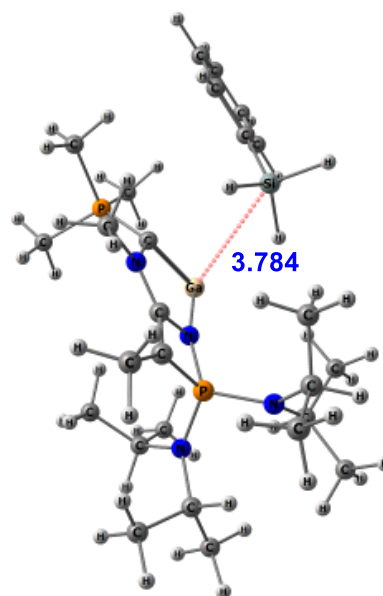
2Ga-Int^{Si-H}

I-Int^{Si-H}

Figure 4.2.11: Optimized geometries of the van der Waals complexes involved in the activation of Si–H bond of SiH$_3$Ph by **1–4** and **I** at M06-D3/def2-TZVP(Toluene) level of theory.
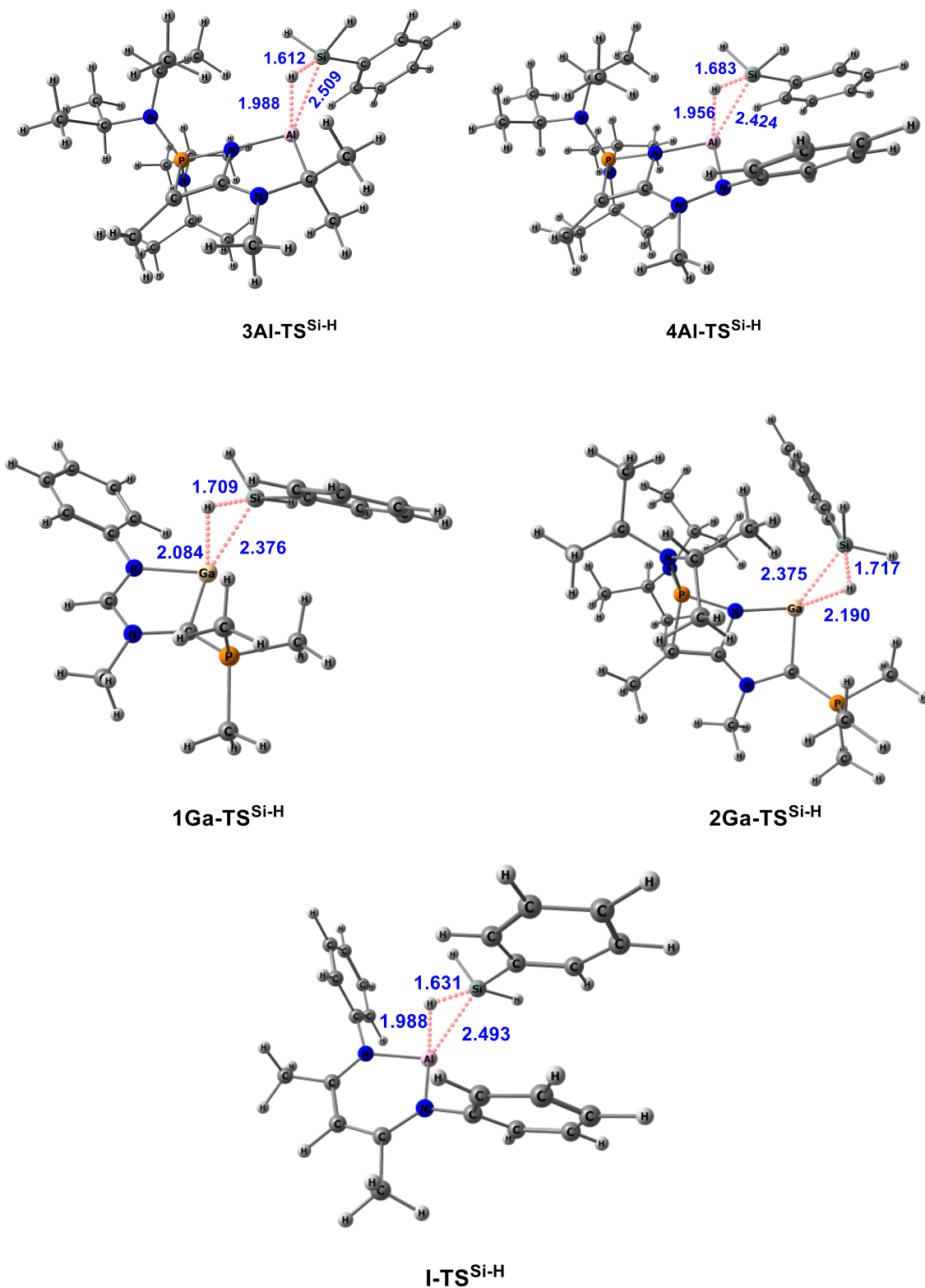

1Al-TS^{Si-H}

2Al-TS^{Si-H}

3Al-TS^{Si-H}

4Al-TS^{Si-H}

1Ga-TS^{Si-H}

2Ga-TS^{Si-H}

I-TS^{Si-H}

Figure 4.2.12: Optimized geometries of the transition states involved in the activation of Si–H bond of SiH₃Ph by **1–4** and **I** at M06-D3/def2-TZVP(Toluene) level of theory.

[4.2.3.4] Activation of Hexafluorobenzene

Activation of the enthalpically robust C–F bond is of considerable interest as this can lead to important organofluorine compounds that are extensively used in various industries like pharmaceuticals, polymers and agrochemicals etc [66-70]. However, activation of C–F bond is a difficult task and often demands forcing reaction conditions or transition metal catalysts [71]. A number of main group compounds are known that are capable of activating C–F bond under mild reaction conditions [21, 72]. For example, in 2015, the groups of Crimmin and Nikonov independently reported the facile splitting of C–F bond for a range of fluorinated molecules with the assistance of Roesky's NacNac aluminium(I) base (**I**) [73,74]. Similarly, more recently, Kretschmer and coworkers employed the gallium counterpart of **I** (**II**) to split the C–F bond for a couple of fluoroarene molecules [23]. This has inspired us to further investigate the potential of **1**–**4** towards activation of C–F bond by considering hexa-fluorobenzene (C_6F_6) as the representative fluoroarene.

The activation of C–F bond of C_6F_6 by group 13 carbenoids may proceeds via two steps [75] as shown in Figure 4.2.13 by considering **2Al** and **2Ga** as the representative
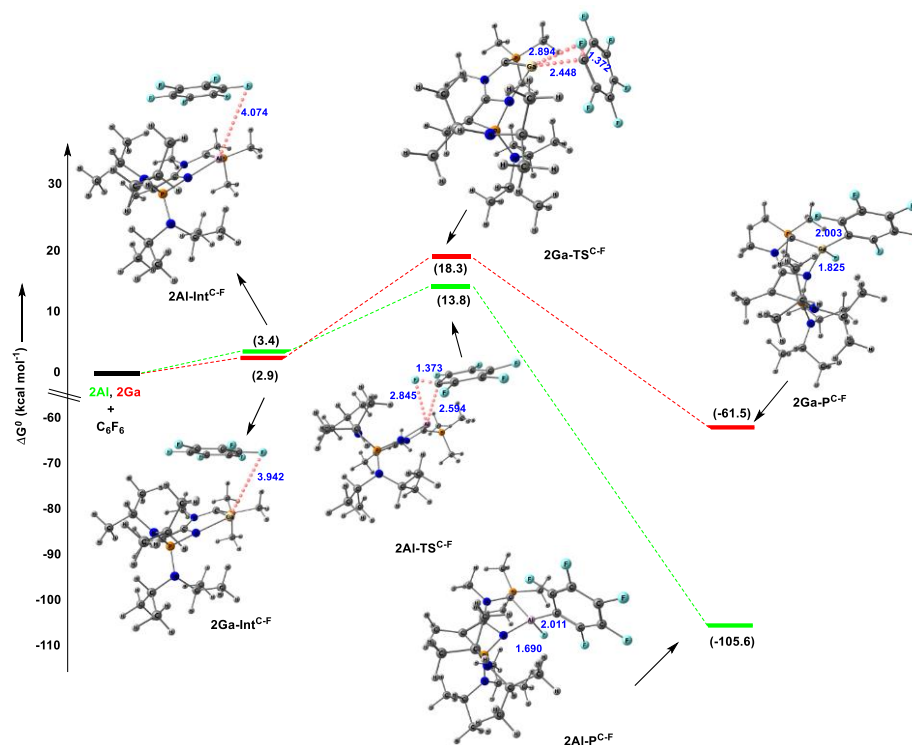

Figure 4.2.13: Energy profile diagram for the activation of C–F bond of C_6F_6 by **2Al** and **2Ga** at M06-D3/def2-TZVP (Toluene) level of theory.

examples. The first step involves the formation of an encounter complex (**2Al-Int$^{C\text{-}F}$–2Ga-Int$^{C\text{-}F}$**) that features weak C–H····F–C interactions and lies slightly higher in energy from their starting reactants (*ca.* 2.9–3.4 kcal mol^{-1}). The encounter complexes proceed through TSs that possess significantly elongated and polarized C–F bonds with the fluorine atom residing in a bridging position between the C$_6$F$_5$ group and the E atom (Figure 4.2.13 and Table 4.2.10). The substantial polarization of the C–F bond as well as the incipient formation of the fluoride ion can be corroborated from the calculated natural charge values which indicate the presence of considerable positive (0.097 to 0.218) and negative (-0.354 to -0.378) charges at the *ipso*-carbon of the C$_6$F$_5$ fragment and bridging fluorine atom respectively (Table 4.2.10). However, despite several attempts, we could not locate the probable TS for C–F activation by **1Ga**. The optimized geometries of the encounter complexes and TSs obtained for activation of C–F bond by **1–4**, **I** and **II** are shown in Figure 4.2.14 and Figure 4.2.15 respectively.

Table 4.2.10: Calculated (M06-D3/def2-TZVP(Toluene)) important geometrical parameters and natural charges at the *ipso*-carbon (q$_C{}^{\delta+}$) of the F$_5$C$_6$ fragment and fluoride atom (q$_F{}^{\delta-}$) and occupancies of the formally vacant p$_\pi$ orbital at the E = Al/Ga center (Occ$_{P_\pi}$) of the transition states involved in the activation of C–F bond of hexafluorobeneze by **1–4**, **I** and **II**. Bond lengths are given in Å and Wiberg Bond Index (WBI) values are given within parentheses.

Molecules	F$^{\delta-}$–C$_6$F$_6{}^{\delta+}$	E–C$_6$F$_6{}^{\delta+}$	E–F$^{\delta-}$	q$_C{}^{\delta+}$	q$_F{}^{\delta-}$	Occ$_{P_\pi}$
I-TS$^{C\text{-}F}$	1.431 (0.739)	2.394 (0.422)	2.401 (0.128)	0.072	-0.387	0.168
II-TS$^{C\text{-}F}$	1.527 (0.612)	2.198 (0.537)	2.328 (0.165)	-0.032	-0.453	0.146
1Al-TS$^{C\text{-}F}$	1.387 (0.807)	2.489 (0.393)	2.718 (0.078)	0.218	-0.361	0.240
2Al-TS$^{C\text{-}F}$	1.373 (0.826)	2.594 (0.357)	2.845 (0.072)	0.176	-0.354	0.220
3Al-TS$^{C\text{-}F}$	1.388 (0.803)	2.571 (0.328)	2.596 (0.098)	0.159	-0.358	0.117
4Al-TS$^{C\text{-}F}$	1.416 (0.761)	2.433 (0.401)	2.448 (0.114)	0.097	-0.378	0.164
2Ga-TS$^{C\text{-}F}$	1.372 (0.821)	2.448 (0.418)	2.894 (0.068)	0.153	-0.360	0.234

The calculated activation energy barriers ($\Delta G°_{TS}{}^{C-F\ddagger}$) obtained for **1–4** lie within 13.8–22.2 kcal mol^{-1}, with the lowest and highest barrier heights being obtained for **2Al** and **4Al**, respectively (Table 4.2.5). Gratifyingly, the calculated $\Delta G°_{TS}{}^{C-F\ddagger}$ values for **1–4** are either substantially lower or comparable to those obtained for **I** and **II** which are known to activate C$_6$F$_6$ under ambient reaction conditions. Moreover, the calculated reaction free energies are found to be remarkably exergonic (-57.0 to -105.6 kcal mol^{-1}) hinting at the feasibility of the C–F bond splitting reaction by **1–4**. Also, the calculated activation barriers for **I** and **II** are found to be comparable to those reported earlier [23, 75a, 75c]. Hence, it can be envisioned that akin to **I** and **II**, all the computationally proposed molecules may be considered as suitable candidates for C–F bond activation.

3Al-Int^{C-F}

4Al-Int^{C-F}

1Al-Int^{C-F}

2Al-Int^{C-F}

2Ga-Int^{C-F}

I-Int^{C-F}

II-Int^{C-F}
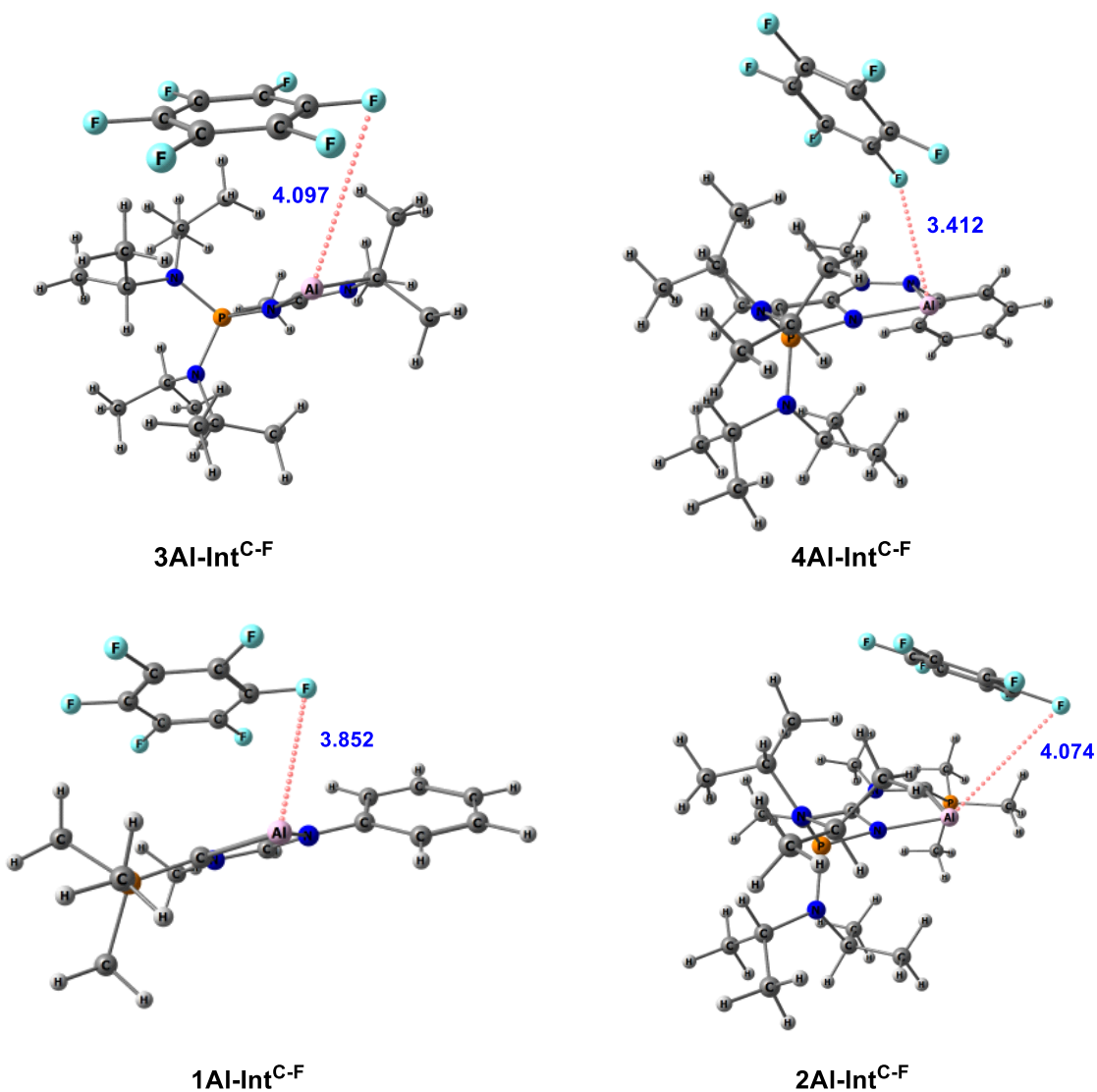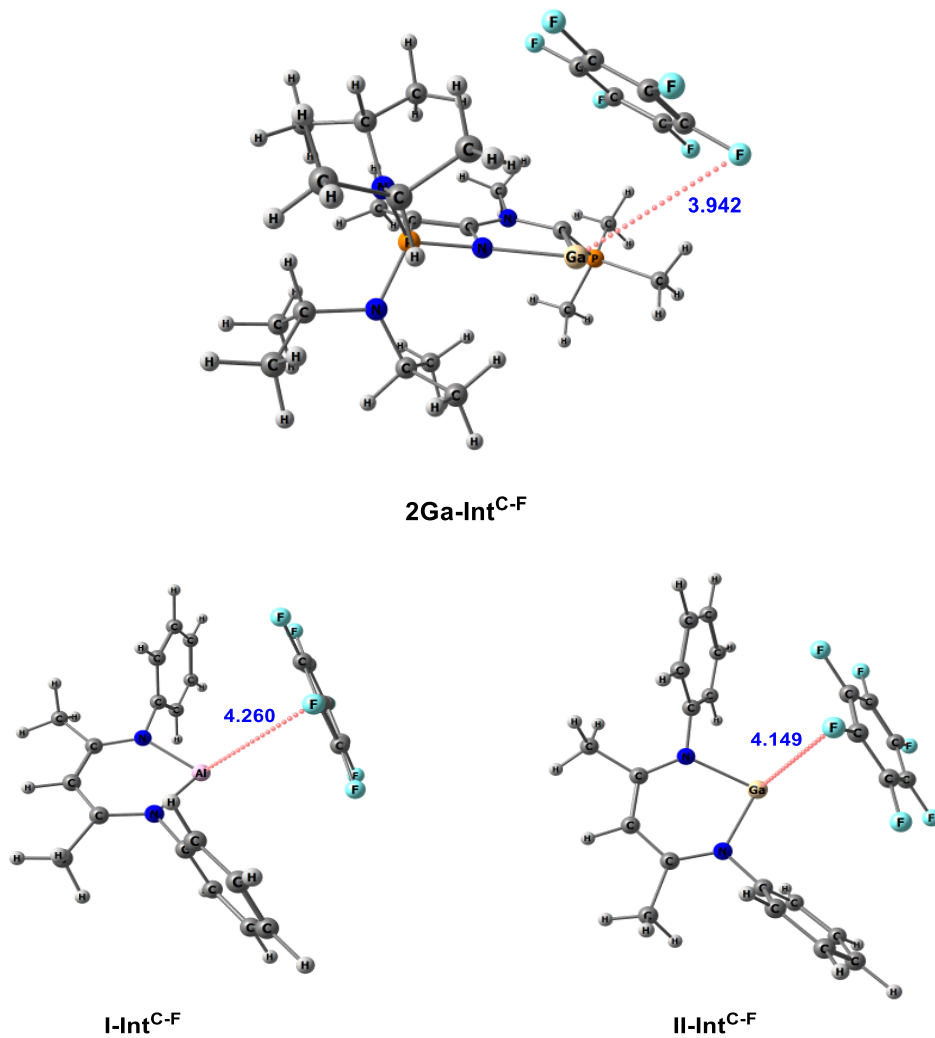
Figure 4.2.14: Optimized geometries of the encounter complex involved in the activation of C–F bond of C_6F_6 by **1–4**, **I** and **II** at M06-D3/def2-TZVP(Toluene) level of theory.
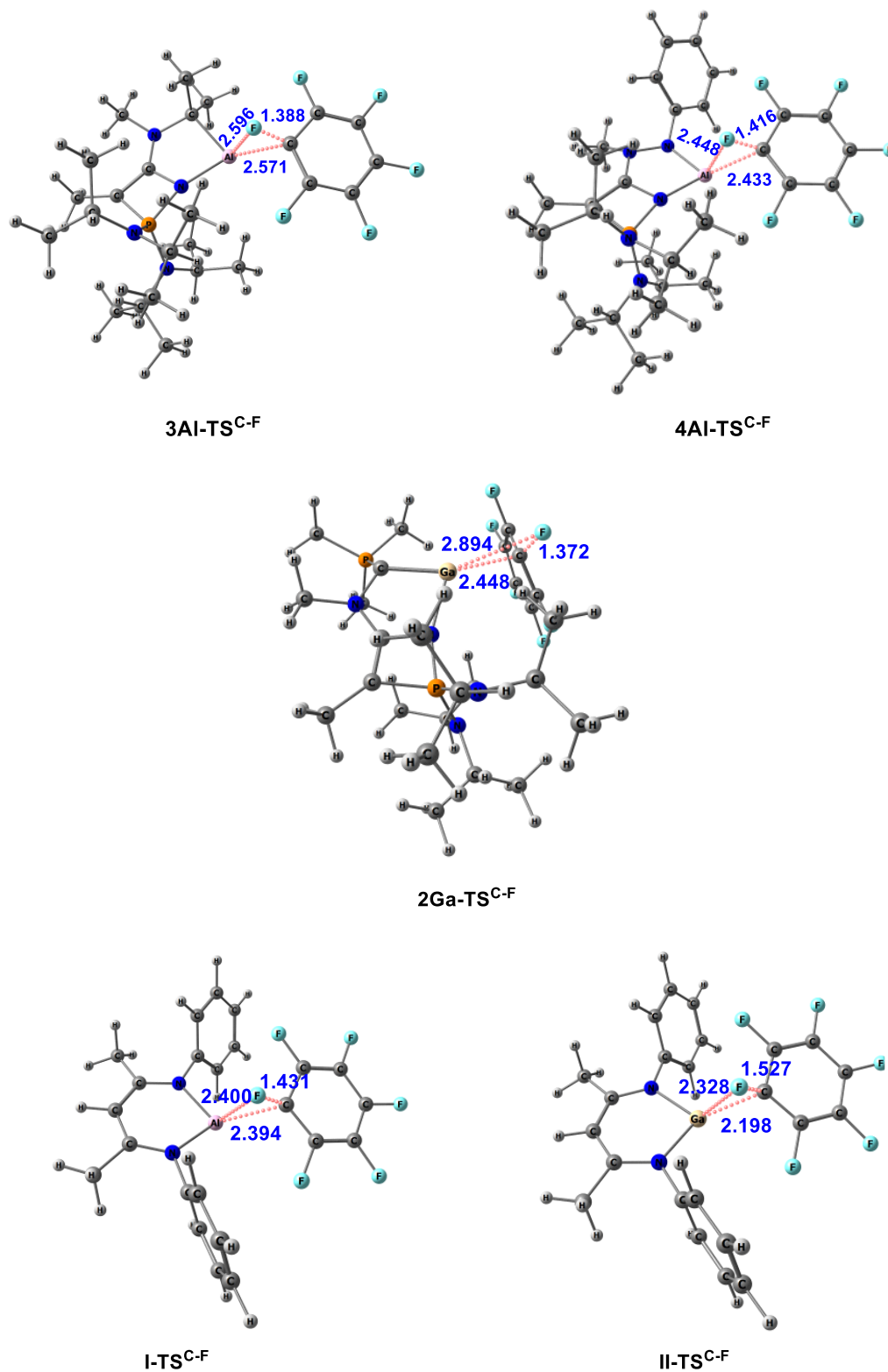

1Al-TS^{C-F}

2Al-TS^{C-F}

3Al-TS^{C-F} **4Al-TS**$^{C-F}$

2Ga-TS^{C-F}

I-TS^{C-F} **II-TS**$^{C-F}$
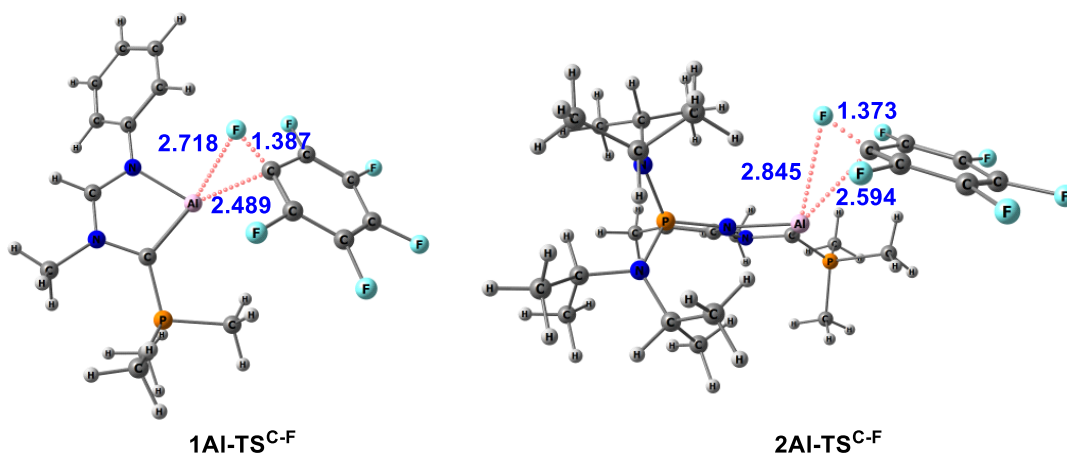
Figure 4.2.15: Optimized geometries of the transition states involved in the activation of C–F bond of C_6F_6 by **1–4**, **I** and **II** at M06-D3/def2-TZVP(Toluene) level of theory.

[4.2.3.5] Reaction with Acetylene (C–H activation *vs*. cycloaddition product)

Activation of the C–H bond is a challenging task and often demands harsh reaction conditions [76-77]. However, recent studies have demonstrated the successful utilization of a variety of main group compounds that can readily cleave enthalpically strong C–H bond under mild reaction conditions [21]. It is pertinent to mention here that Roesky's aluminium carbenoid **I** upon reaction with one equivalent of acetylene favors the formation of a [1+2] cycloaddition product over the C–H bond splitting one [78]. Therefore, in the present study, we have investigated both the possibilities i.e., the formation of the C–H activated product as well as the cycloaddition product by **1**–**4** and compared the energetics with that of **I** and **II**.

The C–H bond insertion reaction by **1**–**4** may proceeds via a single step in which the lone pair of E interacts with the C–H antibonding orbital thereby producing a pseudo anionic CCH fragment that eventually migrates toward the vacant p orbital at E to form the C–H bond cleaved product. The overall process proceeds via a TS that exhibits a substantially elongated (C–H = 1.470–1.585 Å) and polarized C–H bond as shown in Figure 4.2.16 for **1Al** and **2Al** as representative examples (for others, see Table 4.2.11 and Figure 4.2.17). On the other hand, formation of the cycloaddition products by **1**–**4** proceed via two successive steps [79]. The first step involves the formation of an intermediate (**1Al-Int$_{Cy}$** and **2Al-Int$_{Cy}$**, Figure 4.2.16) which is found to be almost at equilibrium for **1Al** and slightly exergonic (-5.0 kcal mol^{-1}) for **2Al**. In the second step, the intermediates pass through TSs (**1Al-TS$_{Cy}$** and **2Al-TS$_{Cy}$**) featuring a substantially elongated C≡C bond (1.349–1.355 Å) to yield the [1+2] cycloaddition product. The optimized geometries of the intermediates as well as the TSs involved in the cycloaddition by **1**–**4** and **I** are shown Figures 4.2.18-4.2.19 respectively.

It is evident from Table 4.2.12 that the formation of the C–H splitting product involves much higher barriers than that for the cycloaddition products–which is indeed in agreement with the experimental findings of Roesky and coworkers who have reported the formation of a cycloaddition product upon reaction of **I** with acetylene [78]. Furthermore,
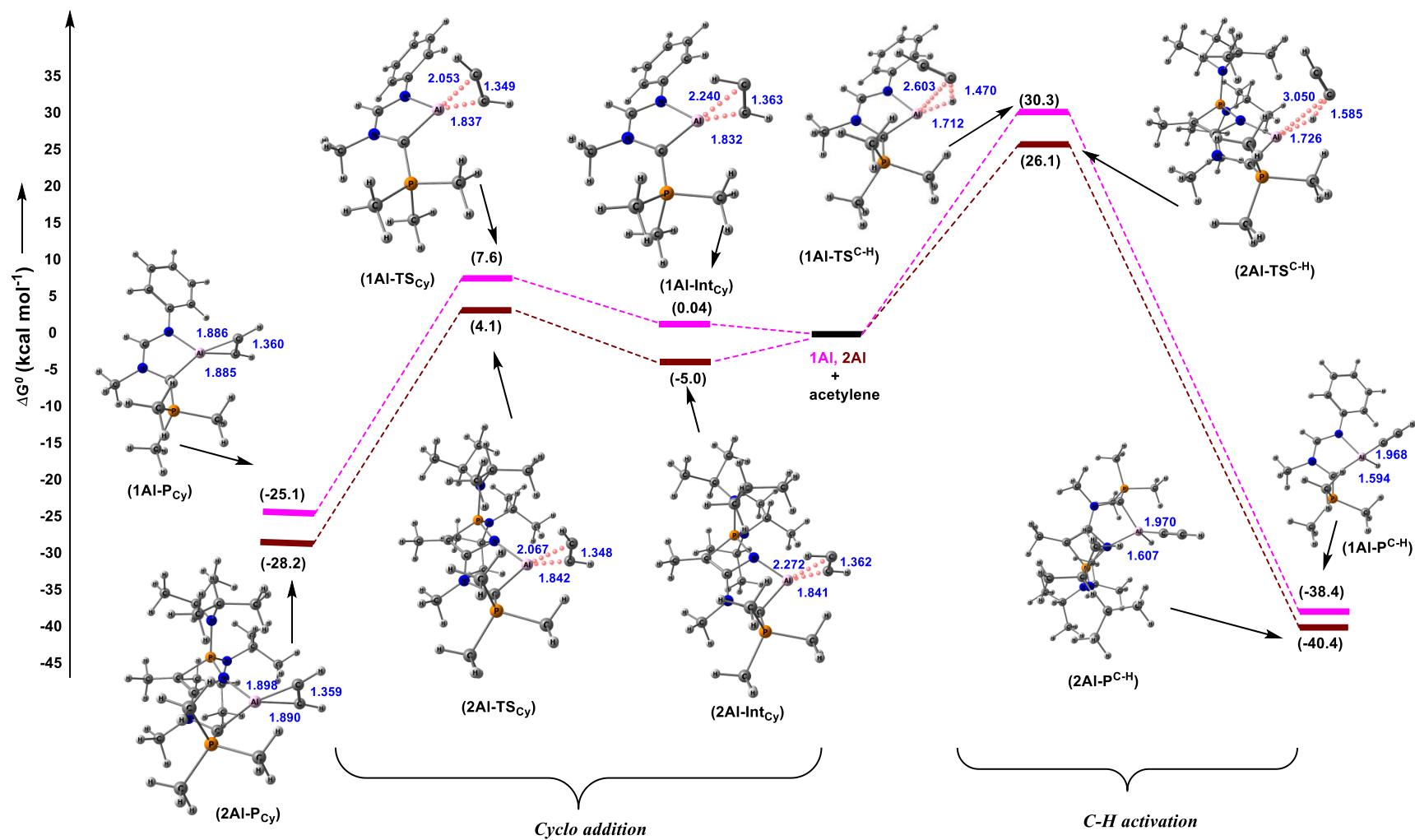
Figure 4.2.16: Energy profile diagram for the formation of the cycloaddition and C–H insertion products by **1Al** and **2Al** at M06-D3/def2-TZVP (Toluene) level of theory.
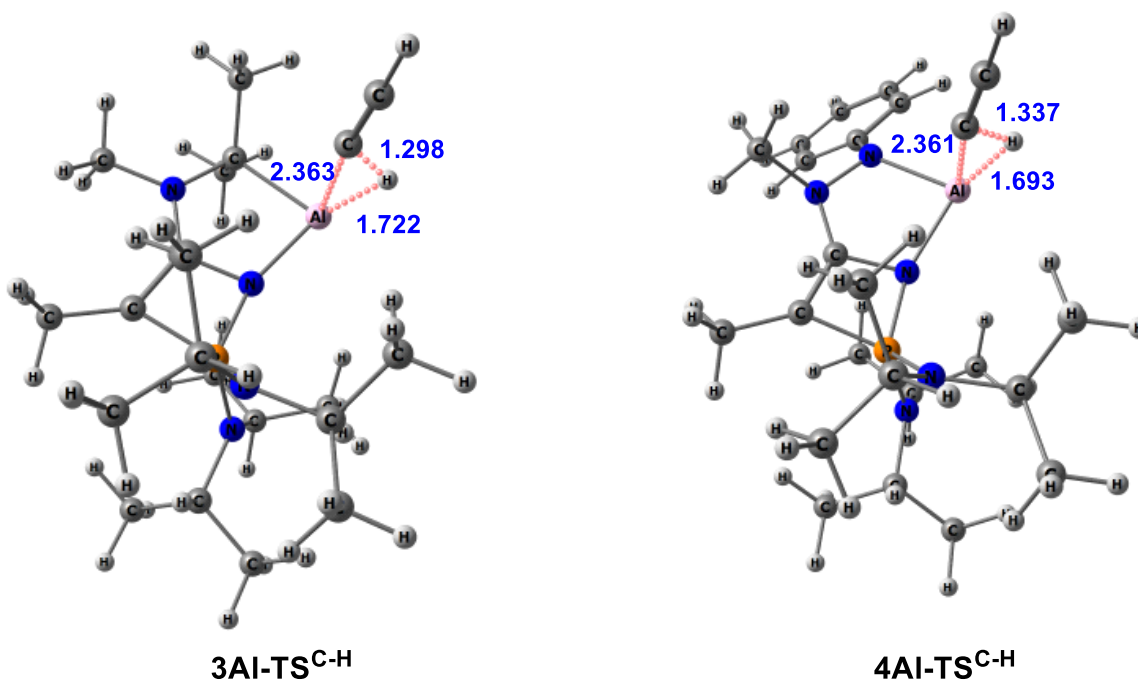
Table 4.2.11: Calculated (M06-D3/def2-TZVP(Toluene)) important geometrical parameters and natural charges at positively polarized hydrogen atom ($q_{H^{\delta+}}$) and carbon atom of the CCH fragment ($q_{CCH^{\delta-}}$) and occupancies of the formally vacant p_π orbital at the E = Al/Ga center (Occ_{P_π}) of the transition states involved in the activation of C–H bond of acetylene by **1–4**, **I** and **II**. Bond lengths are given in Å and Wiberg Bond Index (WBI) values are given within parentheses.

Molecules	$H^{\delta+}$–$CCH^{\delta-}$	E–$CCH^{\delta-}$	E–$H^{\delta+}$	$q_{CCH}^{\delta-}$	$q_H^{\delta+}$	Occ_{p_π}
I-TS^{C-H}	1.347	2.374	1.690	-0.494	0.048	0.408
	(0.472)	(0.443)	(0.494)			
II-TS^{C-H}	1.512	2.430	1.512	-0.477	0.020	0.423
	(0.328)	(0.468)	(0.615)			
1Al-TS^{C-H}	1.470	2.603	1.712	-0.430	-0.067	0.421
	(0.363)	(0.357)	(0.590)			
2Al-TS^{C-H}	1.585	3.050	1.726	-0.414	-0.150	0.232
	(0.290)	(0.283)	(0.643)			
3Al-TS^{C-H}	1.298	2.363	1.722	-0.479	0.065	0.182
	(0.523)	(0.434)	(0.430)			
4Al-TS^{C-H}	1.337	2.362	1.693	-0.495	0.050	0.170
	(0.484)	(0.440)	(0.478)			
1Ga-TS^{C-H}	1.803	3.141	1.613	-0.425	-0.135	0.255
	(0.180)	(0.206)	(0.743)			
2Ga-TS^{C-H}	1.730	3.053	1.730	-0.414	-0.135	0.349
	(0.208)	(0.237)	(0.708)			

1Ga, **2Ga** and **II** involve much higher barriers for the formation of either the C–H activated or the cycloaddition products which perhaps explains why there is no experimental report on activation of acetylene by gallium carbenoids. It is indeed inspiring to note that the proposed aluminium carbenoids (**1Al-4Al**) compute significantly lower barriers than that obtained for the experimentally evaluated **I**, which invites experimental verification.

Table 4.2.12: Calculated (M06-D3/def2-TZVP (Toluene)) activation energy barriers ($\Delta G°_{TS}{}^{C-H\ddagger}$ and $\Delta G°_{TS}{}^{Cy\ddagger}$) and reaction free energies for the formation of intermediates ($\Delta G°_{Int}$), C–H bond insertion and cycloaddition products ($\Delta G°_{Total}{}^{C-H}$ and $\Delta G°_{Total}{}^{Cy}$) obtained for **1–4**, **I** and **II**. The energies are given in kcal mol^{-1}.

Entry	C–H activation		Cycloaddition		
	$\Delta G°_{TS}{}^{C-H\ddagger}$	$\Delta G°_{Total}{}^{C-H}$	$\Delta G°_{Int}$	$\Delta G°_{TS}{}^{Cy\ddagger}$	$\Delta G°_{Total}{}^{Cy}$
1Al	30.3	-38.4	0.04	7.6	-25.1
2Al	26.1	-40.4	-5.0	4.1	-28.2
3Al	30.9	-42.5	-3.8	3.3	-29.8
4Al	35.5	-39.3	3.5	8.7	-24.4
1Ga	39.1	-12.1	16.9	22.4	7.9
2Ga	33.3	-14.4	13.7	20.5	3.4
I	35.9	-41.3	3.3	10.7	-25.6
II	51.9	-10.7	2.4	26.2	13.9

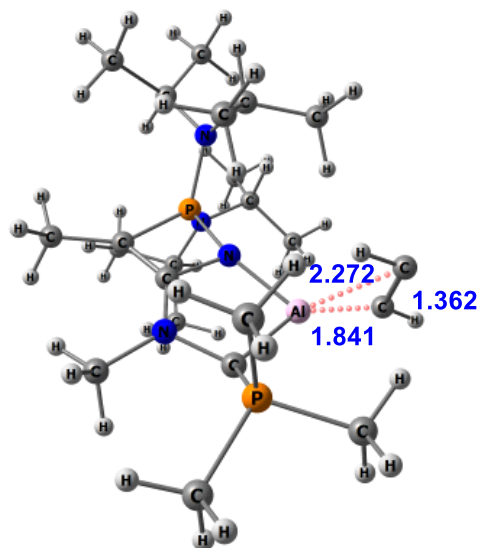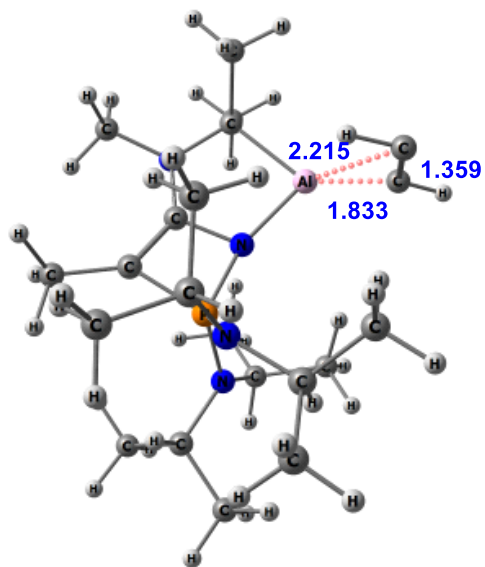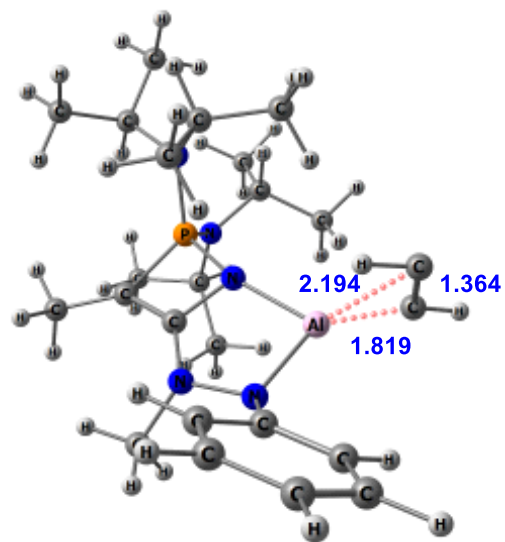**3Al-TS^{C-H}**

4Al-TS^{C-H}
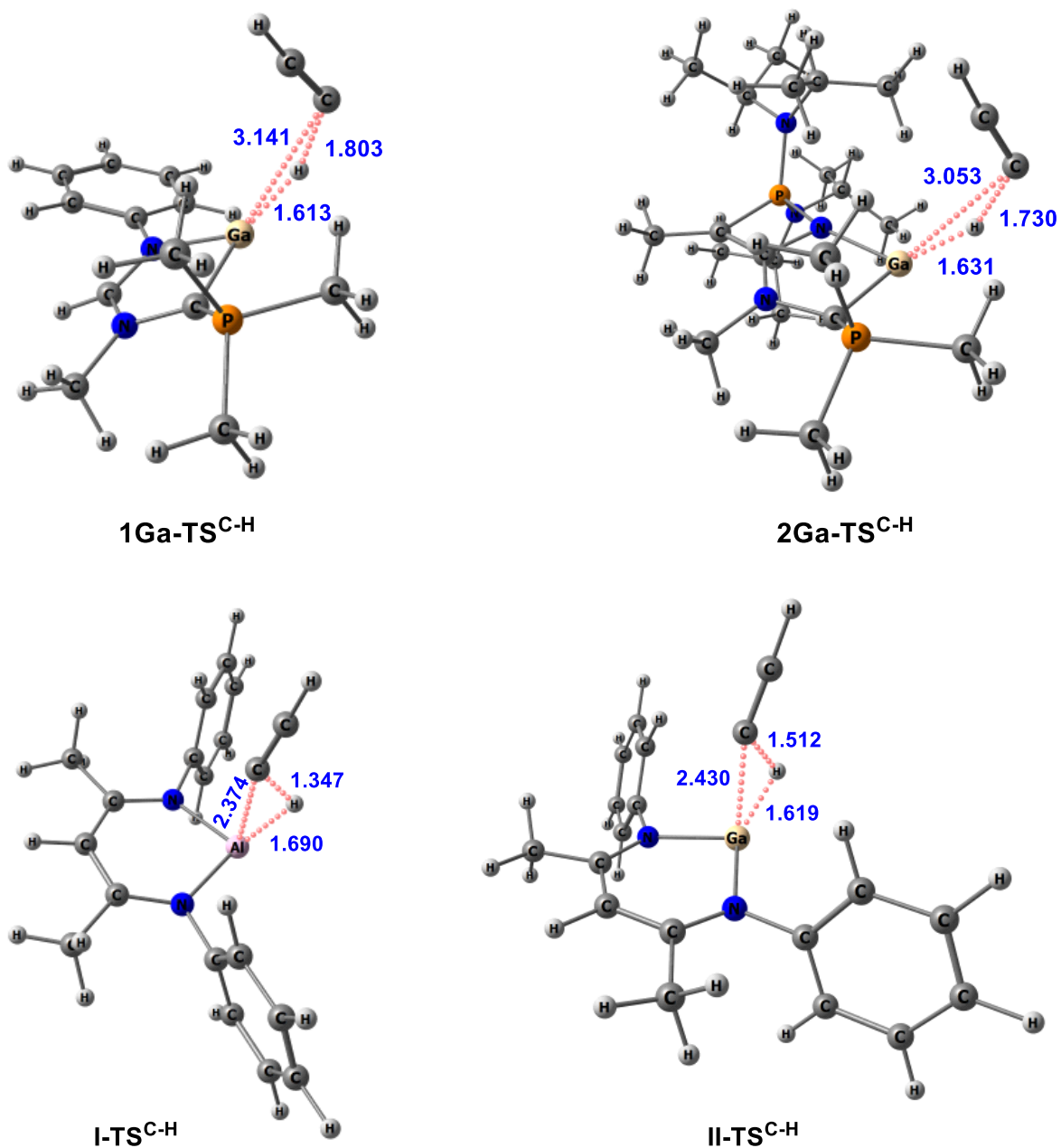
Figure 4.2.17: Optimized geometries of the transition states involved in the activation of C–H bond of acetylene by **1–4** and **I-II** at M06-D3/def2-TZVP(Toluene) level of theory.
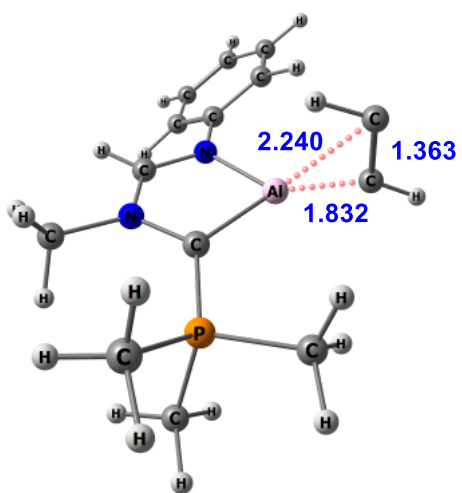
1Al-Int_Cy

2Al-Int_Cy

3Al-Int_Cy
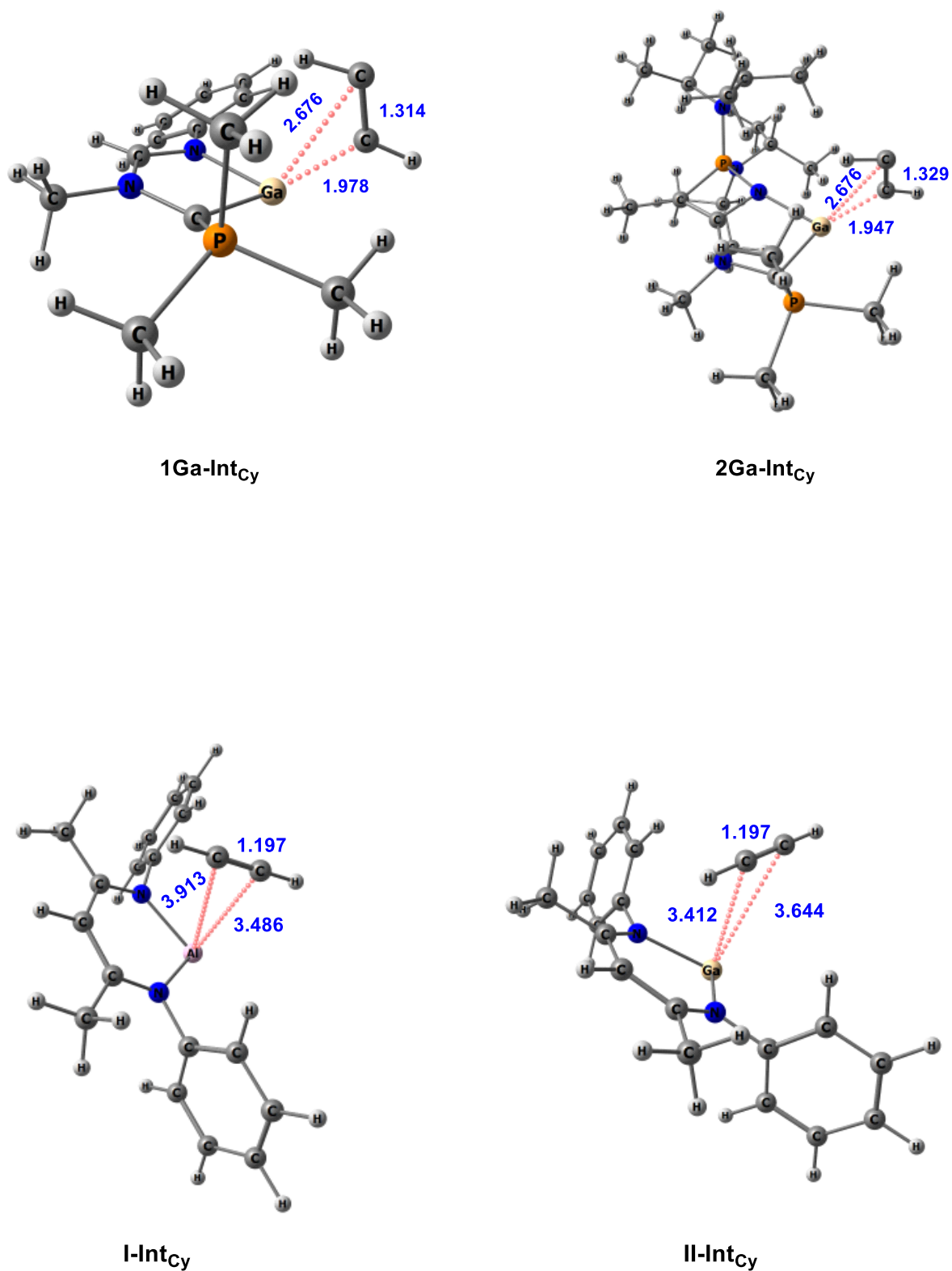

4Al-Int_Cy

1Ga-Int$_{Cy}$

2Ga-Int$_{Cy}$
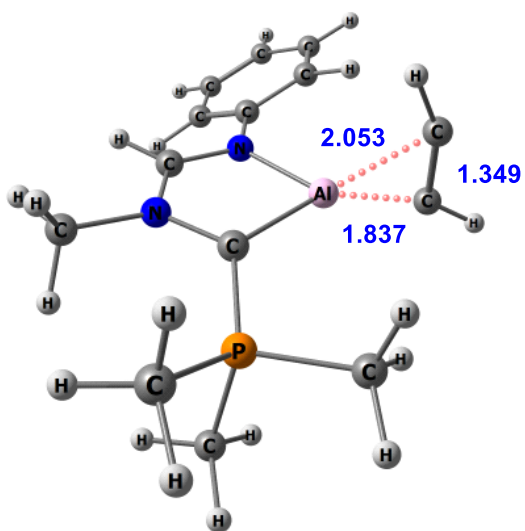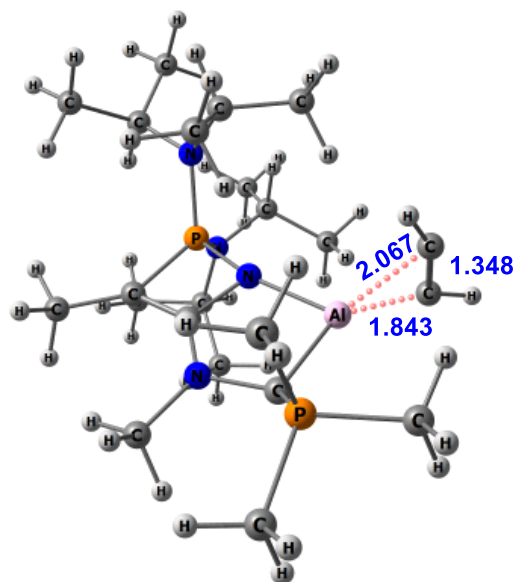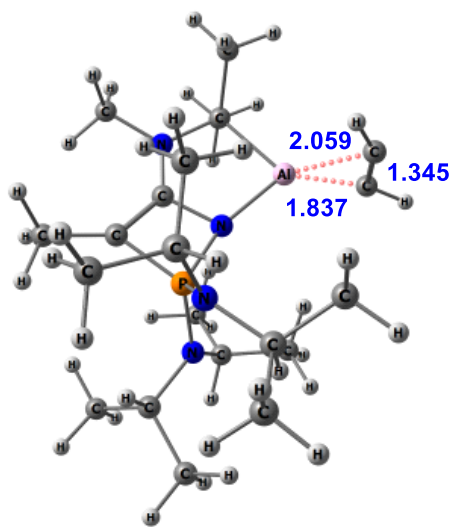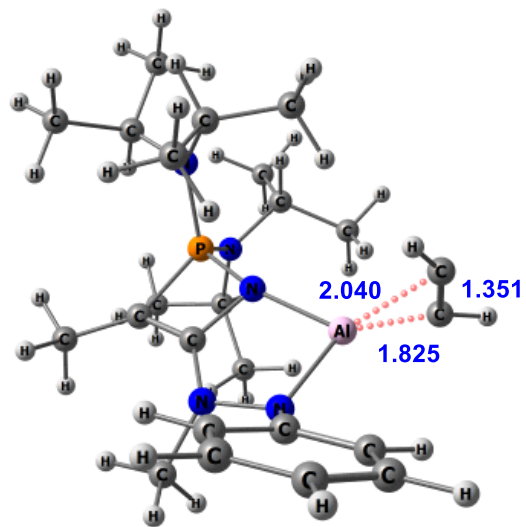
I-Int$_{Cy}$

II-Int$_{Cy}$

Figure 4.2.18: Optimized geometries of the intermediate involved in the formation of the cycloaddition product by **1–4** and **I-II** at M06-D3/def2-TZVP(Toluene) level of theory.

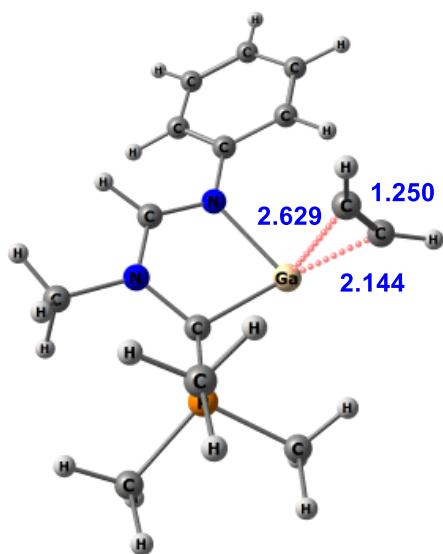**1Al-TS_{Cy}**

2Al-TS_{Cy}

3Al-TS_{Cy}

4Al-TS_{Cy}

1Ga-TS$_{Cy}$

2Ga-TS$_{Cy}$

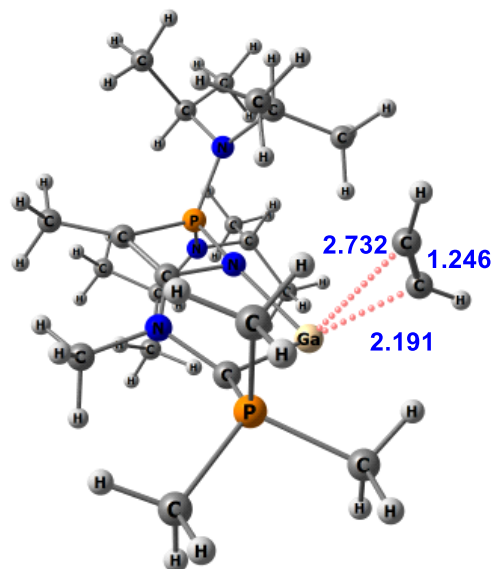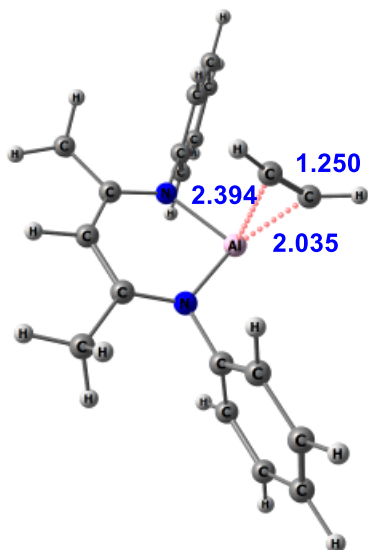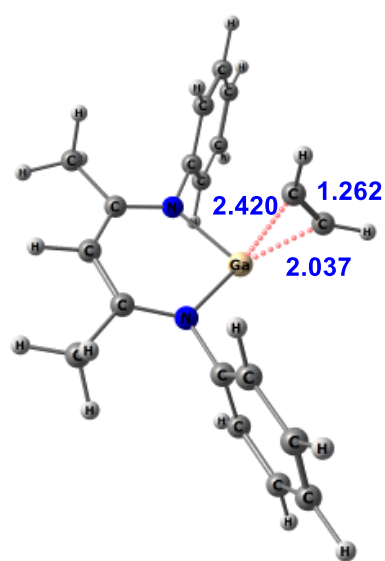**I-TS$_{Cy}$**

II-TS$_{Cy}$

Figure 4.2.19: Optimized geometries of the transition states involved in the formation of cycloaddition product by **1–4**, **I** and **II** at M06-D3/def2-TZVP(Toluene) level of theory.

[4.2.4] Conclusions

Motivated by the lack of isolable neutral monomeric five-membered aluminium carbenoids as well as to contribute to the field of group 13 carbenoids with enhanced ligand properties, density functional theory calculations were carried out on a number of ylide decorated monovalent aluminium and gallium carbenoids (**1**–**4**). All the computationally proposed molecules are found to be substantially nucleophilic and exhibit singlet-triplet energy separation values that are either comparable or higher than those obtained for **I**, **II** and **XIa** indicating that all of them could be considered as potential synthetic targets. In addition, the calculated activation energy barriers obtained for **1**–**4** in different bond activation processes are found to be comparable to those of **I** and **II** which are known to activate a range of small molecules under mild reaction conditions. Therefore, akin to **I** and **II**, all the newly designed ylide anchored group 13 carbenoids may be considered as suitable candidates for small molecule activation and calls for sustained experimental efforts toward their synthesis and isolation. A hint towards their possible isolation came from the synthetic amenability of the cyclic ylide [80] employed towards stabilizing the proposed systems in this study. We hope that if one is successful in the synthesis and isolation of these proposed group 13 carbenoids, then they may find use not only as strong nucleophilic ligands for transition metal catalysis but also may be used as suitable platforms for activation of a range of enthalpically strong bonds under mild reaction conditions.

Due to their better electron donation ability, the ylide decorated borylenes consistently yields lower barrier heights in different σ-bonds activation (H–H and C–F) process than that of their heavier congeners. Therefore, the newly proposed borylenes are expected to perform more efficiently in different enthalpically strong bond splitting process.

All the group 13 and 14 carbenoids considered in our work exhibit suitable ligand properties for their application in different small molecule activation process. Infect, the barrier heights obtained the group 13 and 14 carbenoids are comparable or lower than those of the experimentally evaluated systems (CAAC, DAC, Roesky's Al(I) and Power's Ga(I) carbenoid), indicating they may be considered as an suitable platform for the activation of different enthalpically strong bonds. However, the nucleophilic borylenes which computes substantially lower barrier heights as well as exergonic reaction free energies for different σ-

bond activation process may outperform all other 13 and 14 carbenoids considered in our work.

[4.2.6] Bibliography

[1]   Arduengo III, A. J., Harlow, R. L., and Kline, M. A Stable Crystalline Carbene. *Journal of the American Chemical Society*, 113(1):361-363, 1991.

[2]   Nesterov, V., Reiter, D., Bag, P., Frisch, P., Holzner, R., Porzelt, A., and Inoue, S. NHCs in Main Group Chemistry. *Chemical Reviews*, 118(19):9678-9842, 2018.

[3]   Borthakur, B., Ghosh, B., and Phukan, A. K. The flourishing chemistry of carbene stabilized compounds of group 13 and 14 elements. *Polyhedron*, 197:115049, 2021.

[4]   Vougioukalakis, G. C., and Grubbs, R. H. Ruthenium-Based Heterocyclic Carbene-Coordinated Olefin Metathesis Catalysts. *Chemical Reviews*, 110(3):1746-1787, 2010.

[5]   Samojłowicz, C., Bieniek, M., and Grela, K. Ruthenium-Based Olefin Metathesis Catalysts Bearing *N*-Heterocyclic Carbene Ligands. *Chemical Reviews*, 109(8):3708-3742, 2009.

[6]   Würtemberger-Pietsch, S., Radius, U., and Marder, T. B. 25 years of N-heterocyclic carbenes: activation of both main-group element–element bonds and NHCs themselves. *Dalton Transactions*, 45(14):5880-5895, 2016.

[7]   Martin, D., Soleilhavoup, M., and Bertrand, G. Stable singlet carbenes as mimics for transition metal centers. *Chemical Science*, 2(3):389-399, 2011.

[8]   Bellotti, P., Koy, M., Hopkinson, M. N., and Glorius, F. Recent advances in the chemistry and applications of N-heterocyclic carbenes. *Nature Reviews Chemistry*, 5(10):711-725, 2021.

[9]   Velazquez, H. D., and Verpoort, F. N-heterocyclic carbene transition metal complexes for catalysis in aqueous media. *Chemical Society Reviews*, 41(21):7032-7060, 2012.

[10]   Doddi, A., Peters, M., and Tamm, M. N-Heterocyclic Carbene Adducts of Main Group Elements and Their Use as Ligands in Transition Metal Chemistry. *Chemical Reviews*, 119(12): 6994-7112, 2019.

[11]   Lavallo, V., Canac, Y., Präsang, C., Donnadieu, B., and Bertrand, G. Stable Cyclic (Alkyl)(Amino) Carbenes as Rigid or Flexible, Bulky, Electron-Rich Ligands for

Transition-Metal Catalysts: A Quaternary Carbon Atom Makes the Difference. *Angewandte Chemie International Edition*, 44(35):5705-5709, 2005.

[12]   Hudnall, T. W., and Bielawski, C. W. An *N, N′*-Diamidocarbene: Studies in C−H Insertion, Reversible Carbonylation, and Transition-Metal Coordination Chemistry. *Journal of the American Chemical Society*, 131(44):16039-16041, 2009.

[13]   Asay, M., Jones, C., and Driess, M. *N*-Heterocyclic Carbene Analogues with Low-Valent Group 13 and Group 14 Elements: Syntheses, Structures, and Reactivities of a New Generation of Multitalented Ligands. *Chemical Reviews*, 111(2):354-396, 2011.

[14]   Cui, C., Roesky, H. W., Schmidt, H. G., Noltemeyer, M., Hao, H., and Cimpoesu, F. Synthesis and Structure of a Monomeric Aluminum(I) Compound $[\{HC(CMeNAr)_2\}Al](Ar= 2,6-^iPr_2C_6H_3)$: A Stable Aluminum Analogue of a Carbene. *Angewandte Chemie International Edition*, 39(23): 4274-4276, 2000.

[15]   Hardman, N. J., Eichler, B. E., and Power, P. P. Synthesis and characterization of the monomer $Ga\{(NDippCMe)_2CH\}(Dipp= C_6H_3Pr^i_2-2,6)$: a low valent gallium(I) carbene analogue. *Chemical Communications*, (20):1991-1992, 2000.

[16]   Chu, T., Korobkov, I., and Nikonov, G. I. Oxidative Addition of σ Bonds to an Al(I) Center. *Journal of the American Chemical Society*, 136(25):9195-9202, 2014.

[17]   Bakewell, C., Garçon, M., Kong, R. Y., O'Hare, L., White, A. J., and Crimmin, M. R. Reactions of an Aluminum(I) Reagent with 1,2-,1,3-, and 1, 5-Dienes: Dearomatization, Reversibility, and a Pericyclic Mechanism. *Inorganic Chemistry*, 59(7):4608-4616, 2020.

[18]   Hill, M. S., and Hitchcock, P. B. A mononuclear indium(I) carbene analogue. *Chemical Communications*, (16):1818-1819, 2004.

[19]   Hill, M. S., Hitchcock, P. B., and Pongtavornpinyo, R. Neutral carbene analogues of the heaviest Group 13 elements: Consideration of electronic and steric effects on structure and stability. *Dalton Transactions*, (2):273-277, 2005.

[20]   Zhong, M., Sinhababu, S., and Roesky, H. W. The unique β-diketiminate ligand in aluminum(I) and gallium(I) chemistry. *Dalton Transactions*, 49(5):1351-1364, 2020.

[21]   Chu, T., and Nikonov, G. I. Oxidative Addition and Reductive Elimination at Main-Group Element Centers. *Chemical Reviews*, 118(7):3608-3680, 2018.

[22]   Seifert, A., Scheid, D., Linti, G., and Zessin, T. Oxidative Addition Reactions of Element–Hydrogen Bonds with Different Polarities to a Gallium(I) Compound. *Chemistry– A European Journal*, 15(44):12114-12120, 2009.

[23]   Kysliak, O., Görls, H., and Kretschmer, R. Cooperative Bond Activation by a Bimetallic Main-Group Complex. *Journal of the American Chemical Society*, 143(1):142-148, 2020.

[24]   Hobson, K., Carmalt, C. J., and Bakewell, C. Recent advances in low oxidation state aluminium chemistry. *Chemical Science*, 11(27):6942-6956, 2020.

[25]   Bag, P., Porzelt, A., Altmann, P. J., and Inoue, S. A Stable Neutral Compound with an Aluminum–Aluminum Double Bond. *Journal of the American Chemical Society*, 139(41):14384-14387, 2017.

[26]   Hicks, J., Vasko, P., Goicoechea, J. M., and Aldridge, S. Synthesis, structure and reaction chemistry of a nucleophilic aluminyl anion. *Nature*, 557(7703):92-95, 2018.

[27]   Hicks, J., Vasko, P., Goicoechea, J. M., and Aldridge, S. Reversible, Room-Temperature C—C Bond Activation of Benzene by an Isolable Metal Complex. *Journal of the American Chemical Society*, 141(28):11000-11003, 2019.

[28]   Schwamm, R. J., Anker, M. D., Lein, M., and Coles, M. P. Reduction vs. Addition: The Reaction of an Aluminyl Anion with 1,3,5,7-Cyclooctatetraene. *Angewandte Chemie International Edition*, 58(5): 1489-1493, 2019.

[29]   Schwamm, R. J., Coles, M. P., Hill, M. S., Mahon, M. F., McMullin, C. L., Rajabi, N. A., and Wilson, A. S. A Stable Calcium Alumanyl. *Angewandte Chemie International Edition*, 59(10): 3928-3932, 2020.

[30]   Hicks, J., Vasko, P., Goicoechea, J. M., and Aldridge, S. The aluminyl anion: a new generation of aluminium nucleophile. *Angewandte Chemie International Edition*, 133(4): 1726-1737, 2021.

[31]   Evans, M. J., Anker, M. D., and Coles, M. P. Oxidative Addition of Hydridic, Protic, and Nonpolar E–H Bonds (E= Si, P, N, or O) to an Aluminyl Anion. *Inorganic Chemistry*, 60(7):4772-4778, 2021.

[32]   Grams, S., Eyselein, J., Langer, J., Färber, C., and Harder, S. Boosting Low-Valent Aluminum(I) Reactivity with a Potassium Reagent. *Angewandte Chemie International Edition*, 59(37): 15982-15986, 2020.

[33] Heilmann, A., Hicks, J., Vasko, P., Goicoechea, J. M., and Aldridge, S. Carbon Monoxide Activation by a Molecular Aluminium Imide: C−O Bond Cleavage and C−C Bond Formation. *Angewandte Chemie International Edition*, 59(12):4897-4901, 2020.

[34] Schwamm, R. J., Hill, M. S., Liu, H. Y., Mahon, M. F., McMullin, C. L., and Rajabi, N. A. Seven-Membered Cyclic Potassium Diamidoalumanyls. *Chemistry–A European Journal*, 27(60):14971-14980, 2021.

[35] Mellerup, S. K., Cui, Y., Fantuzzi, F., Schmid, P., Goettel, J. T., Belanger-Chabot, G., Arrowsmith, M., Krummenacher, I., Ye, Q., Engel, V., Engels, B., and Braunschweig, H. Lewis-Base Stabilization of the Parent Al(I) Hydride under Ambient Conditions. *Journal of the American Chemical Society*, 141(42):16954-16960, 2019.

[36] Kurumada, S., Takamori, S., and Yamashita, M. An alkyl-substituted aluminium anion with strong basicity and nucleophilicity. *Nature Chemistry*, 12(1):36-39, 2020.

[37] Sugita, K., Nakano, R., and Yamashita, M. Cycloaddition of Dialkylalumanyl Anion toward Unsaturated Hydrocarbons in (1+2) and (1+4) Modes. *Chemistry–A European Journal*, 26(10):2174-2177, 2020.

[38] Koshino, K., and Kinjo, R. Construction of σ-Aromatic AlB$_2$ Ring via Borane Coupling with a Dicoordinate Cyclic (Alkyl)(Amino)Aluminyl Anion. *Journal of the American Chemical Society*, 142(19):9057-9062, 2020.

[39] Denker, L., Trzaskowski, B., and Frank, R. "Give me five"–an amino imidazoline-2-imine ligand stabilises the first neutral five-membered cyclic triel(I) carbenoides. *Chemical Communications*, 57(22):2816-2819, 2021.

[40] Kretsch, J., Kreyenschmidt, A., Schillmöller, T., Sindlinger, C., Herbst-Irmer, R., and Stalke, D. Group 13 Heavier Carbene Analogues Stabilized by the Bulky Bis (4-benzhydryl-benzoxazol-2-yl) methanide Ligand. *Inorganic Chemistry*, 60(10):7389-7398, 2021.

[41] Falconer, R. L., Byrne, K. M., Nichol, G. S., Krämer, T., and Cowley, M. J. Reversible Dissociation of a Dialumene. *Angewandte Chemie International Edition*, 60(46):24702-24708, 2021.

[42] Fujimori, S., and Inoue, S. Small Molecule Activation by Two-Coordinate Acyclic Silylenes. *European Journal of Inorganic Chemistry*, 2020(33):3131-3142, 2020.

[43]   Nakafuji, S. Y., Kobayashi, J., and Kawashima, T. Generation and Coordinating Properties of a Carbene Bearing a Phosphorus Ylide: An Intensely Electron-Donating Ligand. *Angewandte Chemie International Edition*, 47(6):1141-1144, 2008.

[44]   Fürstner, A., Alcarazo, M., Radkowski, K., and Lehmann, C. W. Carbenes stabilized by ylides: Pushing the limits. *Angewandte Chemie International Edition*, 47(43):8302-8306, 2008.

[45]   Borthakur, B., and Phukan, A. K. Moving toward Ylide-Stabilized Carbenes. *Chemistry–A European Journal*, 21(32):11603-11609, 2015.

[46]   (a) lvarado-Beltran, I., Baceiredo, A., Saffon-Merceron, N., Branchadell, V., and Kato, T. Cyclic Amino(Ylide)Silylene: A Stable Heterocyclic Silylene with Strongly Electron-Donating Character. *Angewandte Chemie International Edition*, 55(52):16141-16144, 2016; (b) Asay, M., Inoue, S., and Driess, M. Aromatic Ylide-Stabilized Carbocyclic Silylene. *Angewandte Chemie International Edition*, 50(41):9589-9592, 2011.

[47]   Del Rio, N., Lopez-Reyes, M., Baceiredo, A., Saffon-Merceron, N., Lutters, D., Müller, T., and Kato, T. N, P-Heterocyclic Germylene/$B(C_6F_5)_3$ Adducts: A Lewis Pair with Multi-reactive Sites. *Angewandte Chemie International Edition*, 56(5):1365-1370, 2017.

[48]   Mohapatra, C., Scharf, L. T., Scherpf, T., Mallick, B., Feichtner, K. S., Schwarz, C., and Gessner, V. H. Isolation of a Diylide-Stabilized Stannylene and Germylene: Enhanced Donor Strength through Coplanar Lone Pair Alignment. *Angewandte Chemie International Edition*, 58(22):7459-7463, 2019.

[49]   Sarbajna, A., Swamy, V. S. V. S. N., and Gessner, V. H. Phosphorus-ylides: powerful substituents for the stabilization of reactive main group compounds. *Chemical Science*, 12(6):2016-2024, 2021.

[50]   Steinert, H., Löffler, J., and Gessner, V. H. Single-Site and Cooperative Bond Activation Reactions with Ylide-Functionalized Tetrylenes: A Computational Study. *European Journal of Inorganic Chemistry*, 2021(47):5004-5013, 2021.

[51]   Bharadwaz, P., and Phukan, A. K. Introducing *N*-Heterocyclic Borylenes: Theoretical Prediction of Stable, Neutral, Monomeric Boron(I) Carbenoids. *Inorganic Chemistry*, 58(9):5428-5432, 2019.

[52]   Zhao, Y., and Truhlar, D. G. The M06 suite of density functionals for main group thermochemistry, thermochemical kinetics, noncovalent interactions, excited states, and

transition elements: two new functionals and systematic testing of four M06-class functionals and 12 other functionals. *Theoretical Chemistry Accounts*, 120(1):215-241, 2008.

[53]   Weigend, F., and Ahlrichs, R. Balanced basis sets of split valence, triple zeta valence and quadruple zeta valence quality for H to Rn: Design and assessment of accuracy. *Physical Chemistry Chemical Physics*, 7(18):3297-3305, 2005.

[54]   Weigend, F. Accurate Coulomb-fitting basis sets for H to Rn. *Physical Chemistry Chemical Physics*, 8(9):1057-1065, 2006.

[55]   Grimme, S.; Antony, J.; Ehrlich, S.; Krieg, H. A consistent and accurate ab initio parametrization of density functional dispersion correction (DFT-D) for the 94 elements H-Pu. *The Journal of Chemical Physics*, 132(15):154104, 2010.

[56]   Cossi, M.; Scalmani, G.; Rega, N.; Barone, V. New developments in the polarizable continuum model for quantum mechanical and classical calculations on molecules in solution. *The Journal of Chemical Physics*, 117(1):43-54, 2002.

[57]   Glendening, E., Reed, A., Carpenter, J., and Weinhold, F. NBO Program 3.1: Madison. WT: 1988.

[58]   Reed, A. E.; Curtiss, L. A.; Weinhold, F. Intermolecular Interactions from a Natural Bond Orbital, Donor-Acceptor Viewpoint. *Chemical Reviews*, 88(6):899-926, 1988.

[59]   Frisch, M. J.; Trucks, G. W.; Schlegel, H. B.; Scuseria, G. E.; Robb, M. A.; Cheeseman, J. R.; Scalmani, G.; Barone, V.; Mennucci, B.; Petersson, G. A.; Nakatsuji, H.; Caricato, M.; Li, X.; Hratchian, H. P.; Izmaylov, A. F.; Bloino, J.; Zheng, G.; Sonnenberg, J. L.; Hada, M.; Ehara, M.; Toyota, K.; Fukuda, R.; Hasegawa, J.; Ishida, M.; Nakajima, T.; Honda, Y.; Kitao, O.; Nakai, H.; Vreven, T.; Montgomery, J. A.; Jr.; Peralta, J. E.; Ogliaro, F.; Bearpark, M.; Heyd, J. J.; Brothers, E.; Kudin, K. N.; Staroverov, V. N.; Keith, T.; Kobayashi, R.; Normand, J.; Raghavachari, K.; Rendell, A.; Burant, J. C.; Iyengar, S. S.; Tomasi, J.; Cossi, M.; Rega, N.; Millam, J. M.; Klene, M.; Knox, J. E.; Cross, J. B.; Bakken, V.; Adamo, C.; Jaramillo, J.; Gomperts, R.; Stratmann, R. E.; Yazyev, O.; Austin, A. J.; Cammi, R.; Pomelli, C.; Ochterski, J. W.; Martin, R. L.; Morokuma, K.; Zakrzewski, V. G.; Voth, G. A.; Salvador, P.; Dannenberg, J. J.; Dapprich, S.; Daniels, A. D.; Farkas, O.; Foresman, J. B.; Ortiz, J. V.; Cioslowski, J.; Fox, D. J., Gaussian 09, Revision D. 01, Gaussian. *Inc., Wallingford CT* **2009**.

[60]   To reduce the computational cost, the Dipp groups attached to the nitrogen atoms of **I** and **II** were replaced with a phenyl group.

[61]   de Vries, J. G., and Elsevier, C. J. (2007). *Handbook of homogeneous hydrogenation*. Wiley-VCH: Weinheim.

[62]   Ogata, H., Lubitz, W., and Higuchi, Y. [NiFe] hydrogenases: structural and spectroscopic studies of the reaction mechanism. *Dalton Transactions*, (37):7577-7587, 2009.

[63]   Dey, S., Das, P. K., and Dey, A. Mononuclear iron hydrogenase. *Coordination Chemistry Reviews*, 257(1):42-63, 2013.

[64]   Shima, S., and Thauer, R. K. A third type of hydrogenase catalyzing H_2 activation. *The Chemical Record*, 7(1):37-46, 2007.

[65]   (a) Zhang, X., and Cao, Z. Insight into the reaction mechanisms for oxidative addition of strong σ bonds to an Al(I) center. *Dalton Transactions*, 45(25):10355-10365, 2016; (b) Villegas-Escobar, N., Gutiérrez-Oliva, S., and Toro-Labbé, A. Catalytic Mechanism of H_2 Activation by a Carbenoid Aluminum Complex. *The Journal of Physical Chemistry C*, 119(47):26598-26604, 2015.

[66]   Ameduri, B.; Sawada, H. (2016). *Fluorinated Polymers: Synthesis, Properties, Processing and Simulation*. Volume 1, Royal Society of Chemistry.

[67]   O'Hagan, D. Fluorine in health care: Organofluorine containing blockbuster drugs. *Journal of Fluorine Chemistry*, 131(11):1071-1081, 2010.

[68]   Amii, H., and Uneyama, K. C−F Bond Activation in Organic Synthesis. *Chemical Reviews*, 109(5):2119-2183, 2009.

[69]   Muller, K., Faeh, C., and Diederich, F. Fluorine in Pharmaceuticals: Looking Beyond Intuition. *Science*, 317(5846):1881-1886, 2007.

[70]   Purser, S., Moore, P. R., Swallow, S., Gouverneur, V. Fluorine in medicinal chemistry. *Chemical Society Reviews,* 37(2):320-330, 2008.

[71]   Kuehnel, M. F., Lentz, D., and Braun, T. Synthesis of Fluorinated Building Blocks by Transition-Metal-Mediated Hydrodefluorination Reactions. *Angewandte Chemie International Edition*, 52(12):3328-3348, 2013.

[72]   Coates, G., Rekhroukh, F., and Crimmin, M. R. Breaking Carbon–Fluorine Bonds with Main Group Nucleophiles. *Synlett*, 30(20):2233-2246, 2019.

[73]   Crimmin, M. R., Butler, M. J., and White, A. J. Oxidative addition of carbon–fluorine and carbon–oxygen bonds to Al(I). *Chemical Communications*, 51(88):15994-15996, 2015.

[74]   Chu, T., Boyko, Y., Korobkov, I., and Nikonov, G. I. Transition Metal-Like Oxidative Addition of C–F and C–O Bonds to an Aluminum(I) Center. *Organometallics*, 34(22):5363-5365, 2015.

[75]   (a) Zhang, X., Li, P., Wang, B., and Cao, Z. Mechanistic Features in Al(I)-Mediated Oxidative Addition of Aryl C–F Bonds: Insights From Density Functional Theory Calculations. *Frontiers in Chemistry*, 7:596, 2019; (b) Pitsch, C. E., and Wang, X. Aluminum(I) β-diketiminato complexes activate C (sp^2)–F and C (sp^3)–F bonds by different oxidative addition mechanisms: a DFT study. *Chemical Communications*, 53(58):8196-8198, 2017; (c) Kim, Y. S., Cho, H., and Hwang, S. Density functional theoretical study on the C–F and C–O oxidative addition reaction at an AI center. *Bulletin of the Korean Chemical Society*, 38(2):282-284, 2017.

[76]   Labinger, J. A., and Bercaw, J. E. Understanding and exploiting C–H bond activation. *Nature*, 417(6888):507-514, 2002.

[77]   For reviews on C-H activation, see the entire issue of *Chemical Reviews,* 2017, 117, 8481-9520

[78]   Zhu, H.; Chai, J.; Fan, H.; Roesky, H. W.; He, C.; Jancik, V.; Schmidt, H. G.; Noltemeyer, M.; Merrill, W. A.; Power, P. P. A Stable Aluminacyclopropene LAl(η^2-C$_2$H$_2$) and Its End-On Azide Insertion to an Aluminaazacyclobutene. *Angewandte Chemie International Edition*, 44(32):5090-5093, 2005.

[79]   Schoeller, W. W., and Frey, G. D. Oxidative Addition of π-Bonds and σ-Bonds to an Al(I) Center: The Second-Order Carbene Property of the AlNacNac Compound. *Inorganic Chemistry*, 55(21):10947-10954, 2016.

[80]   Tejeda, J., Reau, R., Dahan, F., and Bertrand, G. Synthesis and Molecular Structure of a 1,2λ^5-azaphosphete: A Cyclic 4-π-Electron Ylide. *Journal of the American Chemical Society*, 115(17):7880-7881, 1993.